Technical Report

TR-99-18

Site-scale groundwater flow modelling of Beberg

Björn Gylling
Kemakta Konsult AB

Douglas Walker
Duke Engineering and Services

Lee Hartley
AEA Technology

August 1999

Svensk Kärnbränslehantering AB
Swedish Nuclear Fuel
and Waste Management Co
Box 5864
SE-102 40 Stockholm Sweden
Tel 08-459 84 00
+46 8 459 84 00
Fax 08-661 57 19
+46 8 661 57 19

Site-scale groundwater flow modelling of Beberg

Björn Gylling
Kemakta Konsult AB

Douglas Walker
Duke Engineering and Services

Lee Hartley
AEA Technology

August 1999

Keywords: Canister flux, computer modelling, F-ratio, groundwater flow, Monte Carlo simulation, repository, stochastic continuum, SR 97, travel time

Abstract

The Swedish Nuclear Fuel and Waste Management Company (SKB) Safety Report for 1997 (SR 97) study is a comprehensive performance assessment illustrating the results for three hypothetical repositories in Sweden. In support of SR 97, this study examines the hydrogeologic modelling of the hypothetical site called Beberg, which adopts input parameters from the SKB study site near Finnsjön, in central Sweden. This study uses a nested modelling approach, with a deterministic regional model providing boundary conditions to a site-scale stochastic continuum model. The model is run in Monte Carlo fashion to propagate the variability of the hydraulic conductivity to the advective travel paths from representative canister positions. A series of variant cases addresses uncertainties in the inference of parameters and the boundary conditions. The study uses HYDRASTAR, the SKB stochastic continuum (SC) groundwater modelling program, to compute the heads, Darcy velocities at each representative canister position, and the advective travel times and paths through the geosphere.

The Base Case simulation takes its constant head boundary conditions from a modified version of the deterministic regional scale model of Hartley et al. (1998). The flow balance between the regional and site-scale models suggests that the nested modelling conserves mass only in a general sense, and that the upscaling is only approximately valid. The results for 100 realisation of 120 starting positions, a flow porosity of $\varepsilon_f = 1x10^{-4}$, and a flow-wetted surface of $a_r = 1.0\ m^2/(m^3\ rock)$ suggest the following statistics for the Base Case:

- The median travel time is 56 years.
- The median canister flux is 1.2×10^{-3} m/year.
- The median F-ratio is 5.6×10^5 year/m.

The travel times, flow paths and exit locations were compatible with the observations on site, approximate scoping calculations and the results of related modelling studies. Variability within realisations indicates that the change in hydraulic gradient across the hypothetical repository may result in reduced travel times for some areas of the repository. The uncertainties of this study are addressed by a series of variant cases that evaluate the sensitivity of the results to changes in assumptions regarding the boundary conditions and the hydraulic conductivities. The results are most sensitive to the use of boundary conditions derived from a salinity-dependent regional model, transferred to the site-scale model as environmental heads. The results are relatively insensitive to the inclusion of additional possible fracture zones.

Sammanfattning

SR 97 är en säkerhetsanalys av tre hypotetiska djupförvar i Sverige. Denna rapport, utförd som en del av SR 97, beskriver den hydrogeologiska modelleringen av Beberg. Beberg är en hypotetisk plats där indata och parametrar baseras på förhållanden vid Finnsjön som är beläget i Uppland. I studien har en nästlad modellering använts där en deterministisk regional modell ger randvillkor till en stokastisk kontinuum modell i platsskala. Monte Carlo simulering har använts för att propagera variabiliteten i hydraulisk konduktivitet till advektiva partikelbanor som utgår från representativa kapselpositioner. I en serie varianter har osäkerheter vid tolkandet av parametrar och överförandet av randvillkor analyserats. För att beräkna tryck, Darcy-hastigheter (specifika flöden) vid kapselpositioner, advektiva gångtider samt partikelbanor genom geosfären har SKB:s stokastiska kontinuumprogram för grundvattenmodellering, HYDRASTAR, använts.

För basfallet har tidsoberoende tryckrandvillkor från en modifierad version av den regionala modell som beskrivs av Hartley m fl (1998) använts. Vid en jämförelse av flödesbalanserna mellan den regionala och den lokala modellen visar det sig att den nästlade modelleringen bara fungerar i ett generellt perspektiv, och att uppskalningsmetoden av konduktiviteter är approximativ. Resultaten för basfallet vid användande av flödesporositeten $\varepsilon_f = 1 \times 10^{-4}$ och flödesvätta ytan $a_r = 1.0\ m^2/m^3$ ger mätetal för förvarsfunktionen i Beberg enligt följande:

- Medianen för gångtiderna är 56 år.
- Medianen för specifikt flöde vid kapselpostioner är 1.2×10^{-3} m/år.
- Medianen för F-faktorn är 5.6×10^5 år/m.

Partikelbanor, gångtider och simulerade tryck är i överensstämmelse med observationer gjorda på platsen, med förenklade överslagsberäkningar och resultat från andra simuleringar av samma plats. Variabiliteten inom realiseringar indikerar att förändringar i den hydrauliska gradienten över det hypotetiska förvaret kan resultera i förkortade gångtider för vissa områden i förvaret. Osäkerheten i modelleringsansatsen är behandlad genom att utföra en serie av varianter som inriktar sig på känsligheten i antaganden om randvillkor och hydraulisk konduktivitet. Resultaten visar att känsligheten är stor när det gäller randvillkor levererade från en regional modell med salthaltsberoende tryck i form av "densitetsjusterat tryck". Resultaten är relativt okänsliga för ytterligare inlagda tänkbara sprickzoner.

Contents

List of Figures

List of Tables

1 Introduction

1.1 SR 97

Swedish Nuclear Fuel and Waste Management Company (SKB) is responsible for the safe handling and disposal of nuclear wastes in Sweden. This responsibility includes conducting studies into the siting of a deep repository for high-level nuclear waste. The Safety Report 1997 (SR 97) will present a comprehensive performance assessment (PA) of the long-term safety of three hypothetical repositories in Sweden. The PA of each repository will include geosphere modelling to examine the groundwater flow in the hypothetical repository and the possible transport of radionuclides from the emplaced waste packages through the host rock to the accessible environment. The hypothetical repositories, arbitrarily named Aberg, Beberg and Ceberg, take their data from sites previously investigated by SKB.

This report is one of three SR 97 reports regarding site-scale groundwater flow modelling. Walker and Gylling (1998) presents a similar study for the Aberg hypothetical repository, and Walker and Gylling (1999) presents another similar study for the Ceberg hypothetical repository.

1.2 Study Overview

This report presents the hydrogeologic modelling study of the Beberg hypothetical repository. The Beberg site adopts input parameters from the Finnsjön area in east-central Sweden, a site previously investigated by SKB. Walker et al. (1997) summarises the site characterisation studies at Finnsjön and presents several possible representations for the site hydrogeology. This study applies a nested modelling approach to Beberg, with a deterministic regional model providing boundary conditions to a site-scale stochastic continuum model. The model is run in Monte Carlo fashion to propagate the variability of the hydraulic conductivity to the advective travel paths from representative canister positions. A series of variant cases addresses uncertainties in the inference of parameters and the model of fracture zones.

The study uses HYDRASTAR, the SKB stochastic continuum (SC) groundwater modelling program, to compute the heads, Darcy velocities at each representative canister position, and the advective travel paths through the geosphere. The tasks involved in applying HYDRASTAR to Beberg include the interpretation of the hydrogeologic model into HYDRASTAR format, upscaling of parameters, simulation and sensitivity analysis, interpretation and illustration of results, and summary reporting. The report is organised into the following sections:

Sections 1 and 2 introduce SR 97 and the methods used in this study.

Section 3 describes the hydrogeologic interpretation of the Beberg data, and any adjustments to this data relative to previous reports.

Section 4 presents the Base Case simulation and examines several individual realisations and starting positions in detail.

Section 5 presents the variant case simulations.

Section 6 summarises and discusses the study results.

Appendix A defines the summary statistics.

Appendix B summarises additional regional model calculations specific to this study.

Appendix C presents supplemental calculations for rescaling, geostatistical inference and scoping calculations for travel times.

Appendix D summarises all input parameters used in this report.

Appendix E documents the data sources and data deliveries (e.g., SICADA log files for downloading the borehole data).

Appendix F summarises the additional software used in this study for statistical analysis, error checking and graphical display.

Appendix G presents the HYDRASTAR main input file used for the Base Case simulations in this study.

Appendix H documents the coordinate transforms used in this study.

The Finnsjön site also has been the subject of a previous SKB performance assessment, the SKB 91 study (SKB, 1992). That study evaluated the long-term safety of a repository at 600 m depth below ground surface in the Northern Rock Block at Finnsjön. SKB 91 was based on essentially the same site characterisation studies and used a hydrogeologic modelling approach similar to that used in this study. Where appropriate, this report compares the results of this groundwater modelling study to those of SKB 91. These comparisons may be found in Section 4.3.4, Validity of Results, and in Section 6, Summary and Conclusions.

2 Modelling Approach

This study uses a stochastic continuum model of the fractured crystalline host rocks to analyse the groundwater flow and advective flow paths. Geostatistical analysis of hydraulic test data is used to infer a model of spatial correlation for the hydraulic conductivity of the site. Geostatistical simulation is used to create hydraulic conductivity fields for a numerical groundwater flow model, which provides groundwater velocities and stream tubes (flow paths) from the hypothetical waste canisters (Neuman, 1988). The model is run in Monte Carlo fashion for a large number of simulated hydraulic conductivity fields to create an ensemble of possible stream tubes and Darcy groundwater velocities at the representative canister positions (canister fluxes). Separate reports address the subsequent use of these stream tubes and fluxes in transport and biosphere modelling.

The site-scale HYDRASTAR model requires a model domain of adequate grid density to represent the known fractures and adequate extent so that the model reflects the regional flow conditions. These conflicting requirements force this study to adopt a nested modelling approach, with the site-scale model taking its boundary conditions from a regional scale model. This permits the site-scale model to use a relatively dense grid while incorporating the regional flow patterns through constant head (Dirichlet) boundaries on the site-scale domain (Ward et al., 1987). The Base Case and several variants examine this nested approach and the resulting flow balance across the site-scale boundaries.

This study uses SKB's Convex 220 computer to run the HYDRASTAR version 1.7.2 code under a strict source code control system. Several additional SKB programs are used for pre- and post-processing of HYDRASTAR input and output. These include INFERENS, a geostatistical analysis and inference program that is used to regularise the variogram of the data to the model scale; TRAZON, which verifies the stream tube starting positions versus the fracture zones; and HYDRAVIS, a graphical post-processor developed from the commercial software package AVS. The commercial software package STATISTICA post-processes and summarises the statistics of HYDRASTAR output. These pre- and post-processing programs are summarised in Appendix F.

2.1 The PA Model Chain

The software tool for the geosphere portion of the safety analysis consists of a chain of PA models, HYDRASTAR – COMP23 – FARF31—BIO42, developed by SKB for use as a computational tool in the 1995 SKB safety analysis project (SR 95). The end product of the PA model chain is the calculation of the probable dose to the biosphere (Figure 2.1-1). This modular approach allows each component of the repository system to be studied separately, with the results combined at the finish to evaluate the performance. The hydrogeologic model, HYDRASTAR, determines the Darcy groundwater velocities at each stream tube starting position (canister flux) and the

advective travel paths through the geosphere. COMP23 is the near-field model, which uses the canister fluxes to determine the release rate for radionuclides from the representative canisters and into the groundwater flow system. FARF31 uses the release rates from the representative canisters and the travel paths through the groundwater flow system to determine the radionuclide flux through the geosphere. BIO42 is the biosphere module, which takes the radionuclide fluxes from the geosphere and determines the dose to potential receptors (SKB, 1996a). Monte Carlo simulations of the PA chain address uncertainty in the input parameters (e.g., hydraulic conductivity, porosity, etc.).

Note that this report presents only the hydrogeologic modelling study, and consequently discusses only the HYDRASTAR portion of the PA model chain.

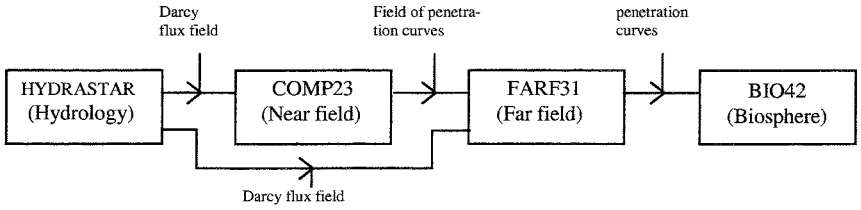

Figure 2.1-1. SKB PA model chain.

2.2 HYDRASTAR

HYDRASTAR is a stochastic groundwater flow and transport modelling program developed as a quantitative tool for support of the SKB 91 safety analysis project (SKB, 1992). A flow chart summarising the HYDRASTAR algorithm is presented in Figure 2.2-1. The current version, 1.7.2, uses the Turning Bands algorithm (Journel and Huijbregts, 1978) to generate realisations of the hydraulic conductivity field conditioned on the observed hydraulic conductivities. Trends in the data may be included implicitly through the use of ordinary kriging neighbourhoods or prescribed explicitly for specific regions. Hydraulic conductivity measurements at the borehole scale are upscaled to the model calculation scale using a regularisation scheme based on Moye's formula (a corrected arithmetic mean of the packer test hydraulic conductivities within a block; see Norman, 1992a, for details). HYDRASTAR uses the governing equation for either time-dependent or steady state groundwater flow in three dimensions, assuming constant density. The solution to this governing equation is approximated by a node-centred finite-difference method to create a linear system of equations. A pre-conditioned conjugate-gradient algorithm solves the system of equations to arrive at a solution for the hydraulic head at each node. The pilot point inverse method (de Marsily et al., 1984) can be used to calibrate the input hydraulic conductivity field to minimise the error between the simulated and observed hydraulic heads. Transport in the resulting velocity field is modelled as pure advection using a particle tracking scheme. The process of conditional geostatistical simulation of hydraulic conductivity, calibration via inverse modelling, and particle tracking can be repeated in Monte Carlo fashion to

develop empirical probability distributions for the hydraulic conductivity field, and the travel paths and arrival times for advected contaminants (SKB, 1996b).

Starprog AB developed and tested the code under contract to SKB, beginning in 1989 (Norman 1991 and 1992a). Various authors have contributed to the development and testing of the code, most notably Norman (1991 and 1992a); Morris and Cliffe (1994); Lovius and Eriksson (1993, 1994); Walker et al. (1997a); and Walker and Bergman (1998). The test problems include comparisons to well-known analytical and numerical solutions, or are taken from the HYDROCOIN series of test problems (OECD, 1983; Hodgkinson and Barker, 1985). The code also has been applied successfully to the Finnsjön site, as part of the SKB 91 Project (Norman, 1992a and SKB, 1992).

This study does not make use of all the available features in the current version of HYDRASTAR. Conditional geostatistical simulation using borehole data is not used. The Moye's formula upscaling of borehole data is only used as part of INFERENS analysis of the data to infer a variogram model. Trends in the hydraulic conductivity are included only as discrete, stepwise changes to represent fracture zones and rock units (i.e., no use of a continuous function as a model of decrease in hydraulic conductivities with depth). The calibration algorithm is not used, nor is the transient simulation of pumping tests.

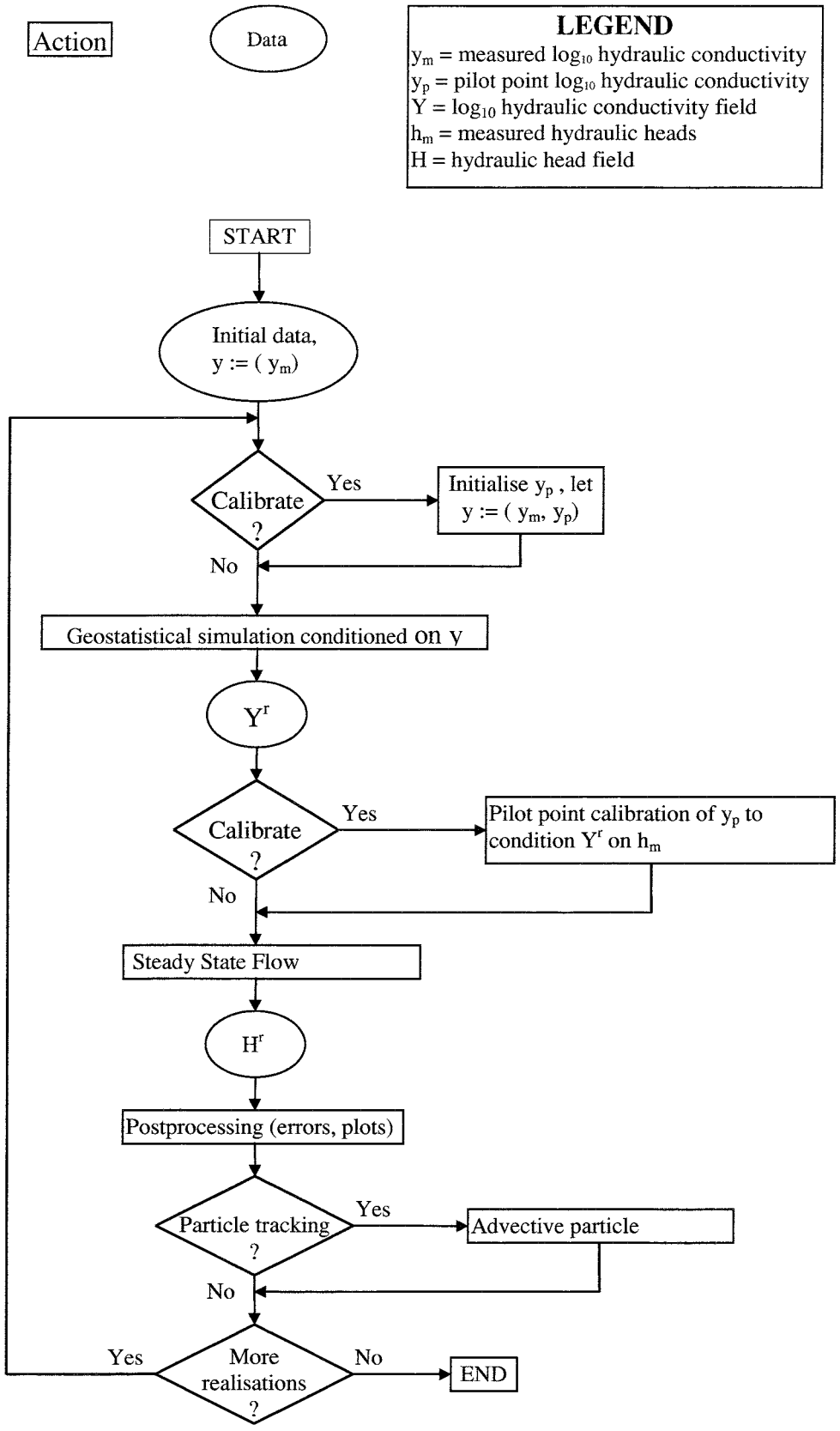

Figure 2.2-1. HYDRASTAR version 1.7 flow chart. Superscript 'r' denotes realisation.

2.3 Development of Modelled Cases

In addition to data analysis, computer simulation, and post-processing of results, the modelling process also requires that a set of relevant cases be analysed. In practice, expert judgement determines which assumptions to test and which uncertainties to evaluate. The result is a base case that represents the expected site conditions, and several variation cases that assess the uncertainty of inferences and assumptions. For this study, a separate group of scientists was convened by SKB, consisting of:

- Johan Andersson (Golder Grundteknik),
- Sven Follin (Golder Grundteknik),
- Björn Gylling (Kemakta),
- Lee Hartley (AEA),
- Jan-Olof Selroos (SKB),
- Anders Ström (SKB), and
- Douglas Walker (DE&S).

This group met during the fall of 1998 to discuss the reasoning behind the modelling assumptions, the derivation of model parameters and the modelling uncertainties. These discussions resulted in the parameters and assumptions that constitute the Base Case addressed in this report. The variant cases evolved to address questions that arose during the study.

3 Model Application

Walker et al. (1997b) summarises the hydrogeology of the site and proposes a preliminary series of parameter sets for the Base Case representing the most expected conditions and several variants to explore the uncertainties. In addition to these parameter sets, HYDRASTAR also requires a geostatistical description of the hydraulic conductivity that is appropriate for the grid scale of interest. Appendix C presents additional computations for rescaling hydraulic conductivities and the inference of additional geostatistical parameters. Where possible, input parameters describing the repository layout, structural model, hydraulic conductivities, etc. are taken directly from SICADA or the authors of the respective reports (See Appendices D and E).

The site-scale HYDRASTAR model also requires a model domain of adequate extent and boundary conditions that reflect the regional flow conditions. The extent of the model domain was evaluated as part of preliminary modelling studies (Gylling et al., 1999). This modelling study uses a nested modelling approach, taking the boundary conditions of the site-scale model from a much larger regional scale model. Appendix B summarises the specific regional model simulations used to generate the boundary conditions for the local scale model.

The following sections describe the application of HYDRASTAR to the Beberg site, including the hydrogeologic conditions and modelling assumptions.

3.1 Site Description

Beberg takes its data from the Finnsjön site, which is located in east-central Sweden, in the northern part of Uppland (Figure 3.1-1). It is approximately 13 km inland from the Baltic Sea in an area corresponding to LMV map sheets Östhammar 12I SV, Östhammar 12I NO and Österlövsta 13I SV. Forsmark, the SKB Final Repository for Radioactive Operational Waste (SFR), is situated 15 km northeast of the Finnsjön site, and the Dannemora Mine is 17 km south of the site. From a hydrogeologic perspective, northern Uppland is notable for the occurrence of saline groundwater at relatively shallow depths and for the presence of relatively shallow, subhorizontal conductive fracture zones.

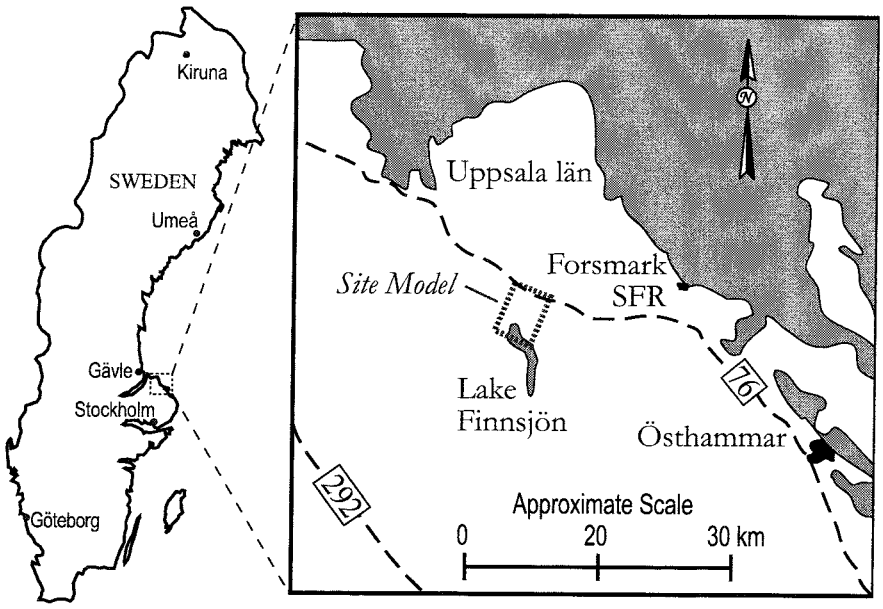

Figure 3.1-1. Location of the Finnsjön site. Dashed lines represent roads.

3.2 Hydrogeology

The geology and hydrogeology of the Finnsjön site have been studied in detail and are summarised in a series of reports (Ahlbom & Tirén, 1991; Andersson et al., 1991; Ahlbom et al., 1992; Stålhös, 1988). Walker et al. (1997) presents a summary of site conditions emphasising continuum modelling.

The ground surface of the Finnsjön region has little relief and is characterised by flat rock outcrops, lakes, bogs and mires. The average elevation is 30 masl, and varies ± 30 m. The regional geology is dominated by coarse-grained granitoids and fine-grained leptites of about 2 billion years of age. The region continues to experience isostatic rebound as a consequence of the last period of continental glaciation, currently at a rate of 5.7 mm/yr. The soil cover is rather thin with numerous bedrock outcrops. The Quaternary deposits are dominated by glacial till. Depressions are mostly occupied by mires and peat bogs. Sand, gravel and glacial clay occur only sparsely. Lineaments in northern Uppland have been interpreted from topographic maps at a scale of 1:250,000. At least two sets of lineaments are present, one trending north to northeast and the other trending northwest. Saline groundwater is common in shallow wells in northeastern Uppland, both near the Baltic Sea and inland.

Carlson and Gidlund (1983) summarised the hydrology of the Finnsjön area, suggesting that precipitation generally exceeds evapotranspiration, resulting in a small net recharge on the land surface. The classical model of topographic drive suggests that recharge will occur in higher elevations near Lake Finnsjön and flow to discharge areas in lower elevations to the northeast. Studies associated with SKB 91 (e.g., Andersson et al., 1991) demonstrated that this general model is consistent with the locations of streams,

mires, observed hydraulic heads, salinity distributions and geochemical data available in the region.

Two characteristics of this region have been widely studied because of their interaction and implications for the long-term safety of a deep repository. One of these characteristics is the presence of subhorizontal fracture zones found in several locations in the region. SKB site characterisation studies revealed one such subhorizontal zone, Zone 2, within the Northern Block of the Finnsjön site. SKB 91 modelling studies indicated that Zone 2 strongly influences groundwater flow, salinity distributions, and consequently the performance of a repository situated under such a zone (Andersson et al, 1991; Lindbom et al., 1991; SKB, 1992). The other notable characteristic of the regional hydrogeology is the occurrence of saline groundwater at relatively shallow depths. This is particularly striking at the Finnsjön site, where the groundwater changes from essentially freshwater above Zone 2 to saline water within and below Zone 2. Shallow saline groundwater is thought to be a consequence of the cycle of depression, innundation and uplift associated with the last period of continental glaciation in this region. Hartley et al. (1998) found that the present-day salinity of Zone 2 can be explained by the slow replacement of relic saline water by modern precipitation, the high conductivity of Zone 2 and a weak hydraulic connection between the subvertical and subhorizontal fracture zones.

3.3 Regional Model and Boundary Conditions

This application of HYDRASTAR uses a nested modelling approach, taking the boundary conditions of the site-scale model from a much larger regional scale model. Hartley et al. (1998) used a salinity-dependent finite element continuum model, NAMMU, to study regional flow patterns under the combined effects of landrise, salinity, freshwater recharge and fracture zone connectivity. The Hartley et al. (1998) model is the basis of the regional flow modelling used by this study to determine boundary conditions for HYDRASTAR. Figure 3.3-1 shows the extent and location of both the regional and site-scale modelling domains.

The model of Hartley et al. (1998) included salinity dependence to investigate the origin and effects of relic saline water observed under Zone 2 in the Northern Rock Block. Hartley et al. (1998) found that the present-day salinity at the site is a transient phenomenon, slowly evolving toward freshwater conditions. The time required to flush salt from the upper levels of the site is highly sensitive to reasonable variations in porosities, but appears to be on the order of a few thousand years. This creates a dilemma for modelling groundwater flow at the site: should the site be modelled for present–day salinities and heads, or for the long-term freshwater conditions? For this modelling study, the choice is limited since HYDRASTAR cannot simulate the density dependent effects of saline groundwater. This study consequently modifies the Hartley et al. (1998) regional model, running a supplemental simulation of the regional model case AltK with freshwater to create the Base Case boundary conditions (Appendix B). Figure 3.3-2 shows the steady-state head values, which are used as Dirichlet (constant head) boundary conditions for the Base Case site-scale model.

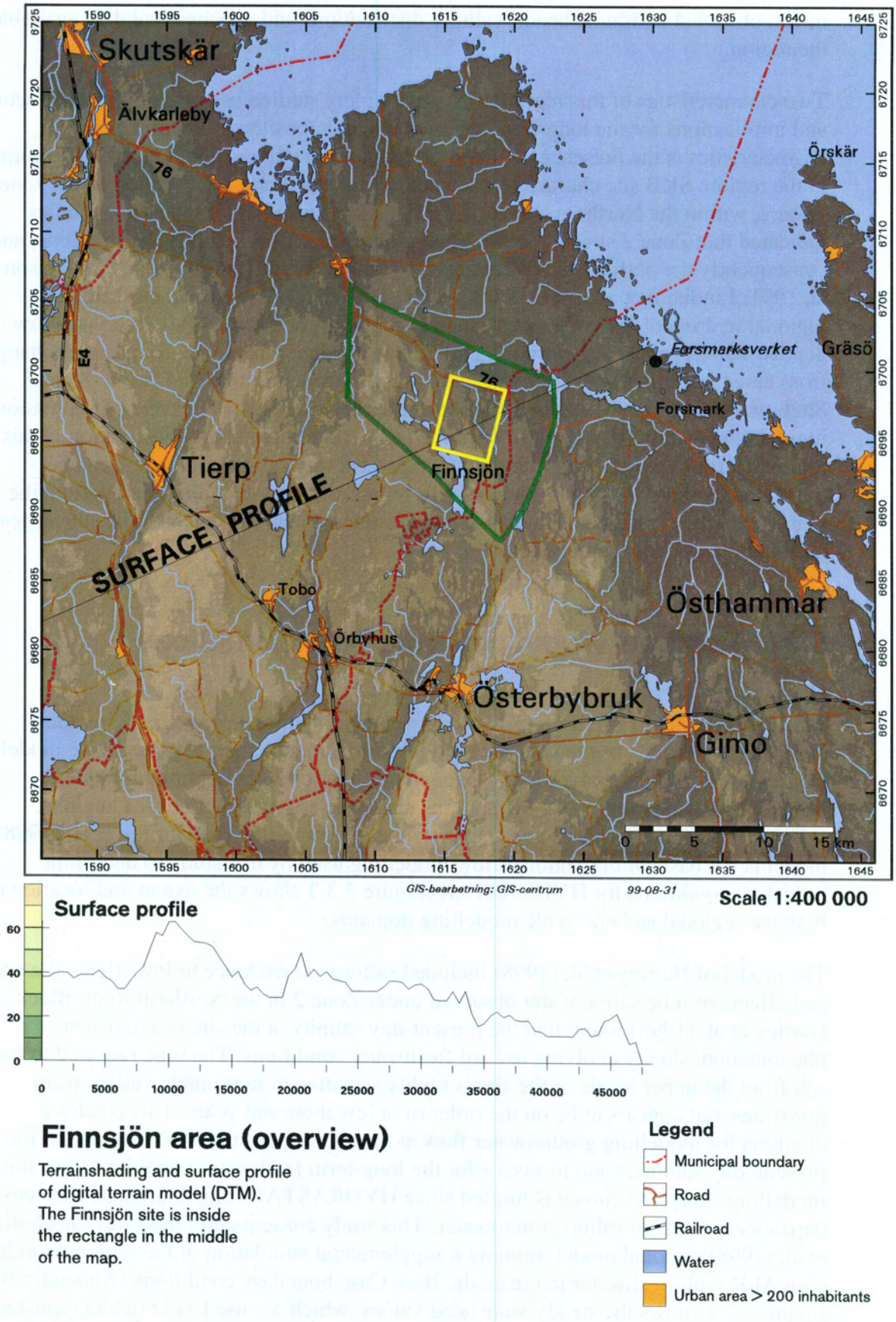

Figure 3.3-1. Finnsjön site map, showing Hartley et al. (1998) regional model and the site-scale model domains (RAK coordinate system)

It is reasonable to evaluate the uncertainties associated with the assumption of freshwater conditions, since this might result in inappropriate heads being specified along the site model domain. This uncertainty is examined by Variant 1, where the Hartley et al. (1998) regional model case AltK generates pressures and salinities along the site-scale model boundaries. The resulting pressures are then converted to environmental heads for use as boundary conditions for the site scale HYDRASTAR model (Appendix B.2). Another supplementary simulation of the Hartley et al. (1998) regional model determined boundary conditions Variant 2 (alternative conductors). The supplemental simulations for the Base Case and Variant 2 of this study were not reported in Hartley et al. (1998), but are documented in Appendix B.

It is important to note that the Base Case of this site-scale modelling study is not the same as the regional base case of Hartley et al. (1998). The Base Case of this study is essentially the AltK case of Hartely et al. (1998), run with freshwater conditions and additional site-scale detail. Variant 3 of this study is essentially the regional base case of Hartley et al. (1998), with additional site-scale detail.

The regional model head values described in Appendix B and pictured in Figure 3.3-2 require some adaptation for use in the smaller scale HYDRASTAR model. The heads predicted by the regional model along the boundaries of the site-scale model domain are used as Dirichlet (constant-head) boundary conditions for the site-scale model. The regional NAMMU model generates the head values using finite element basis functions to interpolate as necessary between the NAMMU nodes for the HYDRASTAR grid spacing of 35 m. A HYDRASTAR subroutine reads the interpolated heads and uses them as boundary conditions for the HYDRASTAR model domain. Although this approach is similar to that used in other nested groundwater models (e.g., Ward et al., 1987; Leake et al., 1998), it is also important to verify that the volumetric flow of water across the boundary is the same (i.e., conservation of mass). The consistency of the boundary flows and the mass balance calculations are discussed further in Section 4.2 and Appendix B.6.

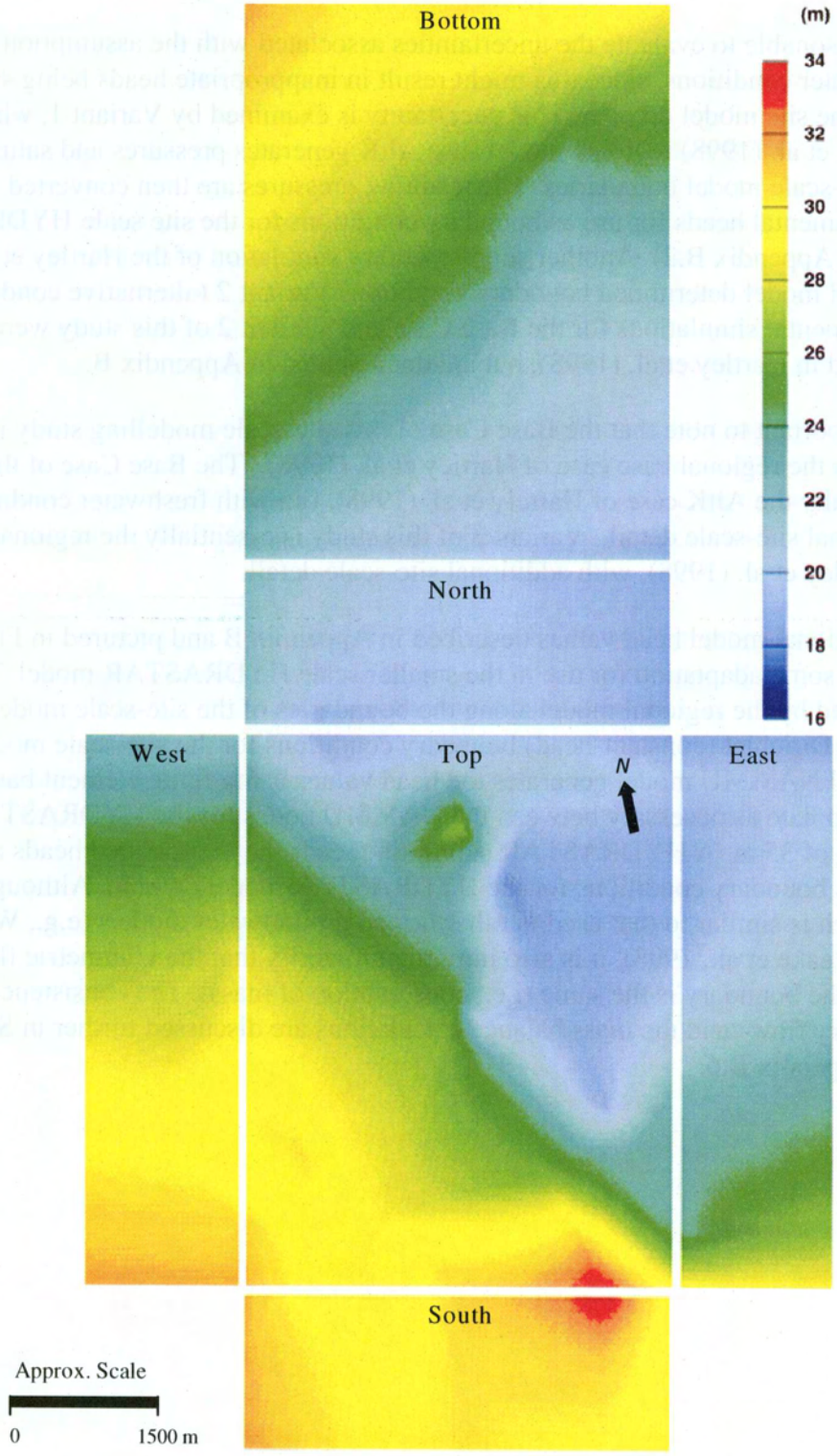

Figure 3.3-2. Constant head boundary conditions for the Beberg Base Case on each face of the model domain (freshwater hydraulic head, in metres).

3.4 Model Grid and Repository Layout

The HYDRASTAR model for this application consists of a 3-dimensional finite difference grid with a uniform grid spacing of 35 m. Preliminary modelling studies by SKB (1992), Gylling et al. (1999), and Hartley et al. (1998) determined a domain location and extent such that a minimum of particle paths would be intercepted by lateral boundaries. Figure 3.4-1 shows the location of the modelled domain, which covers an area of 4130 m by 5355 m and extends to a depth of 1505 m. The modelling domain extends slightly less farther northward than that specified for the SKB 91 modelling study (SKB, 1992). The resulting grid of $119 \times 154 \times 44$ nodes (width, length and depth, respectively) gives a typical size for HYDRASTAR models that can be run on the SKB CONVEX within the project schedule and computer resources.

The performance assessment measures are based on distributions of canister flux, travel paths, and travel times to exit locations in the accessible environment (i.e., ground surface). Ideally, the model grid upper surface would correspond to the ground surface. This is not possible in this study because HYDRASTAR uses a flat plane for the upper model surface. Consequently, the observed ground surface is represented as a horisontal plane with the modelled domain lying below the minimum ground surface elevation (approximately 0 masl). The HYDRASTAR particle tracking algorithm requires a minimum distance of one grid spacing from any model boundary to calculate the velocity vectors, and thus the exit location for these simulations is -35 masl. That is, the performance assessment measures are based on exit locations on a horisontal plane at -35 masl.

Figure 3.4-1 also shows the hypothetical repository tunnel layout, a single-level design specified by Munier et al. (1997, recommended tunnel design). The tunnels of this repository design lie at an elevation of -600 masl, oriented perpendicular to the principal regional stress. The design avoids mapped fracture zones, allowing an exclusion zone whose width depends on the fracture zones' classification. The tunnels are placed no closer than 100 m to zones that are classified as certain (e.g., Zone 1), and no closer than 50 m to those classified as probable (eg., Zone 4). No zones are designated as possible, although some authors have speculated that additional subhorizontal and subvertical zones are possible at the site (Ahlbom and Tirén, 1991; Andersson et al., 1991; Saksa and Nummela, 1998). These zones are discussed in Section 5.2. This study represents the hypothetical waste canisters with 120 locations uniformly scattered over the repository tunnels (Figure 3.4-2). HYDRASTAR uses these 120 representative locations as starting positions for the stream tubes and the subsequent travel time, canister flux and F-ratio calculations.

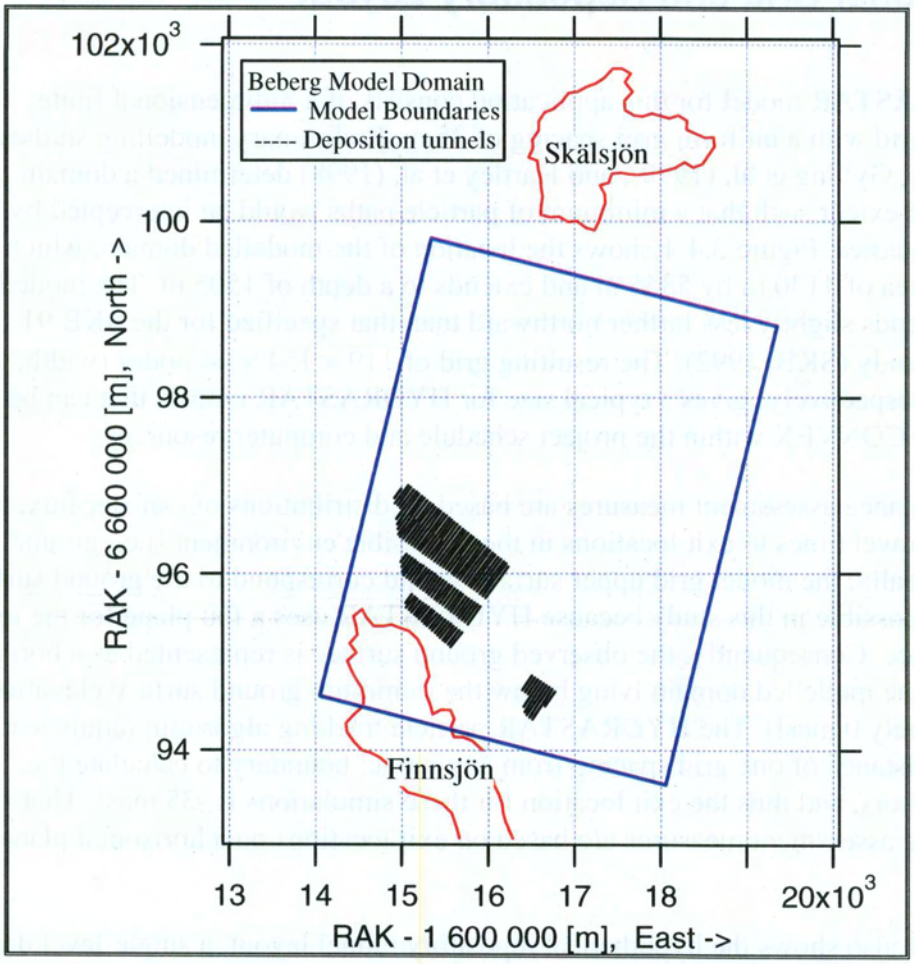

Figure 3.4-1. Beberg site-scale model domain (blue line). Tunnels of the hypothetical repository at -600 masl are shown projected to ground surface (plan view, offset RAK coordinates in metres).

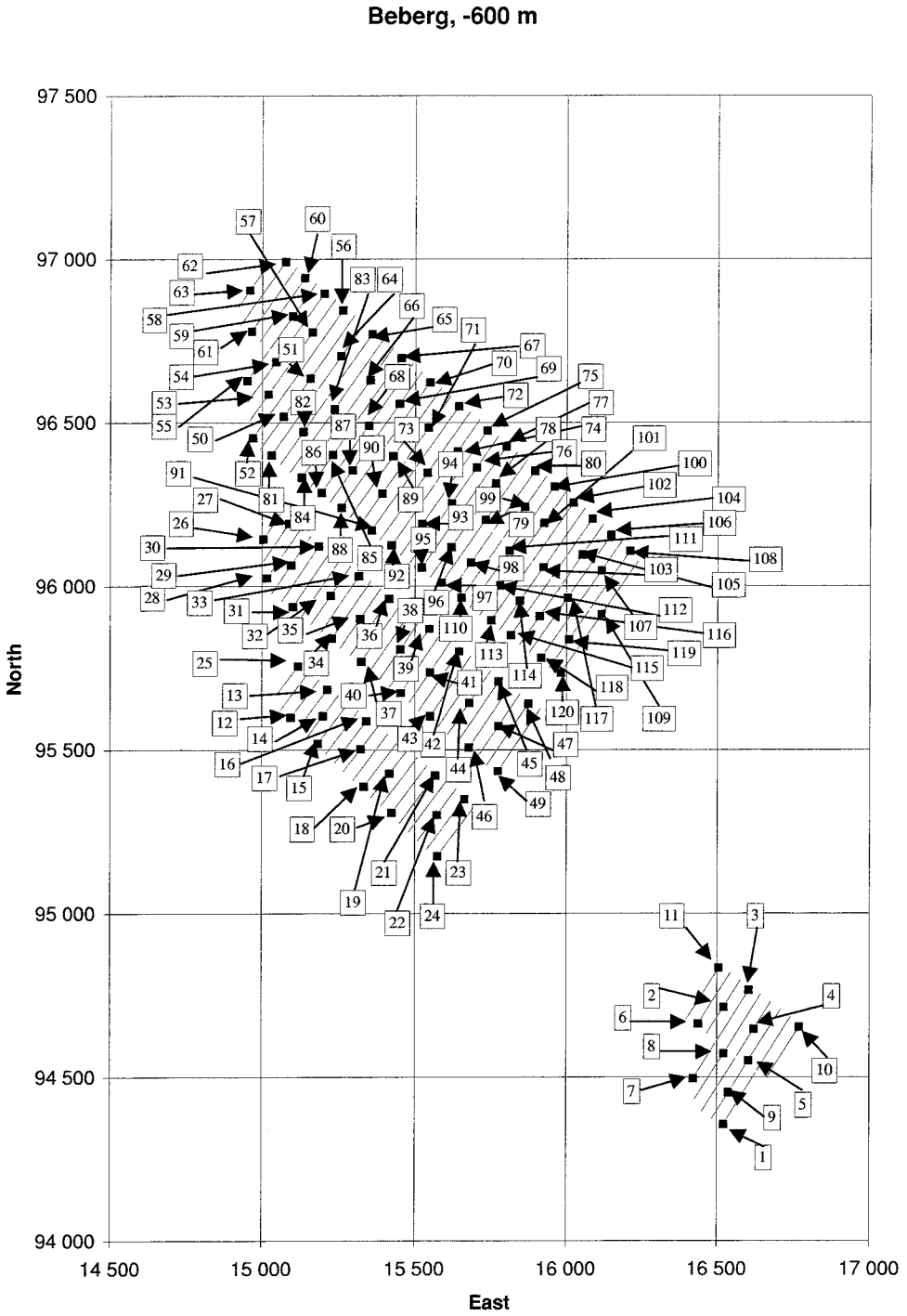

Figure 3.4-2. Beberg hypothetical repository tunnel layout at -600 masl. Numbered locations are 120 stream tube starting locations as representative canister positions (plan view, offset RAK coordinates, in metres).

3.5 Input Parameters

HYDRASTAR's input parameters require a structural, hydraulic, and geostatistical description of the site, all at an appropriate scale. This study uses the site-scale description based on hydrogeologic information found in Anderson et al. (1991) and Walker et al. (1997). The site investigations identified a number of relatively conductive fracture zones between 5 to 100 m in width. Studies associated with the characterisation of Zone 2 suggested that the fractured zones and their interconnections can be very complex. Most important is that, while the fracture zones can be highly conductive in the plane of the fracture, they can have very low hydraulic conductivity perpendicular to the plane of the fracture. Thus the assumption that the fracture zones are uniformly conductive features is uncertain at Beberg (Anderson et al., 1991). Fractures elsewhere in the site (i.e., those not included in the deterministic zones) are collectively included in the hydraulic conductivity estimates for the rock mass. Consequently, the hydraulic conductivity data is divided into two populations based on the site structural model (Walker et al., 1997b):

- Rock Domain (RD) – relatively unfractured rocks outside the deterministic conductors. On the site-scale, this is denoted SRD.

- Conductor Domain (CD) – rocks within the deterministic conductors. On the site-scale, the set of conductors is collectively referred to as SCD.

The principal source of hydraulic conductivity data is the injection and pumping tests performed in the cored boreholes (Figure 3.5-1). These tests were interpreted and the measurements reported for various depths, rock types, etc. as described by Anderson et al. (1991) and Walker et al. (1997). The interpreted hydraulic conductivities for the 3 m packer tests were taken directly from the SKB SICADA database and analysed with the SKB geostatistical inference code INFERENS.

One important conclusion of the Hartley et al. (1998) regional modelling study was that the preliminary base case parameters provided in Walker et al. (1997) could not reproduce the salinity distribution in the Northern Block. Specifically, Hartley et al. (1998) found that vertical fractures with constant hydrualic conductivities created a strong hydraulic connection from the surface to great depth, rapidly flushing saline water from below Zone 2. This kept RCD1, the preliminary representation of no depth dependence inferred from the interpreted hydraulic conductivities proposed by Walker et al. (1997), from reproducing the observed high salinity levels in and below Zone 2. This led Hartley et al. (1998) to a revised representation of hydraulic conductivity for the fracture zones in the regional model, case AltK, that included depth-dependent hydraulic conductivity in the fracture zones (Appendix C.1). The regional model case was able to reproduce the present-day salinity distribution, and consequently this study assumes a similar representation of depth-dependent hydraulic conductivity of the SCD for the site-scale Base Case. This model of the SCD is uncertain, and is evaluated by an alternative hydrogeologic interpretation in Variant 3 of this study (Section 5.3).

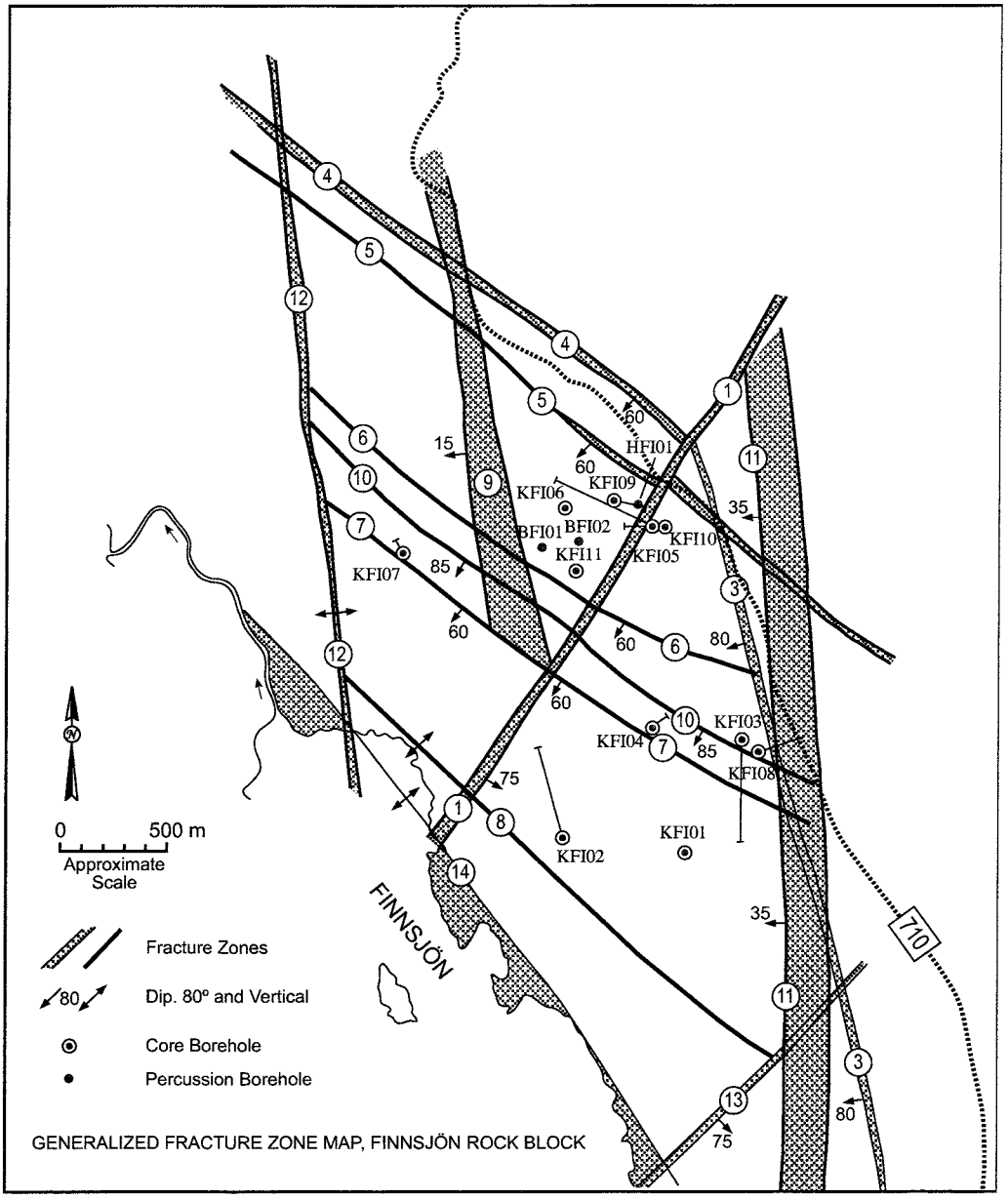

Figure 3.5-1. Finnsjön site and SKB boreholes, after Ahlbom and Tirén (1991).

The scale of the intrepreted hydraulic conductivitiy measurements (as inferred from the packer length) is much different from the proposed model grid scale. As discussed in Walker et al. (1997), hydraulic conductivity is a scale-dependent parameter, which requires that the measured hydraulic conductivities be upscaled to the finite difference grid scale of the model. This study uses the upscaling approach described in Appendix C.2. The following sections present both the geometric means of the test-scale and model-scale hydraulic conductivities for the conductor domain and the rock domain.

3.5.1 Site-Scale Conductor Domain (SCD)

The geometries of the hydraulic conductor domains are defined by the major discontinuities described in Andersson et al. (1991) and represented as planar features of constant width (Figure 3.5-2). The resulting values are provided below in Table 3.5-1. SCD represents the mapped fracture zones as hydraulically conductive features, with the locations and orientations as given in Andersson et al. (1991). Hydraulic conductivities of SCD are based on the 3 m packer test data corresponding to conductive fracture zones identified by Anderson et al. (1991, Table 4.3-2). As described in Section 1.6, the SCD geometric means are upscaled from 3 m to 35 m using the Äspö regression relationships (Appendix C). The hydraulic conductivity of Zone 2 is inferred from the interference test results presented in Andersson et al. (1991). This study assumes that the measurement scale of the interference tests in Zone 2 is approximately 100 m, and correspondingly downscales the reported values to the finite difference block scale of 35 m using the Äspö scale relationships. Table 3.5-1 presents the interpreted and upscaled hydraulic conductivities that are used in the Base Case representation for hydraulic conductors (SCD) at Beberg.

It should be noted that several of the fracture zones have hydraulic conductivities approximately equal to the rock mass (e.g., zones 6, 9 and 10; see Table 3-6). Because these low conductivity zones will behave approximately the same as the rock mass and might interrupt important conductors (e.g., zone 11), they are omitted from the SCD set for the Base Case simulations. The repository layout of Munier et al. (1997) avoids these zones, however, since they may represent structural weakness in the host rock. Variant 2 evaluates the uncertainty of omitted zones 6, 9 and 10, along with other possible fracture zones (Section 5.2).

Table 3.5-1. Site-scale conductor domain (SCD) properties for the Beberg Base Case, inferred from 3 m tests, upscaled to 35 m. Below –100 masl, K is reduced by a factor of 12.3 (i.e., [$Log_{10}K$ below -100 masl] = [$Log_{10}K$ above -100 masl] - 1.09).

Zone	Width	Median Log_{10} K (m/s)	
		3 m	35 m
1*	20	-5.66	-4.68
2	100	-4.50**	-4.86
3	50	-6.82	-5.99
4	10	-6.35	-4.26
5	5	-6.35	-4.26
6***	5	-8.39	-6.56
7	5	-7.39	-5.30
8	5	-7.39	-5.30
9***	50	-7.94	-7.10
10***	5	-8.34	-7.51
11	100	-7.22	-6.38
12	25	-6.10	-5.27
13	20	-5.66	-4.68
14	100	-6.10	-5.27

* also known as the Brändan fracture zone
** interference test value, assumed scale of 100 m. Zone 2 assumes no depth dependence in this representation. Value given is for <-100 masl.
*** omitted from the Base Case SCD.

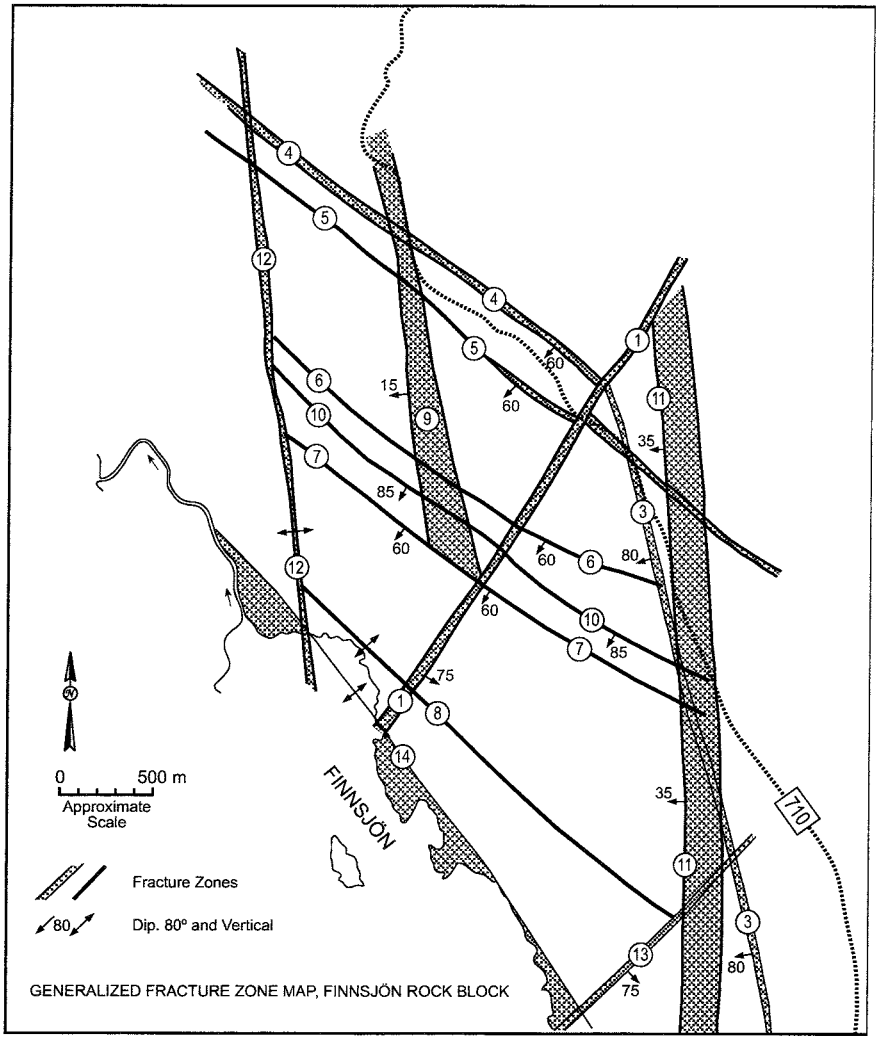

Figure 3.5-2. Beberg site-scale conductor domains (SCD), after Ahlbom and Tirén (1991).

3.5.2 Site-Scale Rock Domain (SRD)

Based on observations during the site investigations, the Finnsjön site is divided into Northern and Southern Rock Blocks by Zone 1 (the Brändan zone; see Walker et al., 1997; see also Figure 3.5-3 in this report). The geometric mean hydraulic conductivities for these rock blocks are based on the interpreted hydraulic conductivities of the 3 m packer tests. The areas outside the rock blocks that define the Finnsjön site are assigned the geometric mean of the SGU well data (i.e, slightly lower than the hydraulic conductivity than the Southern Rock Block, similar to Axelson et al., 1991). As with the conductor domains, these values must be rescaled to the 35 m finite difference grid scale, as presented in Table 3.5-2. The apparent depth dependence of conductivities is addressed by a uniform step decrease in conductivity below -100 masl by a factor of approximately 10. Variant 3 addresses the uncertainties associated with this representation of the spatial distribution of hydraulic conductivities.

Table 3.5-2. Site-scale rock mass domain (SRD) for Beberg Base Case, inferred from 3 m test data. Below –100 masl, K is reduced by a factor of 12.3 (i.e., [Log_{10}K below –100 masl] = [Log_{10}K above - 100 masl] -1.09).

SRD	Arithmetic Mean Log_{10} K (m/s)	
	3 m	35 m
SRD North	-7.35	-6.42
SRD South	-7.51	-6.78
SRD other	-6.95 *	-7.16

* SGU data arithmetic mean log_{10} K at approximately 67 m scale

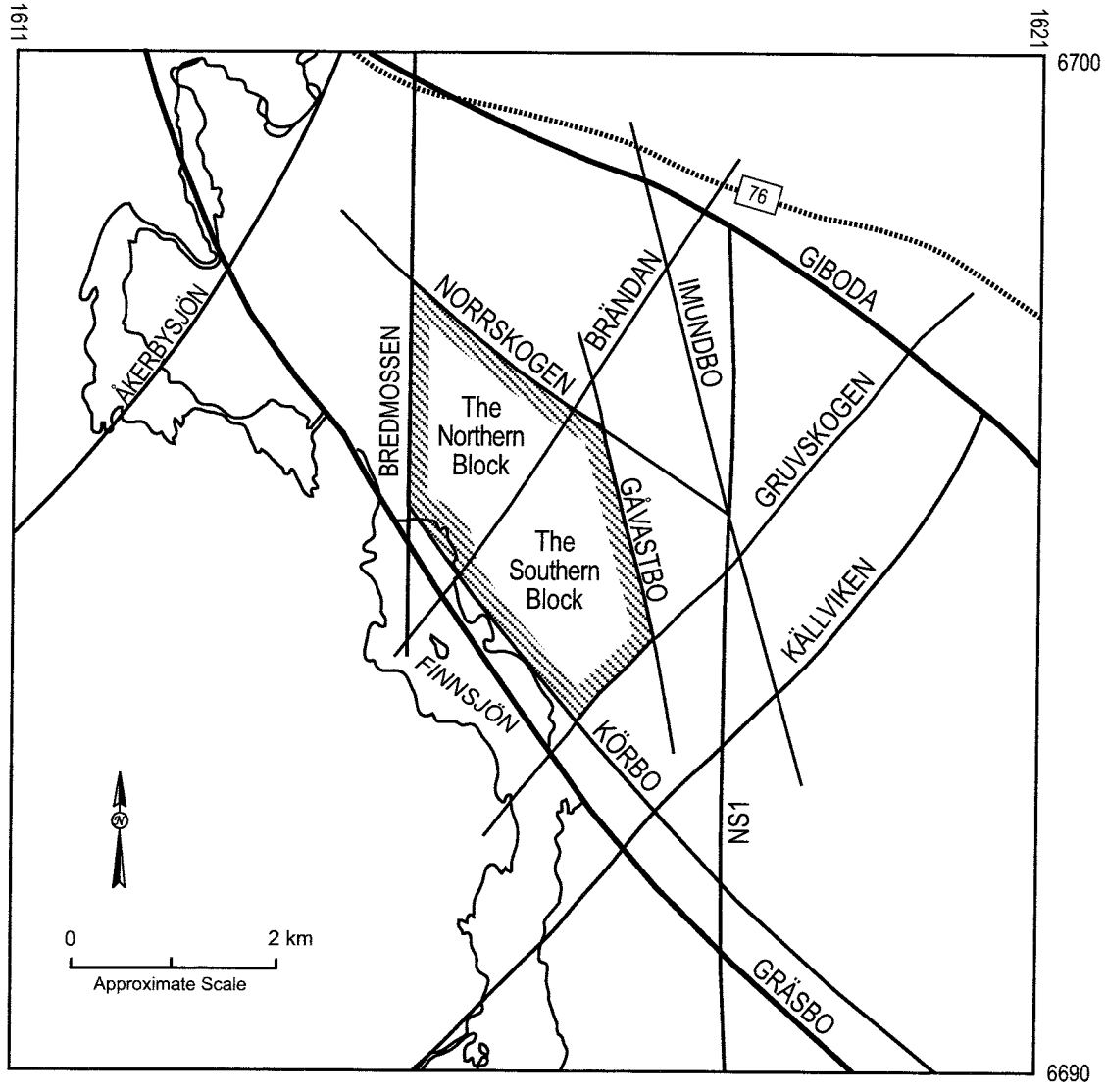

Figure 3.5-3. Beberg site-scale rock domains (SRD), after Andersson et al. (1991).

3.5.3 Geostatistical Model

The Beberg site-scale geostatistical model of hydraulic conductivity consists of the rock blocks described for SRD, SCD and a single variogram model. It is essentially the AltK case of the regional model, rescaled to 35 m. As is discussed in Walker et al. (1997), the variogram must be adjusted (regularised) to account for the difference between measurement and grid scales. Note that only one variogram model can be specified in HYDRASTAR for both domains. Consequently, this study infers a regularised variogram model based on the upscaled 3 m packer test data in the rock domain for both SRD and SCD (Walker et al., 1997). The interpreted conductivities are taken from cored boreholes KFI03 through KFI08, as found in SICADA. The SKB code INFERENS was used to upscale the 3 m data to 35 m and fit a model variogram to the rock mass data (Appendix C.2). Results of this analysis indicated the following variogram model for the hydraulic conductivity at a 35 m grid scale (Figure 3.5-4):

- Exponential model, isotropic;
- Practical range of 247 m; and
- Zero nugget, Log_{10} variance 0.69.

The rock blocks (SRD) and conductors (SCD) are treated as step changes in the mean of the logarithm of block conductivities (0 order trends in $Log_{10} K_b$), with values provided in Tables 3.5-1 and 3.5-2. Figures 3.5-5 and 3.5-6 show the HYDRASTAR representation of the SCD, and Figures 3.5-7 and 3.5-8 show the combination of the SCD and SRD via plots of the deterministic $Log_{10} K$ field. The combined effects of this geostatistical model of Beberg are illustrated in Figure 3.5-9, which presents a single realisation of the Base Case hydraulic conductivity field.

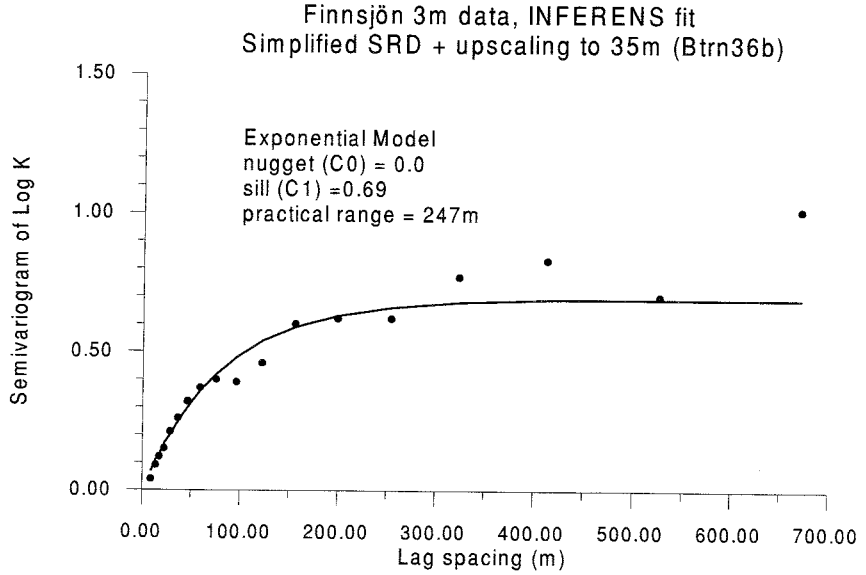

Figure 3.5-4. Semivariogram of log_{10} hydraulic conductivity for Beberg rock domain, based on 3 m test data in rock domain, upscaled to 35 m and fitted via INFERENS.

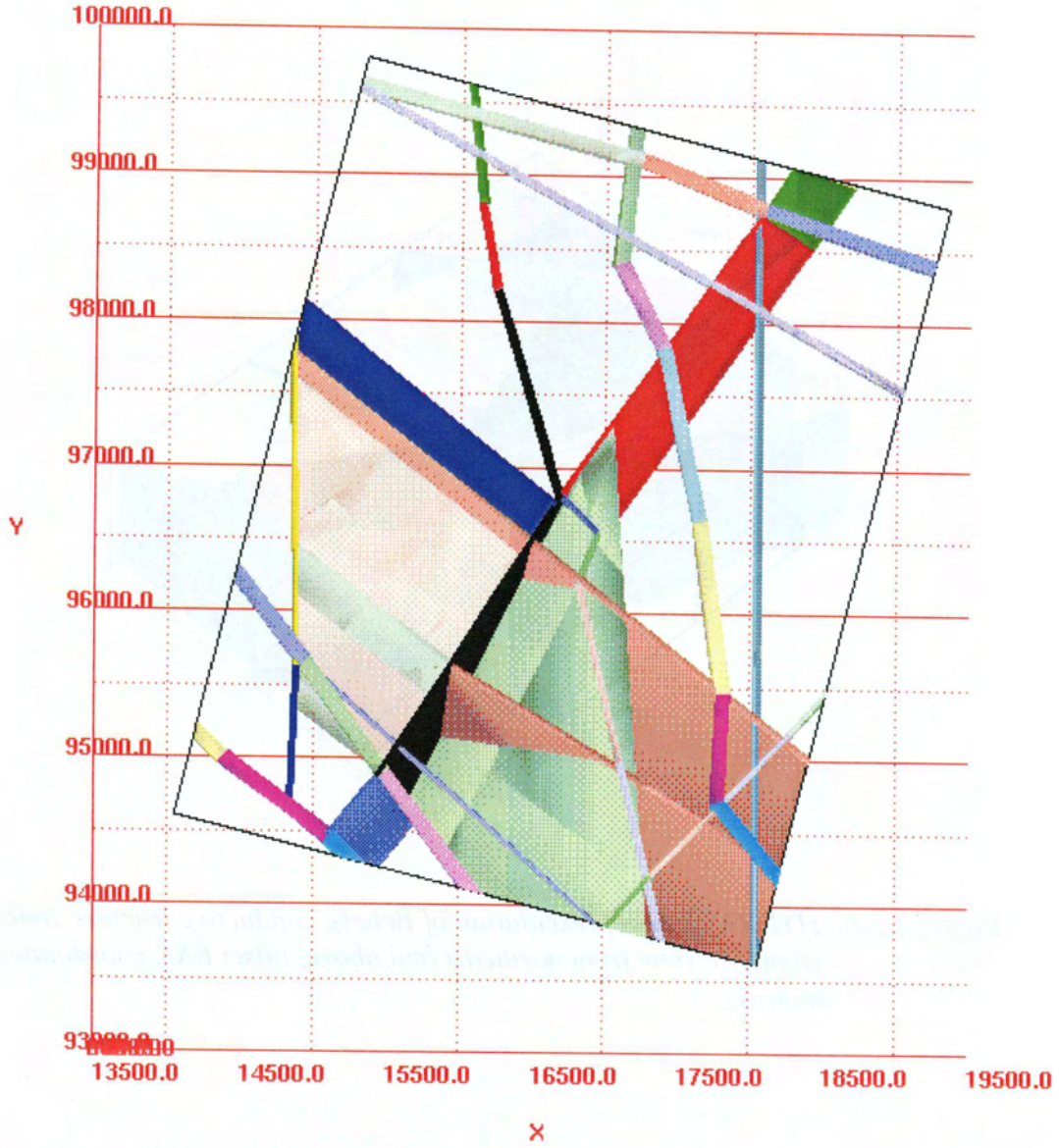

Figure 3.5-5. HYDRASTAR representation of Beberg conductor fracture zones (SCD, in plan view, offset RAK coordinates in metres).

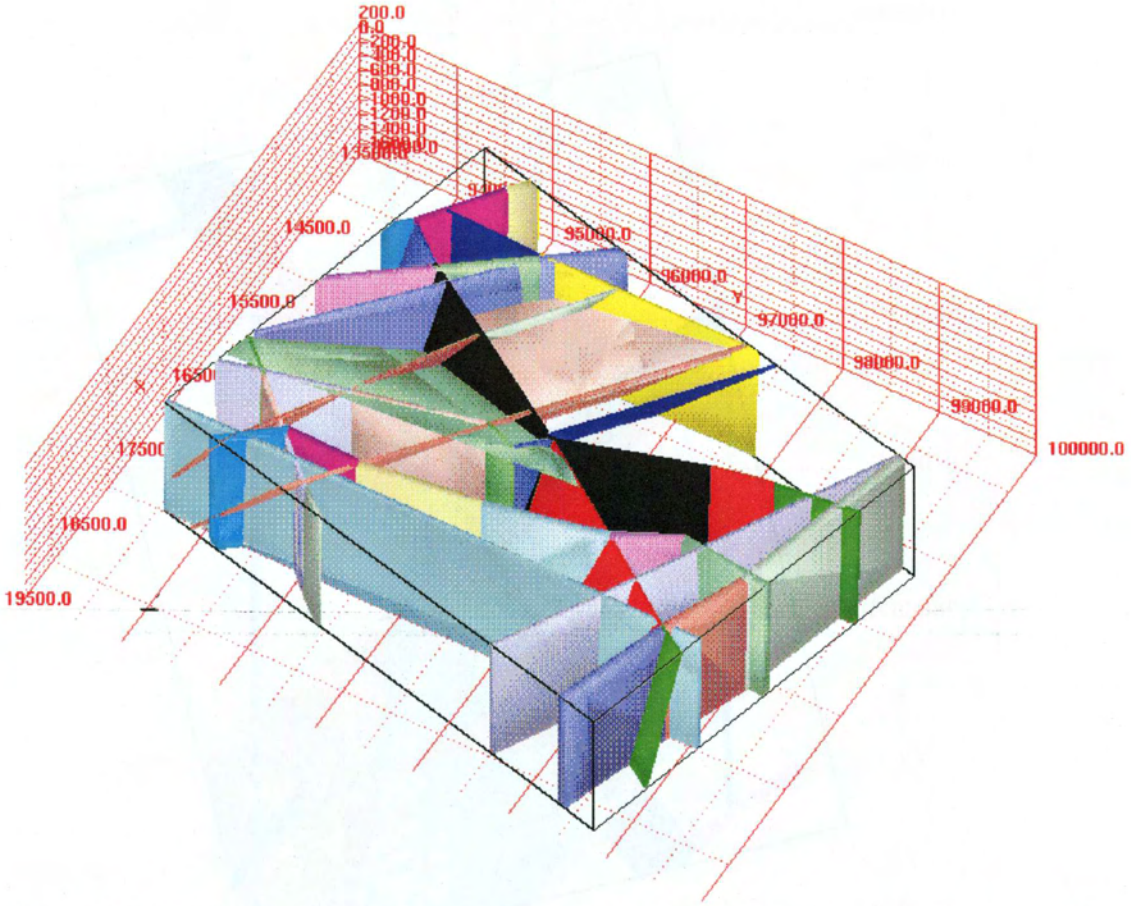

Figure 3.5-6. HYDRASTAR representation of Beberg conductive fracture zones (SCD, isometric view from northeast and above, offset RAK coordinates in metres).

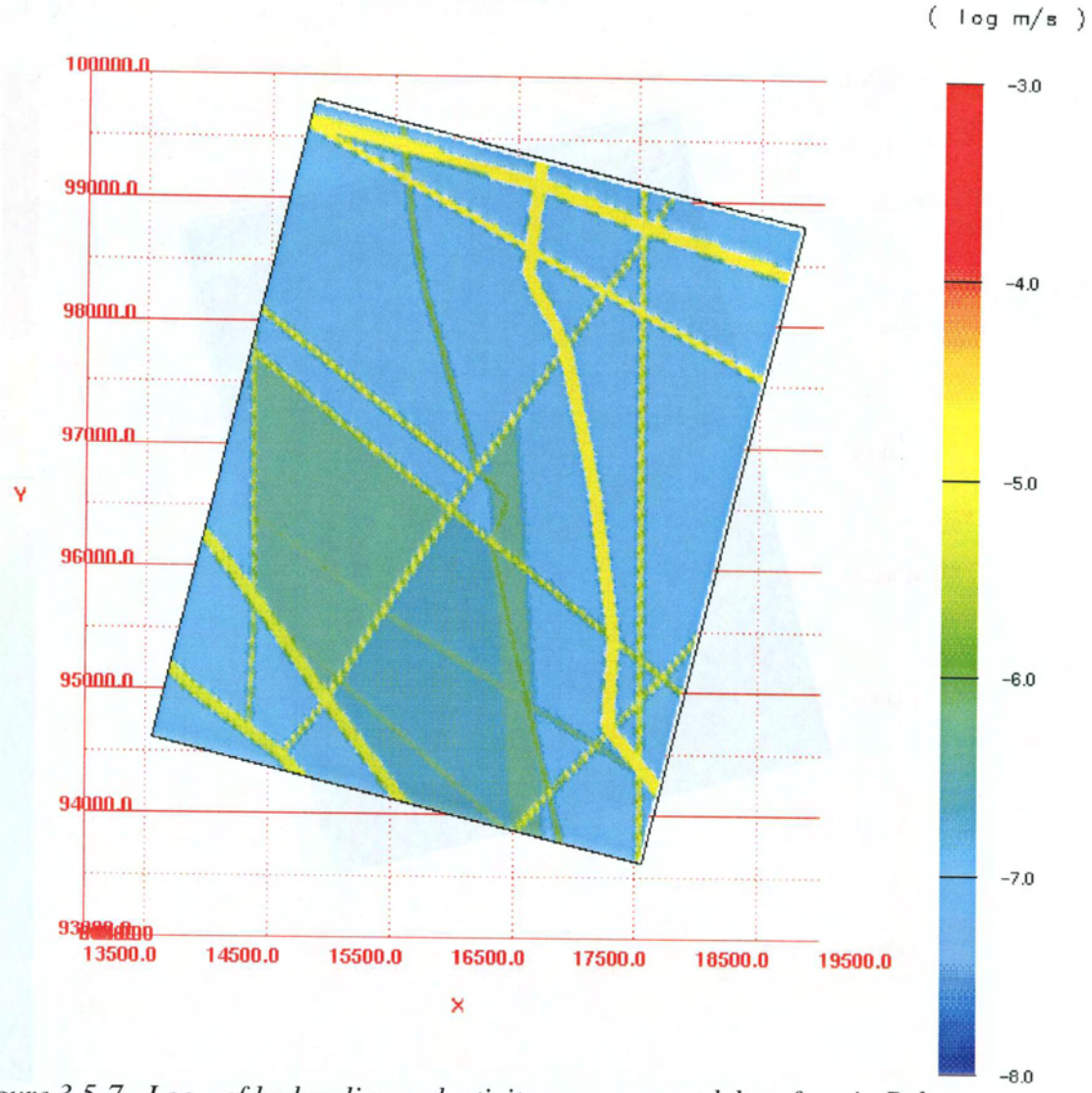

Figure 3.5-7. Log_{10} of hydraulic conductivity on upper model surface in Beberg Variant 4 (deterministic representation of hydraulic conductivity, offset RAK coordinates in metres).

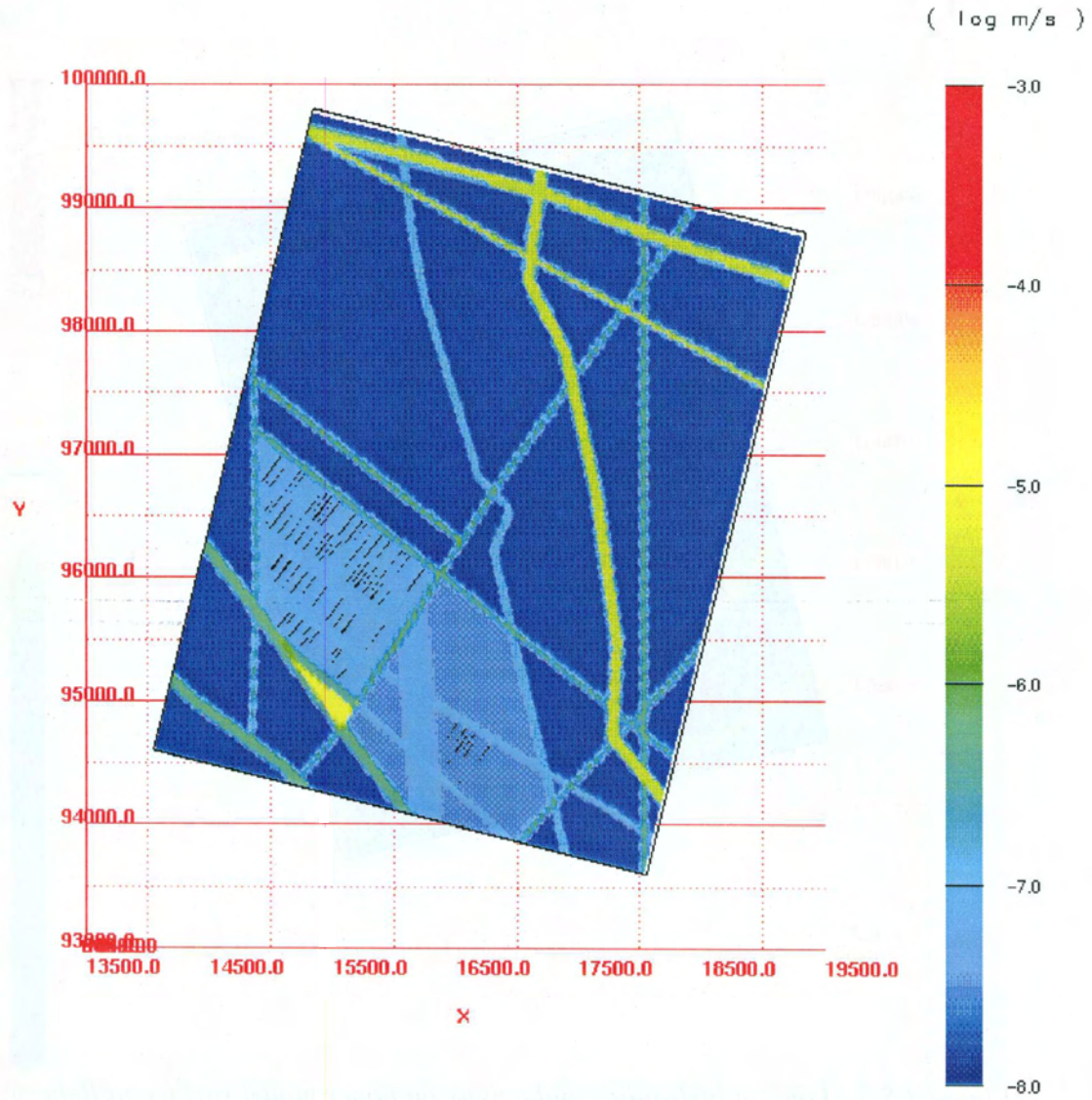

Figure 3.5-8. Log_{10} of hydraulic conductivity on a plane cutting through repository level in Beberg Variant 4 (deterministic representation of hydraulic conductivity, offset RAK coordinates in metres).

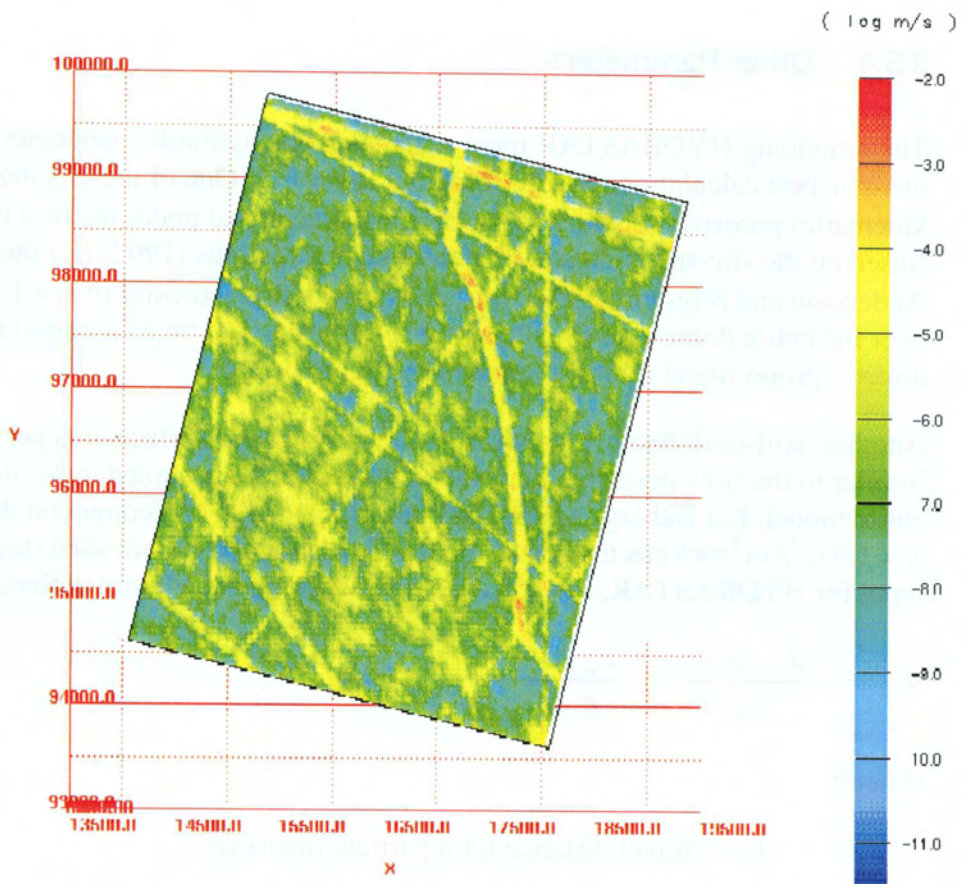

a)

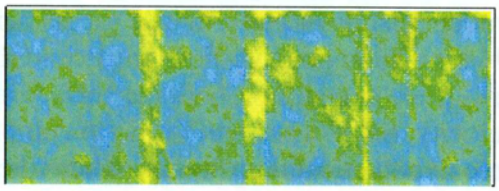

b)

Figure 3.5-9. One realisation of Log$_{10}$ of hydraulic conductivity for the Beberg Base Case in a) plan view on the upper model surface and b) elevation view on the southern model surface (offset RAK coordinates in metres).

3.5.4 Other Parameters

The remaining HYDRASTAR input parameters are hydraulic parameters required for the transport calculations and performance measures. One of these is the flow (or kinematic) porosity, ε_f, which is not easily characterised under the best of conditions. Based on the site-specific data of Brandberg and Skagius (1992) and the study of Andersson and Stigsson (1999), this study uses a flow porosity of $\varepsilon_f = 1 \times 10^{-4}$, uniform over the entire domain. It should be noted that the travel times reported in this study are directly proportional to this assumed flow porosity.

Another hard-to-define parameter is a_r, the flow-wetted surface area per rock volume. Similar to the flow porosity, the flow-wetted surface is assumed to be uniform over the entire model. For Beberg, Andersson and Stigsson (1999) recommend the value $a_r = 1.0\ m^2/(m^3\ rock)$ as the best estimate. This parameter is not used directly as model input for HYDRASTAR, but it is used in calculating the F-ratio, defined as:

$$F = \frac{d_w a_r}{q_w} = \frac{t_w a_r}{\varepsilon_f}$$

Where:

d_w = travel distance for a particle [metres];

q_w = Darcy velocity = $v \cdot \varepsilon_f$ [metres/year];

a_r = specific surface per rock volume for a travel path [m^{-1}]; and

ε_f = flow (kinematic) porosity [.].

The F-ratio [years/m] is a ratio of resisting to driving forces for transport, which has been used to compare model results in performance assessments (SKI, 1997). The F-ratio is useful in evaluating the repository performance in the case of sorbing nuclides, where the transit time depends on both the surface area available for sorption and on the advective velocity. SR 97 uses the F-ratio to compare the geosphere performance for the three hypothetical repositories, where the flow-wetted surface varies from site to site. Although the F-ratio is calculated for all cases, it is a simple multiple of the travel time and is therefore plotted only for the Base Case.

4 Base Case

This section of the report presents the simulation and analysis for the Base Case, which represents the expected site conditions described in Section 3. It is the reference case for comparison to all other cases in this study. A premodelling study by Gylling et al. (1999) examined the extent of the domain and suggested a volume likely to contain all exit locations. Boundaries for this domain are specified head (Dirichlet) boundaries, taken from the steady-state head values of a deterministic, freshwater simulation of the regional model (i.e., a supplemental simulation of Hartley et al., 1998, case AltK; see also Appendix B.1 of this report). Mapped fracture zones are modelled as conductive features and included as deterministic conductor domains (SCD). The site-scale hydraulic conductivity field is created with an unconditional simulation (i.e., no direct use of measured hydraulic conductivities), prescribing the mean of $\log_{10}$ hydraulic conductivity for each rock unit.

The Base Case uses 100 realisations of the hydraulic conductivity field, each with 120 starting positions, to estimate the distributions of travel time and canister fluxes. All statistics are calculated with respect to the common logarithm transforms ($\log_{10}$) to facilitate summary and display. No formal test for the lognormality of these results has been performed or is inferred.

4.1 Monte Carlo Stability

A practical consideration in Monte Carlo simulation studies is that statistics of interest for the model results be stable with respect to the number of realisations. That is, the number of realisations is adequate for reliable estimates of the variability of the results. This study monitored the stability of the estimators of the median travel time and median canister fluxes with respect to the number of realisations. Figures 4.1-1 and 4.1-2 present the medians of the logarithm of travel time and the logarithm of canister flux, respectively, versus the number of realisations. The plots indicate these statistics are approximately constant after 35 realisations, with less than 1% deviation from the median travel time or median canister flux for additional realisations. This suggests that for the purposes of this study, a total number of 100 realisations is adequate for estimating the medians of the performance measures.

The stability of the sample median should not be taken to imply that higher moments, such as the sample variance, are also stable. Estimators of higher moments and the extreme quantiles of distributions are usually much less efficient than the median or the mean (Larsen and Marx, 1986). In general, estimating these moments with a similar degree of accuracy requires many more realisations than are needed for stable estimators of the median (Hammersley and Handscomb, 1975). Consequently, the higher-order statistics may not have stabilised and should be used cautiously.

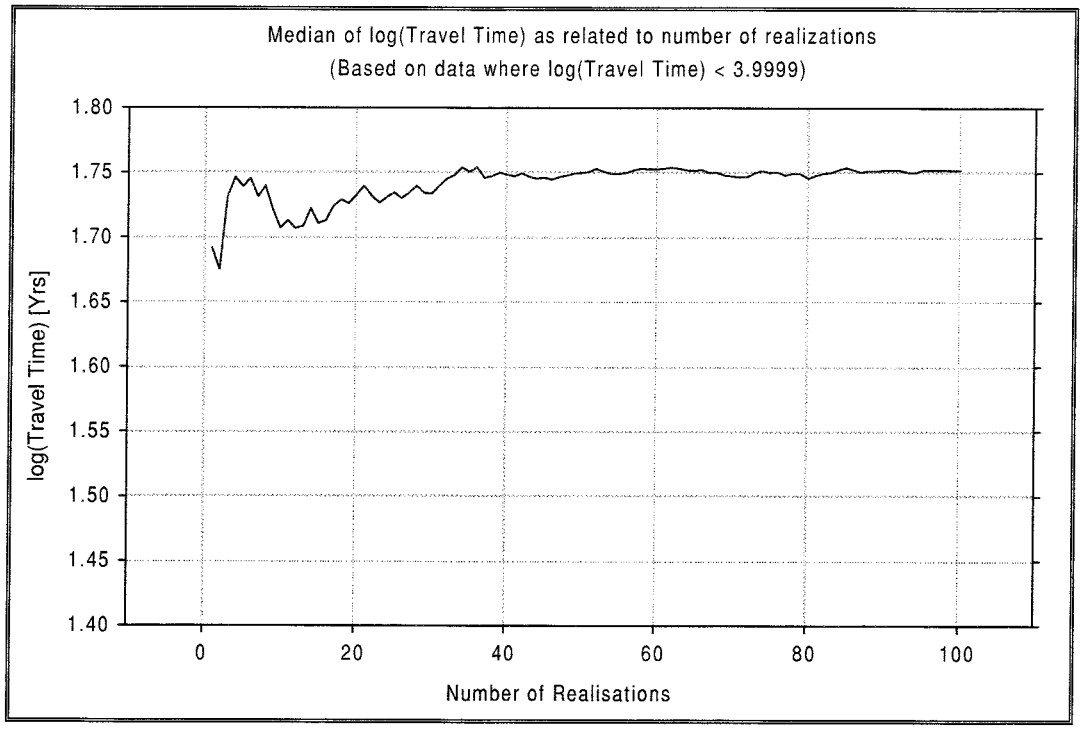

Figure 4.1-1. Monte Carlo stability in the Beberg Base Case. Median travel time versus number of realisations. Results for 120 starting positions, a flow porosity of $\varepsilon_f = 1x10^{-4}$, and travel times less than 10,000 years.

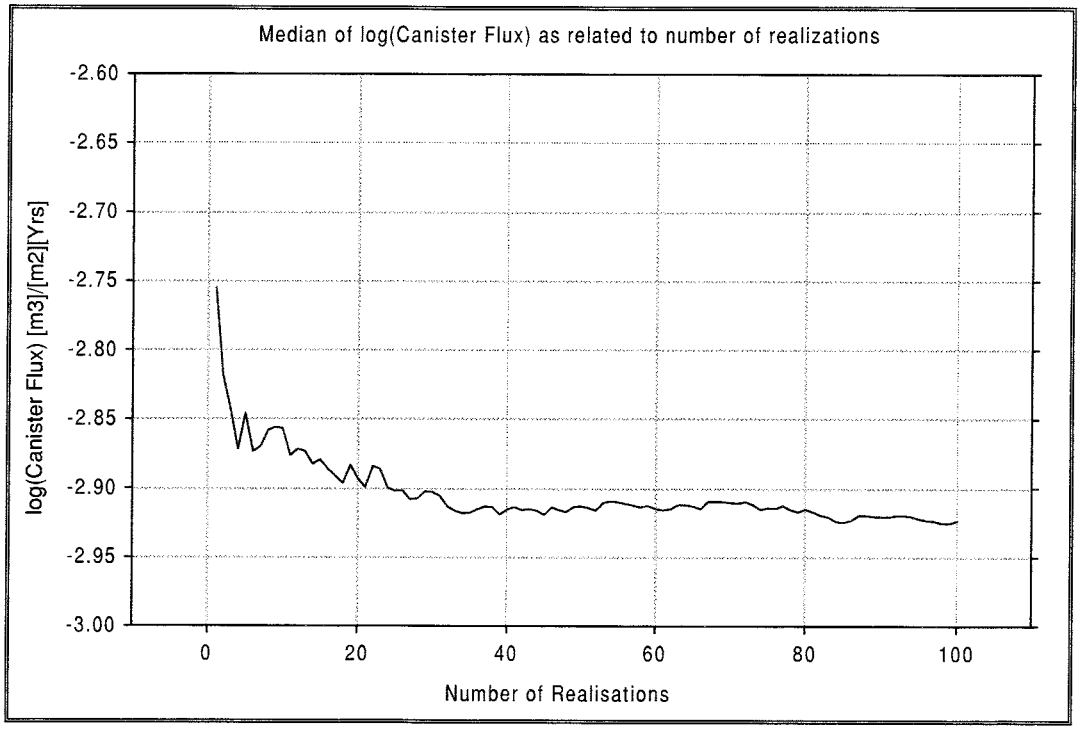

Figure 4.1-2. Monte Carlo stability in the Beberg Base Case. Median canister flux versus number of realisations. Results for 120 starting positions.

4.2 Boundary Flux Consistency

Stochastic continuum theory suggests that, under certain conditions, there exists an effective hydraulic conductivity, K_e, that satisfies:

$$\langle \vec{q} \rangle = -K_e \nabla \langle \vec{h} \rangle$$

Where:

$\langle \vec{q} \rangle$ = the expected flux

$\nabla \langle \vec{h} \rangle$ = the expected gradient.

K_e is useful for nested models in that it can be used to estimate the expected value of the flux in a smaller domain (Dagan, 1986; Rubin and Gómez-Hernández, 1990). This suggests that a regional model with a homogeneous hydraulic conductivity of K_e could be used to determine the expected boundary fluxes of a site-scale model subdomain. If the rescaling of the geometric mean hydraulic conductivity is correct, then the boundary flux of the regional model should be consistent with the average boundary flux of the site-scale stochastic continuum model. That is, the site-scale stochastic continuum model should conserve mass in an average sense with respect to the regional model fluxes.

Walker et al. (1997) suggested that the upscaling of block scale hydraulic conductivity could be calibrated using this relationship, adjusting the mean block hydraulic conductivity until the boundary fluxes of the ensemble matched the regional scale fluxes. However, there are several drawbacks to using that approach for this study. For example, the existence of K_e requires that the domain be stationary (statistically homogeneous), a condition that may be violated by the fracture zones interrupting the Beberg host rocks. Although individual rock blocks may be stationary, K_e also requires that the domain be extensive and under uniform flow conditions. Furthermore, the NAMMU model used by Hartley et al. (1998) uses an approximate algorithm to determine the mass balance over regional model subdomains, introducing additional errors in the regional mass balance calculation. Because of these limitations, this study does not adjust the mean block hydraulic conductivity to improve the flow balance between the models. However, as a check on the nested modelling and the upscaling of hydraulic conductivity, this study calculates the net volumetric flow of water across the boundaries. These flows are also reported as a mass balance for the regional and site models individually as a check on model internal consistency.

The regional model of Hartley et al. (1998) used a deterministic hydraulic conductivity field of fracture zones and rock mass, with density-dependent flow effects of saline groundwater. For the Base Case of this study, the Hartley et al. (1998) regional model Case AltK was rerun using freshwater conditions to determine the expected boundary heads and flows for the Base Case of the site scale model. Appendix B.1 summarises

the details of this regional simulation and its results. Variant 1 addresses the consequences of using other regional models and boundary transfer algorithms (Section 5.1). Lovius (1998) describes the computation of boundary fluxes for a HYDRASTAR model domain, yielding the net volumetric flow of water over each boundary.

Figure 4.2-1 and the corresponding Table 4.2-1 summarise the boundary flows of the regional and Base Case site-scale models. Each term in the table represents the net flow across a surface of the site-scale domain, and consequently does not reflect the complex distribution of inflows and outflows on each of the surfaces. The top surface, for example, has a net recharge due to precipitation, but also discharges to the mires and streams near the site. Note that the site-scale mass balance calculations carry only three significant digits, and thus contribute some error (Lovius, 1998).

Although both models qualitatively agree with the observed northeasterly direction of regional flow, there are several features to note regarding these flows. One of these features is that the regional mass balance has a residual (inflow – outflow) of approximately 50%. This residual is attributed to the approximate interpolation method used for calculating fluxes within finite elements of the regional model. Where the mass balance control surfaces do not coincide with element surfaces, the accuracy of this interpolation is limited. The accuracy of the interpolation also decreases as the contrast in hydraulic conductivities increases. It is important to note that regional model does, however, use a numerical method that is mass-conservative and a linear equation solver that is exact. Consequently, this interpolation error is unrelated to the accuracy of the heads assigned to the site-scale model boundaries (Appendix B.6).

Table 4.2-1 also presents the boundary flows for the site-scale model as the arithmetic mean of five realisations of the site model. The average site-scale flows tend to overpredict the flows of the regional model by approximately 50%. The majority of the discrepancy is seen on the upper model surface, where the regional model predicts a net recharge but the site-scale model predicts a net discharge. Note, however, that the regional residual is approximately equal to the net flow over any of the regional model surfaces, suggesting that such disagreement is within the limited accuracy of the regional mass balance. Although the regional mass balance residual limits further comparison of the nested models, it is possible that some of this discrepancy between the models may be attributable to mismatches in zone geometries or to the upscaling of hydraulic conductivities. Variant 4, the deterministic case, evaluates the upscaling of hydraulic conductivities in more detail (Section 5.4).

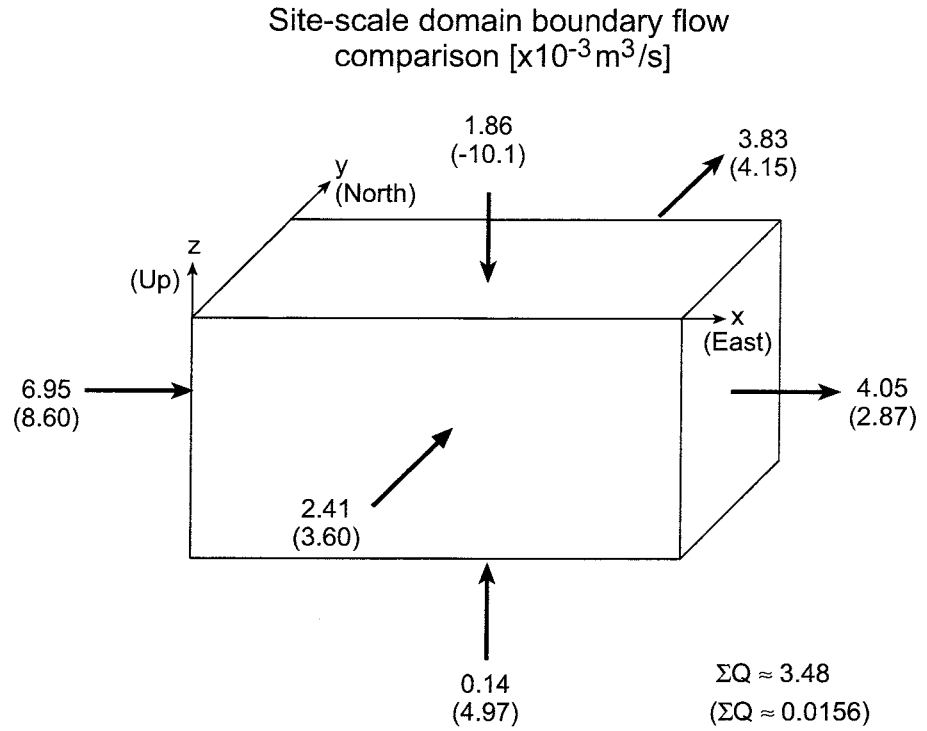

Figure 4.2-1. Consistency of Beberg Base Case boundary flows, regional versus site-scale models. The arithmetic mean flow of five realisations of the site-scale model are shown in parentheses. Arrows denote the regional flow direction.

Table 4.2-1. Boundary flow consistency for the Beberg Base Case, regional model versus site-scale model.

Model Surface	Net Flow Through Site Model Surfaces ($m^3/s \times 10^{-3}$)	
	Regional (AltK+ freshwater)	**Base Case (5 realisations)**
West	6.95 (in)	8.602 (in)
East	4.05 (out)	2.870 (out)
South	2.41 (in)	3.600 (in)
North	3.83 (out)	4.154 (out)
Bottom	0.14 (in)	4.967 (in)
Top	1.86 (in)	10.130 (out)
Total Inflow	11.36	17.169
Total Outflow	7.88	17.154
Mass balance (In – Out)	3.48	0.0156

4.3 Ensemble Results

4.3.1 Travel Time and F-ratio

In each realisation, HYDRASTAR calculates the travel times for a particle to be advected from each starting position (release position) to the model surface. The resulting stream tubes are used later in one-dimensional transport calculations in the PA model chain. Although the advective travel time is a common statistic for comparing variant simulations, it is important to note that HYDRASTAR allows only a homogenous flow porosity to be specified for the entire domain. Consequently, the travel time in any stream tube is directly proportional to this homogeneous flow porosity. This study simply uses the flow porosity of $\varepsilon_f = 1 \times 10^{-4}$, and leaves further analysis of the flow porosity to the transport modelling studies associated with SR 97.

Figure 4.3-1 presents the frequency histogram of the common logarithm of travel time for 100 realisations. Each of these realisations has 120 starting positions as representative canister locations. A few outliers are seen at the upper tail of the histogram, corresponding to travel times of 10,000 years. This 0.7% consists of stream tubes that are intercepted by the side and bottom boundaries and fail to exit the upper surface of the model (see Sections 4.3.3 and 4.4). In this circumstance, HYDRASTAR sets the travel times for these stream tubes to the default maximum travel time of 10,000 years.

The use of the default travel time slightly affects the performance measure statistics, as shown in Table 4.3-1 for the Base Case. To evaluate this effect, this study calculates the statistics both with and without the travel times greater than 10,000 years. The means and variances of the travel time and F-ratio change slightly if stream tubes with the default travel time of 10,000 years are deleted. In contrast, the canister flux statistics are virtually unaffected by this censoring, as are the medians of travel time and F-ratio. For the remainder of this study, the performance measure statistics are calculated both with and without the travel times greater than 10,000 years. For the sake of brevity, the discussions will emphasise the medians of all measures and the statistics of travel time and F-ratio for travel times less than 10,000 years. The canister flux will be summarised with statistics computed for the full set of stream tubes (no deletions). The variances and medians of the performance measures are emphasised in bold in the summary tables (e.g., Table 4.3-1). The effects of this censoring on subsequent performance assessment calculations are beyond the scope of this study.

Table 4.3-1 summarises the ensemble results, presenting the statistics for the 100 Monte Carlo realisations of the 120 starting positions for travel time, as well as canister fluxes and F-ratio. With the intercepted stream tubes deleted, the median of the travel time is 56 years, with an interquartile range from 29 years to 104 years.

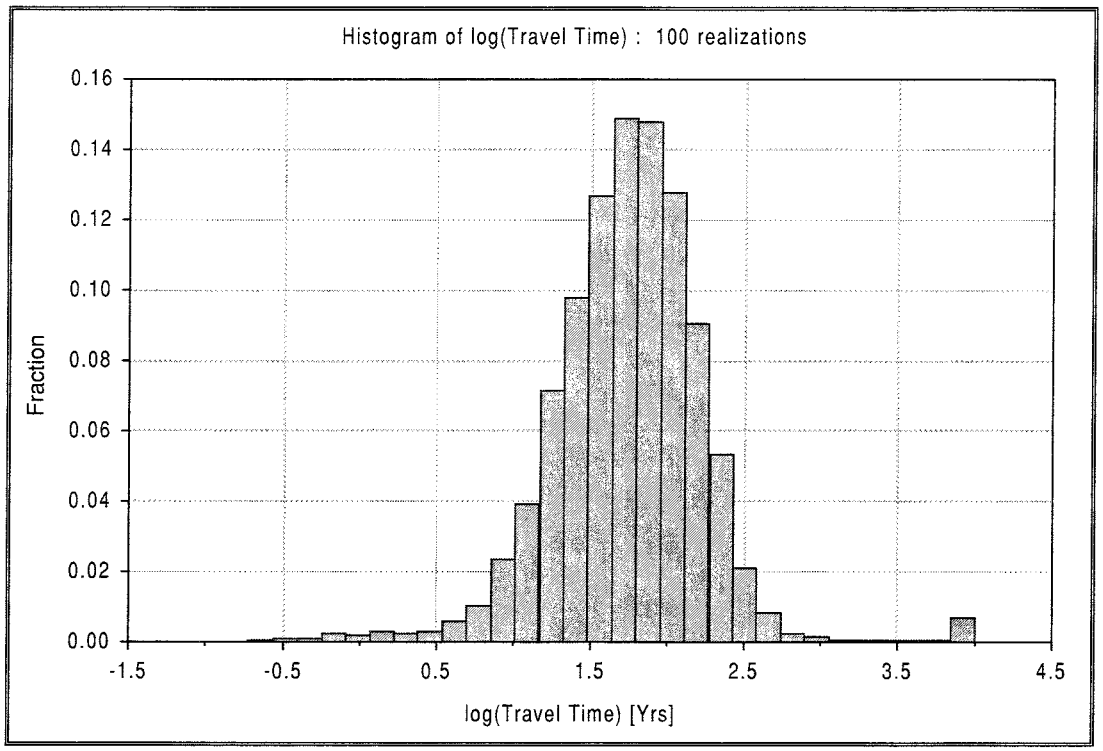

Figure 4.3-1. Relative frequency histogram of log_{10} travel time for Beberg Base Case. Results for 100 realisations of 120 starting positions and a flow porosity of $\varepsilon_f = 1x10^{-4}$.

Table 4.3-1. Summary statistics for the Beberg Base Case. Results for 100 realisations of 120 starting positions, a flow porosity of $\varepsilon_f = 1x10^{-4}$ and flow-wetted surface $a_r = 1.0\ m^2/(m^3\ rock)$. Approximately 0.7% of the stream tubes fail to exit the upper surface. Statistics in bold are discussed in text.

	All values			Travel Times > 10,000 years deleted		
	$Log_{10}\ t_w$	**$Log_{10}\ q_c$**	**Log_{10} F-ratio**	**$Log_{10}\ t_w$**	**$Log_{10}\ q_c$**	**Log_{10} F-ratio**
Mean	1.733	-2.895	5.733	1.718	-2.894	5.718
Median	1.755	**-2.923**	5.755	**1.752**	-2.923	**5.752**
Variance	0.237	**0.423**	0.237	**0.203**	0.424	**0.203**
5th percentile	0.983	-3.881	4.983	0.982	-3.881	4.982
25th percentile	1.462	-3.322	5.462	1.459	-3.321	5.459
75th percentile	2.023	-2.519	6.023	2.018	-2.518	6.018
95th percentile	2.389	-1.828	6.389	2.367	-1.826	6.367

Figure 4.3-2 presents a box plot of the simulated travel times by realisation, which shows a wide range of variability. Several realisations result in short travel times for positions 26 and 80, both of which lie near fracture zones. Another feature of the travel time box plot is that several positions have an upper range limit of 10^4 years. These are positions that occasionally have stream tubes that fail to exit the upper model surface,

and thus are assigned the default maximum travel time of 10,000 years. Figure 4.3-3 presents the number of realisations with travel times less than 1 year and 10,000 years, by stream tube number. Similar to the box plot of travel times by position number, this plot also suggests that starting positions 12, 15, 18, 20 and 24 have reduced travel times in some realisations (see Figure 3.4-2). The utility program TRAZON (Appendix F) confirms that these starting positions are not physically within fracture Zone 8, but are approximately 50 m away (i.e., the width of the exclusion zone). However, some realisations of the hydraulic conductivity field have strong connections between Zone 8 and these starting positions, allowing the stream tubes to travel rapidly up Zone 8 to Zone 2, and from there to exit locations to the northeast. Although such an effect is highly dependent on the model grid spacing and the strength of spatial correlation, these results suggest that either reducing the grid spacing or increasing the width of the exclusion zone might change the simulated repository performance.

Individual starting positions are discussed in greater detail in Section 4.5, and individual realisations are discussed in Section 4.6.

Figure 4.3-4 shows the frequency histogram of the common logarithm of F-ratio for 100 realisations (travel times less than 10,000 years). This histogram is essentially identical to the histogram of $\log_{10}$ travel times (Figure 4.3-1) because the F-ratio is a simple multiple of the travel time (see Section 3.5.4). This report presents the F-ratio for all variants, but in the interest of brevity will present the histogram of F-ratio only for the Base Case. With the intercepted stream tubes deleted, the median of the F-ratio is 5.6×10^5 year/m, with an interquartile range from 2.9×10^5 year/m to 1.0×10^6 year/m.

4.3.2 Canister Flux

HYDRASTAR calculated the canister fluxes (Darcy groundwater velocity) at each of the 120 stream tube starting positions. Table 4.3-1 summarises the results for the canister flux, which indicate a median canister flux of 1.2×10^{-3} m/year and an interquartile range from 4.8×10^{-4} m/year to 3.0×10^{-3} m/year. Figure 4.3-5 presents the frequency histogram for the $\log_{10}$ canister flux for 100 realisations, each with 120 starting positions. This histogram and the associated statistics (Table 4.3-1) show a slightly positive skewness, in contrast to the $\log_{10}$ travel time frequency histogram and statistics, which show a slightly negative skewness (Figure 4.3-4). Taken together, these suggest that the $\log_{10}$ canister flux is inversely correlated to $\log_{10}$ travel time, as is indicated by Figure 4.3-6. This might not be true for models that use a spatially variable porosity, rather than the homogeneous porosity used in HYDRASTAR. Figure 4.3-7 presents a box plot of canister fluxes by realisation, which indicates a variability of almost three orders of magnitude.

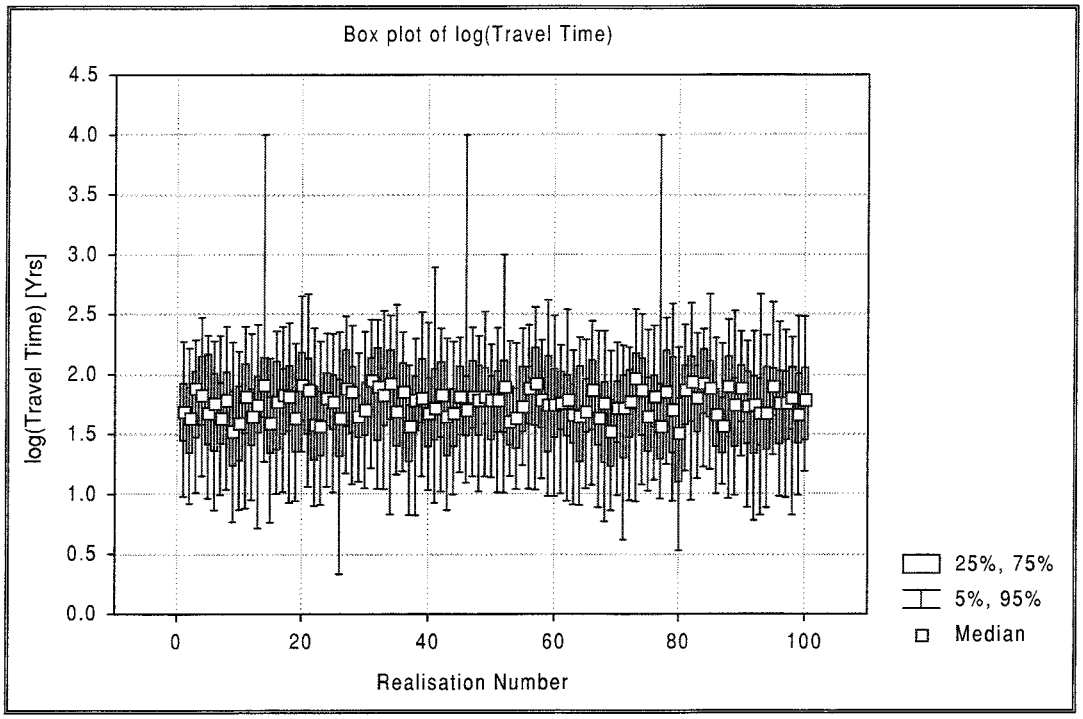

Figure 4.3-2. Travel times by realisation number for Beberg Base Case. Results for120 starting positions and a flow porosity of $\varepsilon_f = 1x10^{-4}$.

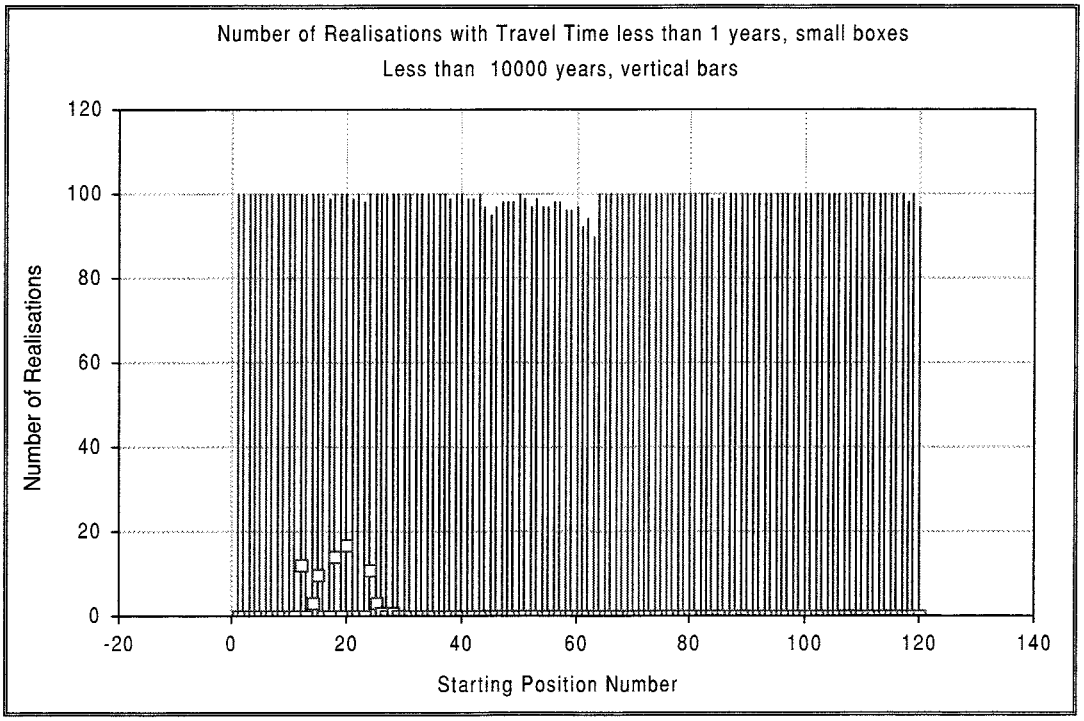

Figure 4.3-3. Number of realisations with travel times less than 1 year (squares) and 10,000 years (lines), by stream tube number for the Beberg Base Case. Results for 100 realisations and a flow porosity of $\varepsilon_f = 1x10^{-4}$.

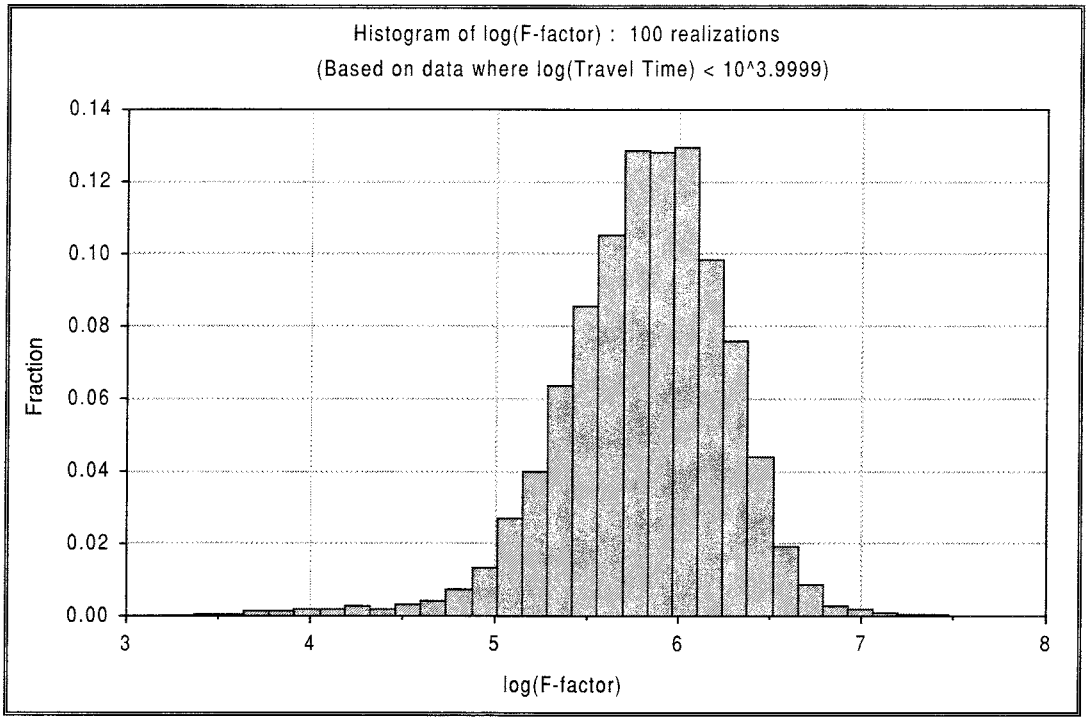

Figure 4.3-4. Relative frequency histogram of log_{10} F-ratio for the Beberg Base Case. Results for100 realisations of 120 starting positions, a porosity of $\varepsilon_f = 1x10^{-4}$ and a flow-wetted surface of $a_r = 1.0\ m^2/(m^3\ rock)$.

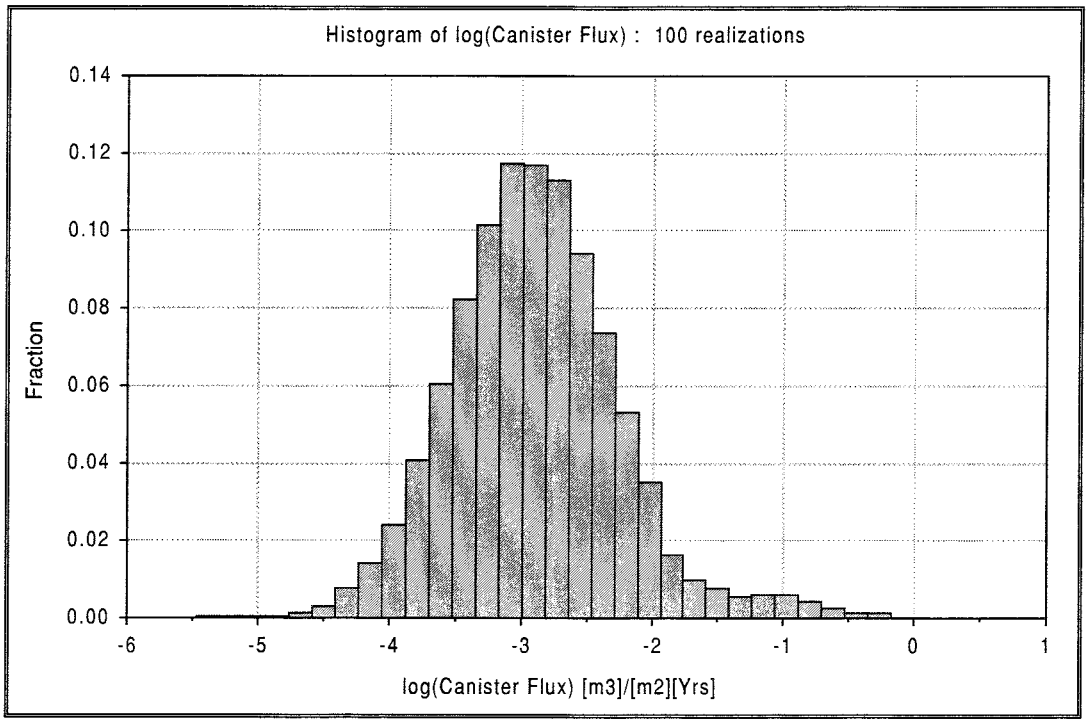

Figure 4.3-5. Relative frequency histogram of log_{10} canister flux for the Beberg Base Case. Results for 100 realisations of 120 starting positions.

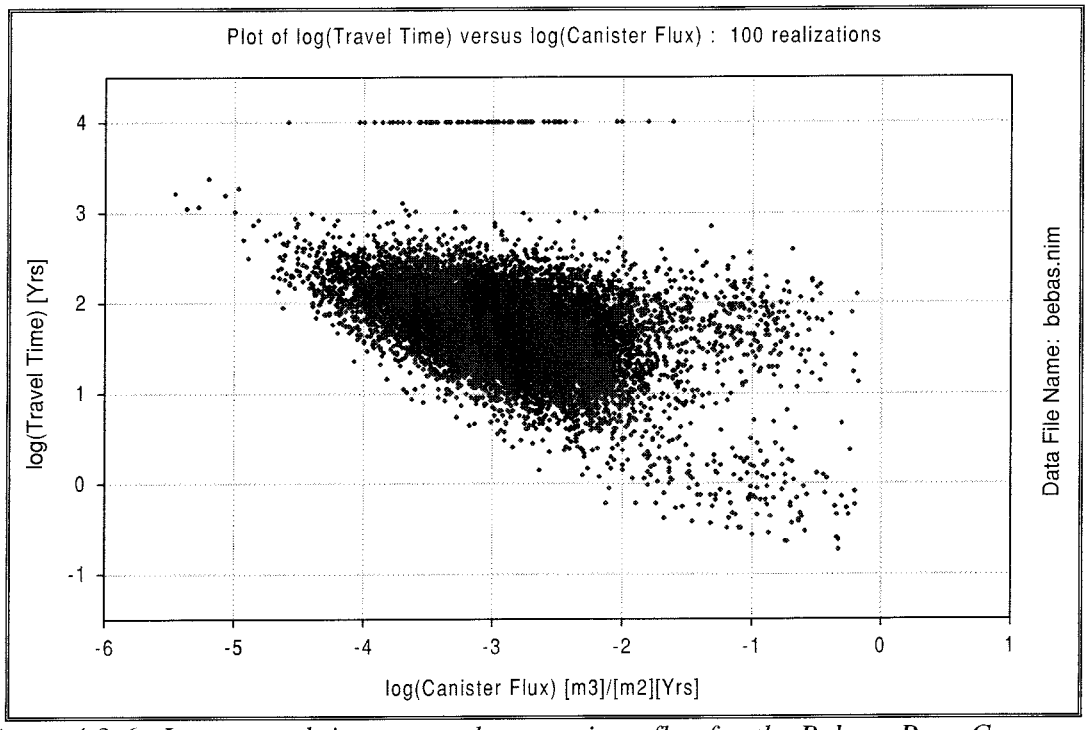

Figure 4.3-6. Log_{10} travel time versus log_{10} canister flux for the Beberg Base Case. Results for 100 realisations of 120 starting positions and a flow porosity of $\varepsilon_f = 1x10^{-4}$.

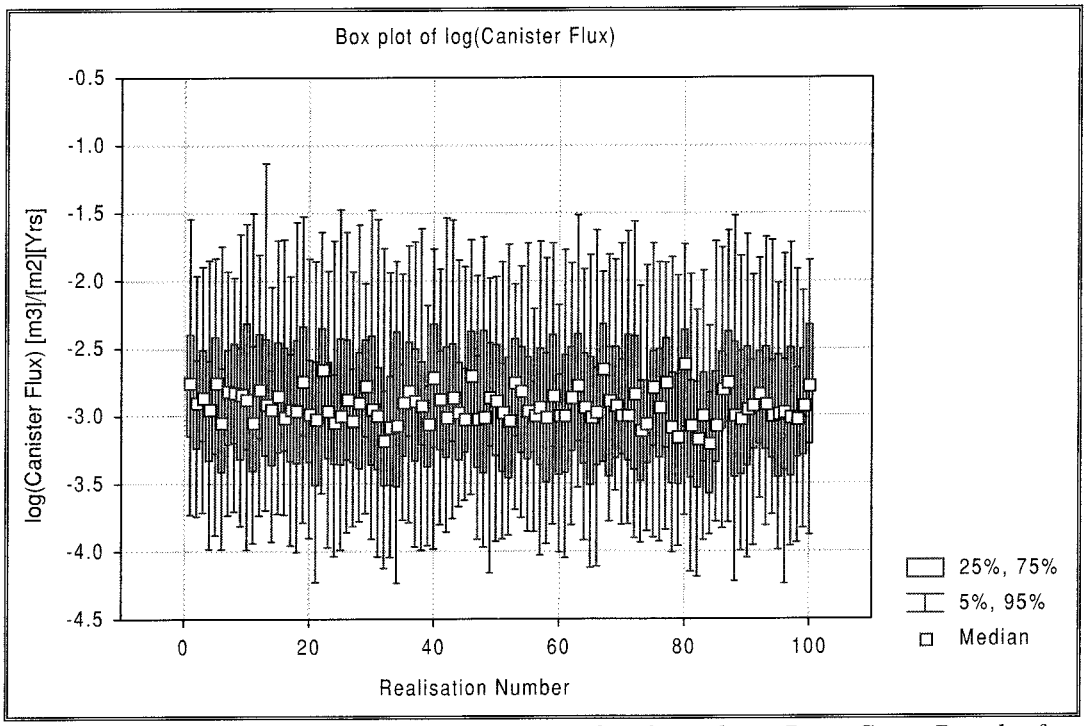

Figure 4.3-7. Log_{10} canister flux by realisation for the Beberg Base Case. Results for 100 realisations of 120 starting positions.

4.3.3 Exit Locations

HYDRASTAR calculates the exit locations for each of the stream tubes as the last point on the travel path before it exits the domain. Figure 4.3-8 presents a map of the exit locations on the model surface (-35 masl). As discussed earlier in this section, the flo paths are predominantly northeastward to discharge areas, reflecting the pattern of regional groundwater flow. The discharge areas tend to be organised around the regional fracture zones lying to the northeast of the repository. The majority of the exit locations are in the Imundbo Zone, while the longest stream tubes follow Zone 3 to the north (Figure 4.3-9). The exceptions to this pattern are the stream tubes that are trapped at the model's side and bottom boundaries (approximately 0.7% of all stream tubes).

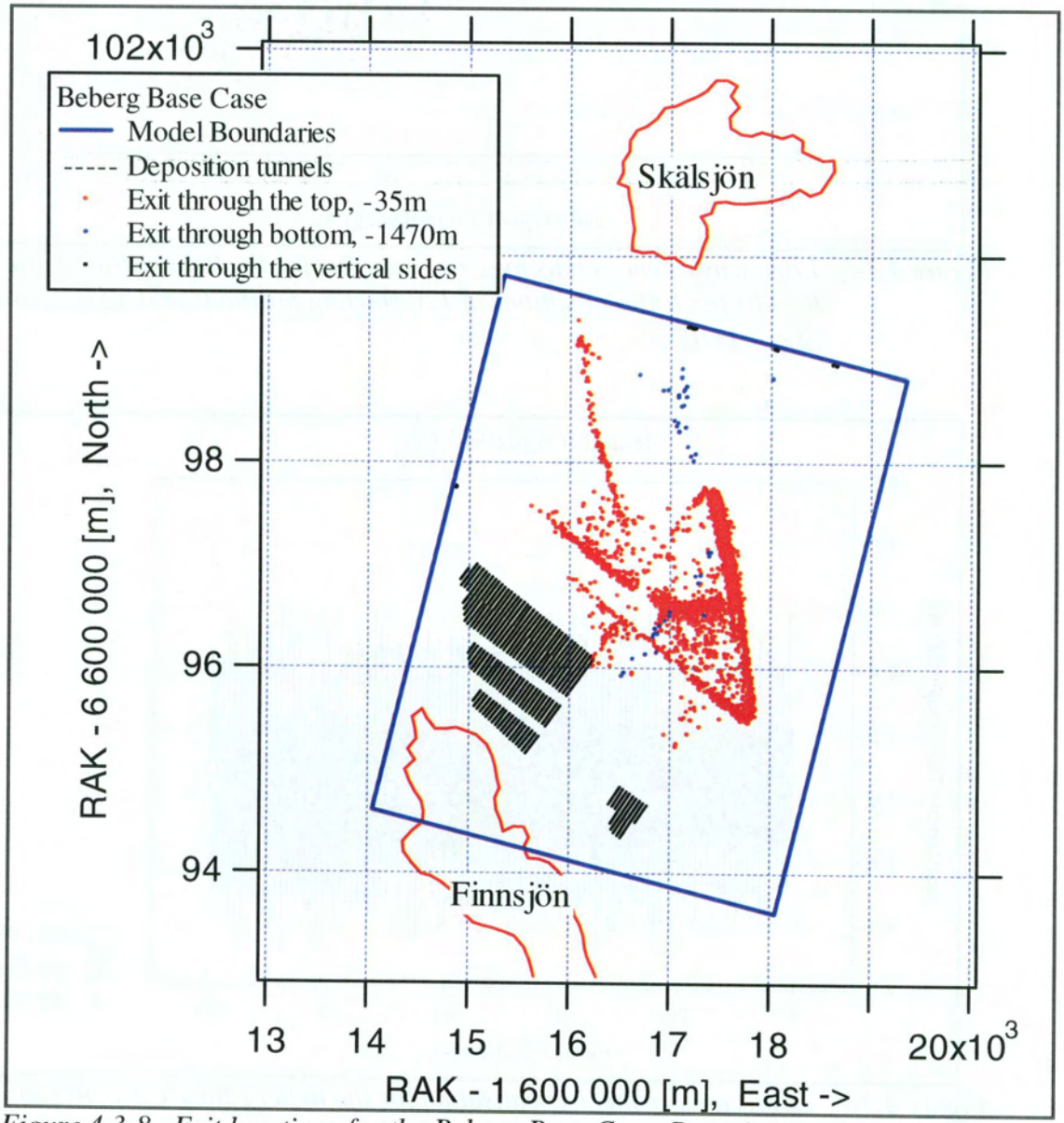

Figure 4.3-8. Exit locations for the Beberg Base Case. Repository tunnels at -600 masl shown projected up to the model surface. Results for 100 realisations of 120 starting positions (offset RAK coordinates in metres).

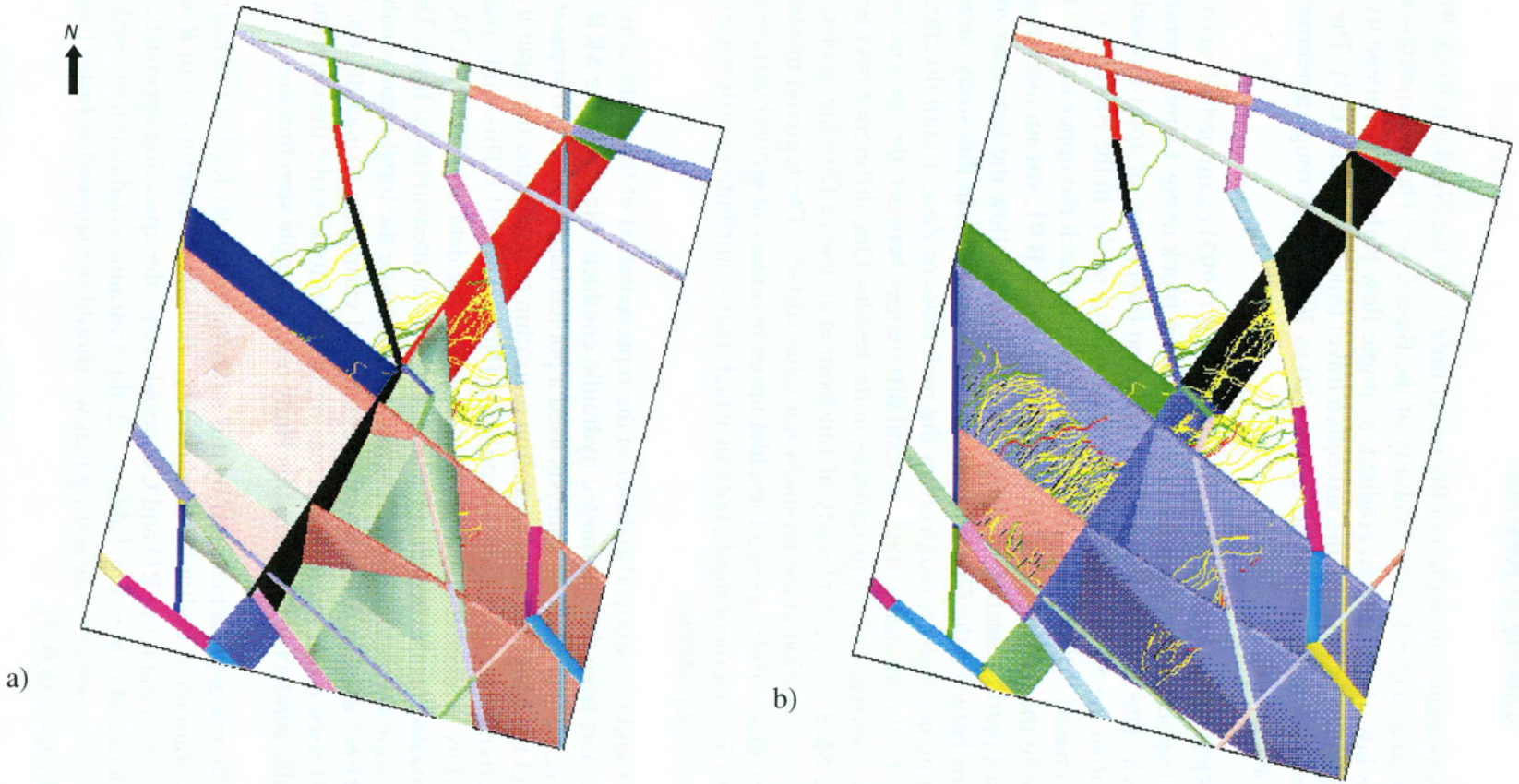

Figure 4.3-9. Stream tubes for the Beberg Base Case realisation number 1, relative to a) the full set of fracture zones (SCD), and b) with Zones 2 and 11 rendered invisible to facilitate viewing.

4.3.4 Validity of Results

An approximate calculation of the travel time from the Northern Rock Block was performed as a check on the validity of the Base Case. These computations used Darcy's law, the estimated gradient, a simple flow path, and the mean hydraulic conductivities to estimate the advective travel time (Appendix C.3). The results showed that the travel times should be between 20 to 70 years, in rough agreement with the Base Case results.

In the SKB 91 study of the Finnsjön site, SKB (1992) examined advective travel times from a hypothetical repository in the Northern block using a similar modelling approach. The SKB 91 study found a median travel time of approximately 100 years, longer than the 56 years of the Base Case of this study. In the SKB 91 study, approximately 50% of the stream tubes failed to reach the upper model surface in contrast to the 0.7% that failed in this study. In SKB 91, stream tubes tended to migrate northeast until contacting the Imundbo zone, then follow the Imundbo zone to exit locations between the Giboda zone and Lake Skälsjön. In this study, stream tubes tend to migrate northeast through either the rock mass or Zone 1 until diverted up to ground surface by the Imundbo zone. Several differences between the approaches used by these studies contribute to the differences in the results. One difference between the studies is that the SKB 91 regional study of Lindbom et al. used a Dirichlet (constant head) upper boundary condition at the groundwater table surface. The regional model of this study (Hartley et al., 1998) used a Dirichlet upper boundary at ground surface elevation and a coarser finite element mesh, both of which may contribute to differences in gradients and recharge patterns.

SKB 91 and this study also differ in the representation of hydraulic conductivity. Both studies start from the interpreted hydraulic conductivities from the SKB SICADA database, but the SKB 91 analysis used a pooled data set (i.e., no separation of RD from CD) and the Moye's-based upscaling algorithm to determine the input hydraulic conductivities for conditional simulation (Norman, 1991). This study uses the values inferred by Walker et al. (1997) that separated the data into RD and CD, then compensated for the censoring effect of the lower measurement limit. The resulting means were then empirically upscaled to determine the input mean conductivities, with INFERENS used to determine the regularised variogram (Appendix C). In addition, SKB 91 used a continuously decreasing function to describe the depth dependence of hydraulic conductivity, where this study uses a simple step function.

The different approaches used by this study and SKB 91 lead to markedly different representations of hydraulic conductivity, including the definition of Rock Domains, the separation of data into RD and CD populations, the upscaling approach, and the depth dependence. As shown in Table 4.3-2, the hydraulic conductivities used in this study generally are greater, suggesting that we should see somewhat faster travel times in this study than in SKB 91.

Taken collectively, the differences in the approaches suggest that the travel times of this study are roughly comparable to those of SKB 91, given the differences in inferred hydraulic conductivities. The reduced travel times appear to be attributable to the

overall increase in hydraulic conductivities used in this study. It is also important to note that the differences in results are minor in the context of performance assessment.

Table 4.3-2. Comparison of the hydraulic conductivity in selected zones of SKB 91 and Beberg Base Case site-scale models.

Zone	Arithmetic mean $log_{10}K$ (m/s) at -50 masl		Arithmetic mean $log_{10}K$ (m/s) at -500 masl	
	SKB-91 (36 m scale)	Base Case (35 m scale)	SKB-91 (36 m scale)	Base Case (35 m scale)
1	-4.52	-4.68	-6.75	-5.77
4	-4.72	-4.26	-6.95	-5.35
Imundbo	-4.36	-4.26	-6.59	-5.35
SRD North	(1)	-6.42	(1)	-7.51
SRD South	(1)	-6.78	(1)	-7.87
SRD Other	-5.71	-7.16	-7.94	-8.25

Note: (1) Only one rock mass value was used in the SKB 91 study.

Lastly, the boundary flow consistency (Section 4.2) indicates that the site-scale model may predict greater outflow to ground surface than the regional model. Although the inaccuracy of the regional mass balance prohibits further analysis, note the following:

- The flow patterns and exit locations are compatible with observed recharge and discharge areas;
- The exit locations are roughly comparable to those of SKB 91; and
- The exit locations and travel times are roughly comparable to those of the regional model used to determine the boundary conditions for this study (Appendix B.5).

4.4 Individual Realisations

There are several strategies that could be used to select several realisations that are in some sense representative of the ensemble. For example, we could select a realisation whose travel time or canister flux is close to the median of the ensemble of the realisations. However, the probability of each realisation in a Monte Carlo set is equal by definition, so that no single realisation can be said to be representative of the ensemble. Consequently, three realisations are examined to illustrate the variability between realisations, with somewhat more detail on realisation number one.

Figure 4.4-1 presents the stream tubes for realisation number one, whose stream tubes reflect the topographically-driven northeasterly flow pattern at the site, with stream tubes. The particles released at repository level tend to drift northward through the rock mass until contacting Zones 1, 4 or the Imundbo fracture zone. The exit locations of the entire ensemble and specific regions of the repository are discussed in Section 4.1.5.

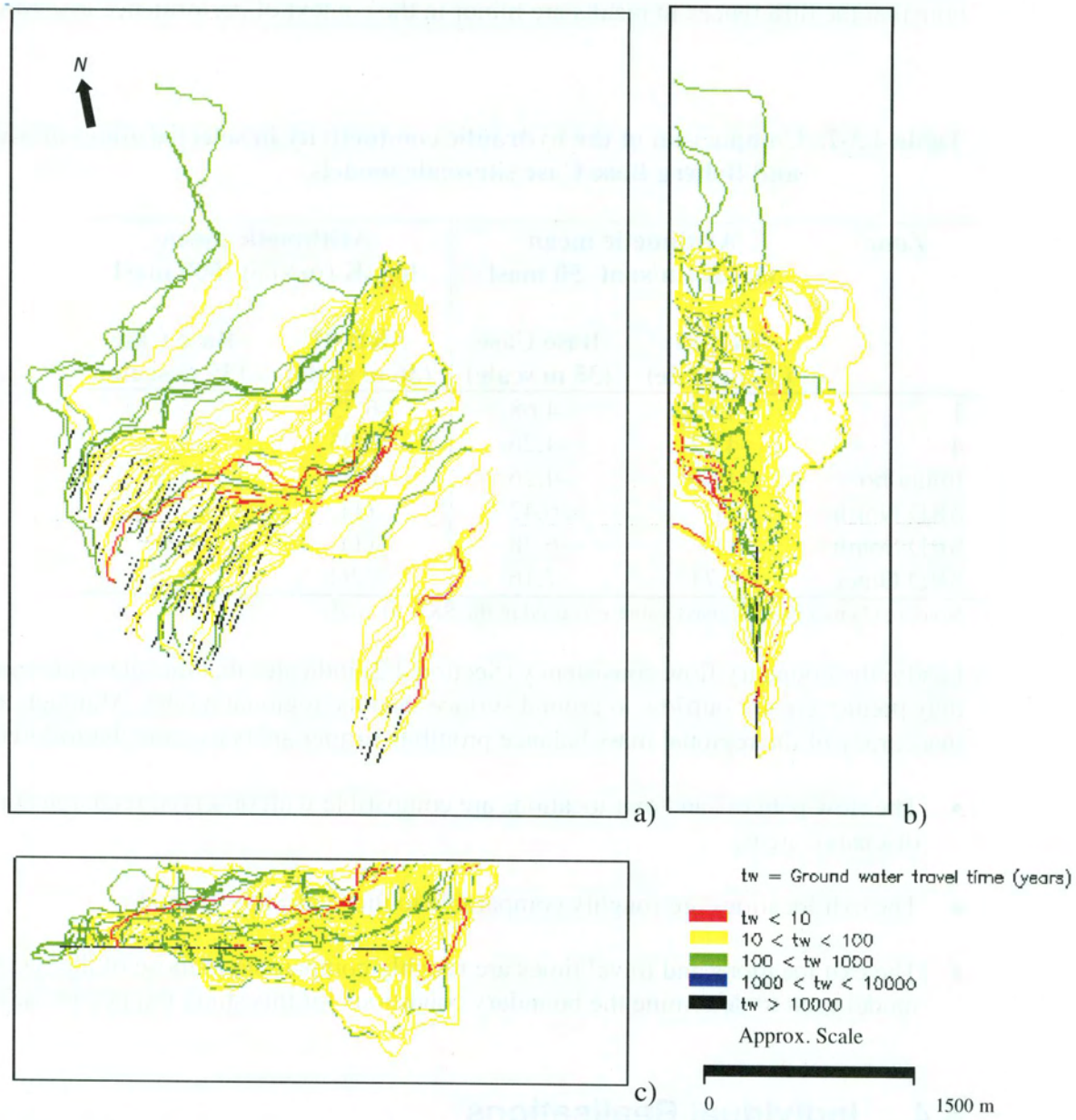

Figure 4.4-1. Stream tubes in realisation 1 of the Beberg Base Case in a) plan view (looking downward), b) elevation view from east and c) elevation view from south. Results for 120 starting positions and a flow porosity of $\varepsilon_f = 1x10^{-4}$.

To examine the variability between realisations, this study selects the three realisations at random and examines them to get a sense of their overall behaviour. (Note that these are actually the first three realisations, whose sequence is randomised by the random number generation). Figure 4.4-2 presents the flowpaths for these three realisations of the Base Case, illustrating the variability of flowpaths between realisations (see also Variant 4). In all three realisations, the dominant flowpath from starting positions in the Northern Block is through the rock mass to Zone 1, and then to exit at the intersection of Zone 1 and the Imundbo zone. In some realisations, the starting positions in the extreme northwestern end of the Northern Block do not follow the dominant flow path of Zone 1- Imundbo, but instead are intercepted by Zone 3 and travel northward toward Skälsjön. For the Southern Block, the stream tubes tend to travel northeastward through the rock mass to exit along the Imundbo Zone. These stream tubes demonstrate the influence of the fracture zones, which are deterministic features even though the occurrence and characteristics are uncertain for all the fracture zones in the SCD representation. In the particular case of the Imundbo Zone, the dominant pathway at the site, the properties are inferred indirectly from boreholes and measurements in nearby zones (i.e., there are no hydraulic tests available for the Imunbo Zone). Variants 3 and 4 evaluate the uncertainties of the SCD representation of the fracture zones.

Table 4.4-1 and Figure 4.4-3 present the summary statistics and floating histograms of the performance measures for these realisations. The results indicate a range of median travel times from 44 to 76 years and a range of median canister fluxes from 1.29×10^{-3} to 1.78×10^{-3} m/yr. Although the range in median travel times is approximately a factor of two, such variability is rather small in the context of performance assessment. That is, for the purposes of performance assessment, the differences between realisations are considered rather small.

Figures 4.4-3, 4.4-4, and 4.4-5 present plots of the performance measures for these three realisations by starting position number, illustrating the variability within and between the realisations. For some starting positions, the variability of $\log_{10}$ canister flux is as much as 1.5 orders of magnitude (e.g., starting position number 1). For $\log_{10}$ travel time, starting positions 20 and 24 show a much greater level of variability than positions (approximately 2 orders of maginitude versus 1 order of magnitude, respectively). As discussed in Section 4.3, this may be attributable to the closeness of starting positions 20 and 24 to Zone 8.

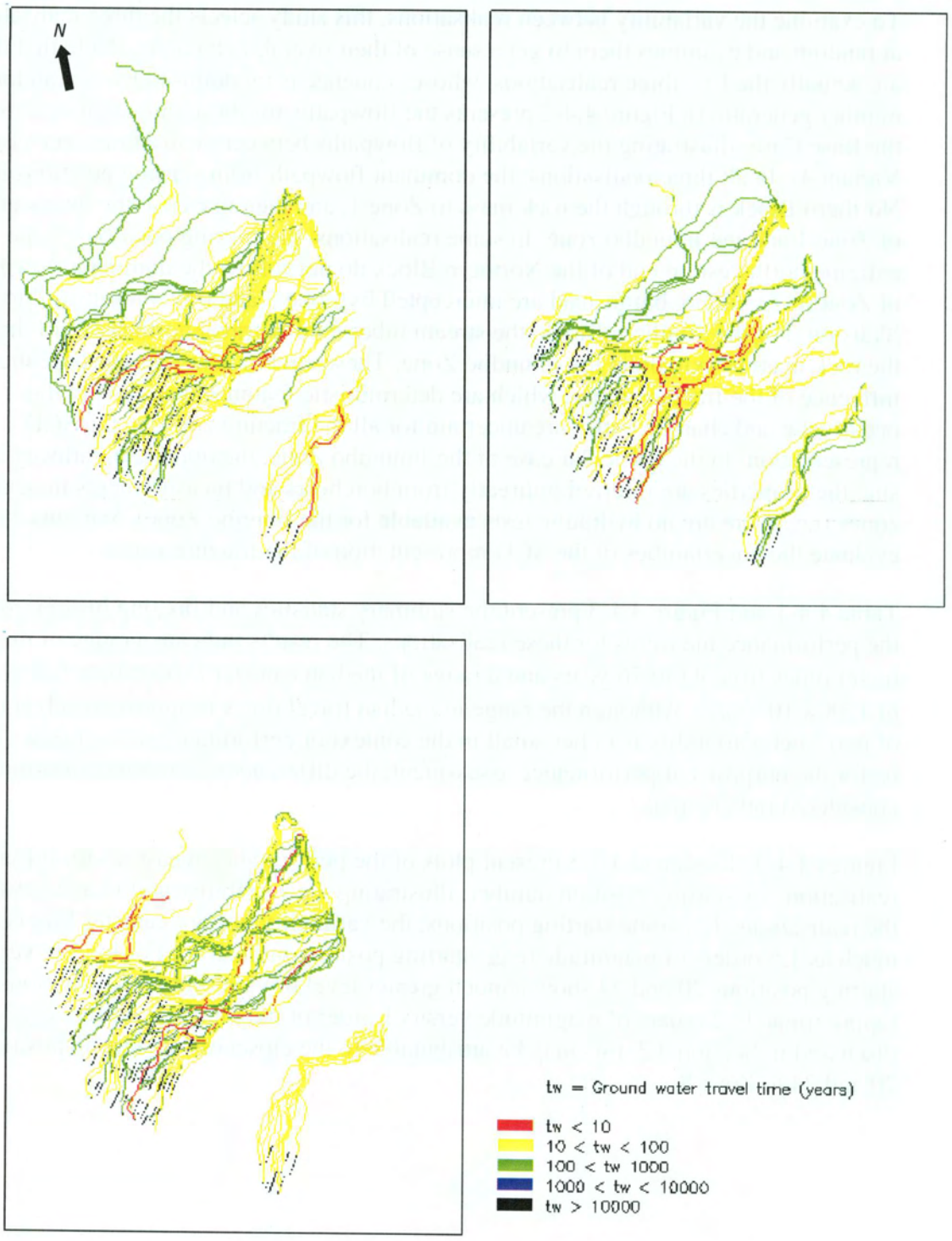

Figure 4.4-2. Stream tubes for three realisations of the Beberg Base Case (plan view). Results for 120 starting positions and a flow porosity of $\varepsilon_f = 1x10^{-4}$.

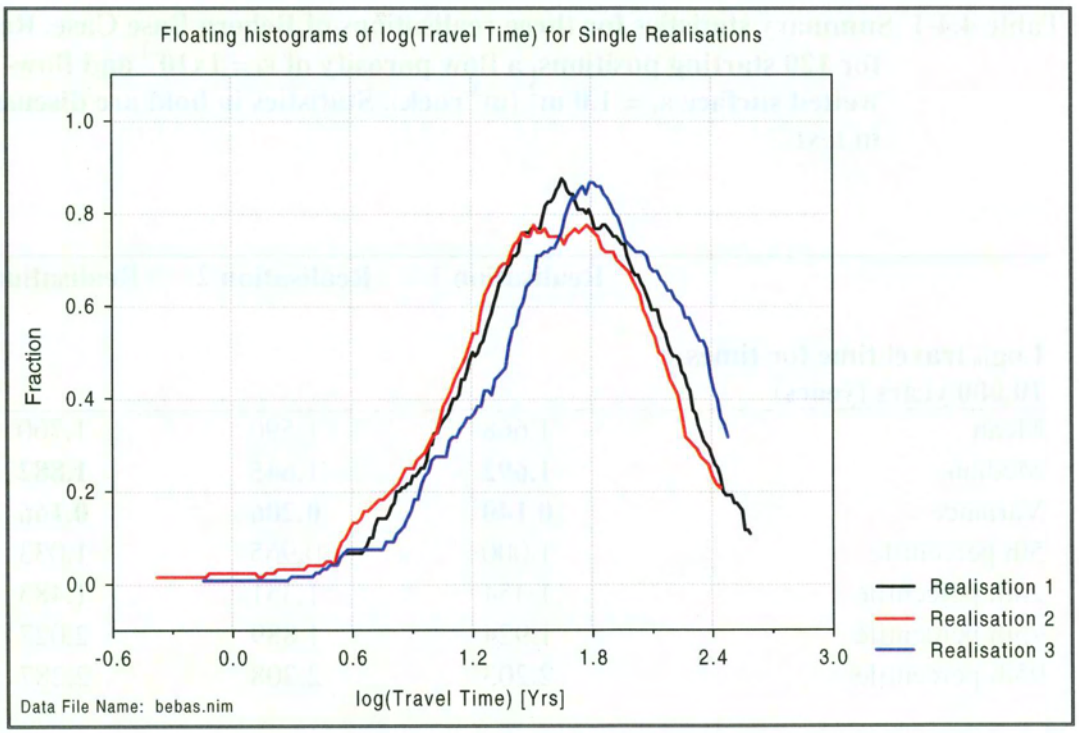

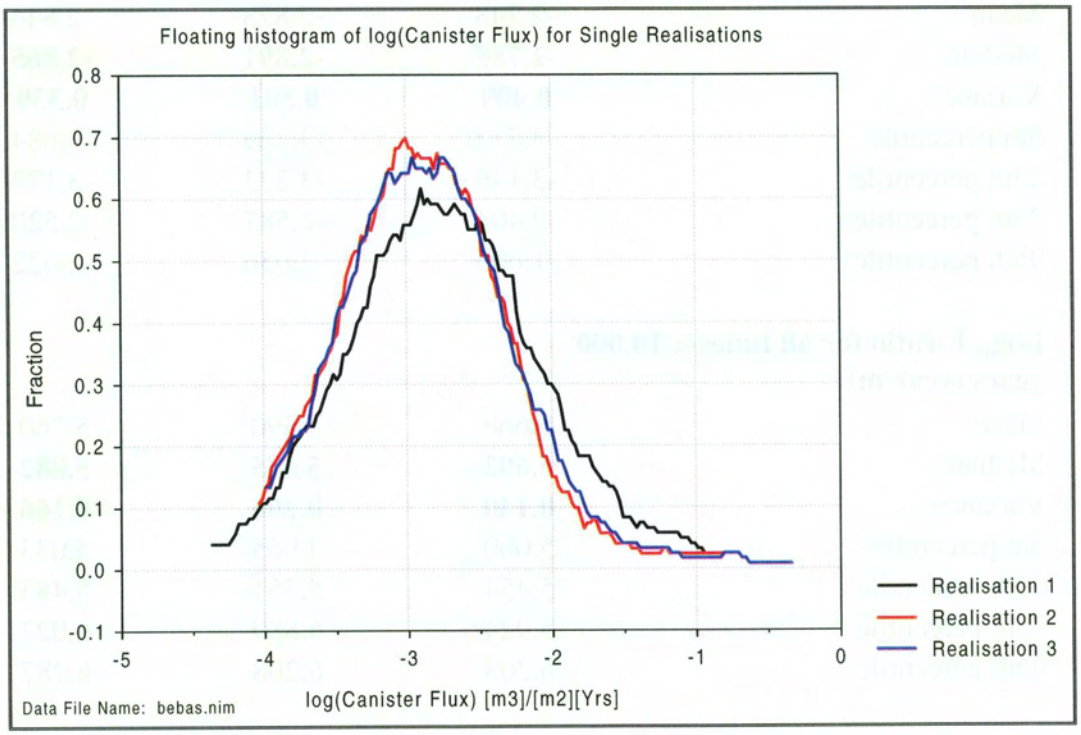

Figure 4.4-3. Floating histograms of a) log_{10} travel time and b) log_{10} canister flux for three realisations of the Beberg Base Case. Results for 120 starting positions and a flow porosity of $\varepsilon_f = 1x10^{-4}$.

Table 4.4-1 Summary statistics for three realisations of Beberg Base Case. Results for 120 starting positions, a flow porosity of $\varepsilon_f = 1x10^{-4}$ and flow-wetted surface a_r = 1.0 $m^2/(m^3$ rock). Statistics in bold are discussed in text.

	Realisation 1	Realisation 2	Realisation 3
Log_{10} travel time for times < 10,000 years (years)			
Mean	1.668	1.590	1.760
Median	**1.692**	**1.645**	**1.882**
Variance	**0.140**	**0.206**	**0.166**
5th percentile	1.000	0.965	1.033
25th percentile	1.454	1.351	1.483
75th percentile	1.924	1.889	2.027
95th percentile	2.203	2.208	2.287
Log_{10} canister flux for all times (m/year)			
Mean	-2.748	-2.878	-2.844
Median	**-2.755**	**-2.891**	**-2.865**
Variance	**0.409**	**0.301**	**0.339**
5th percentile	-3.713	-3.729	-3.684
25th percentile	-3.146	-3.223	-3.177
75th percentile	-2.404	-2.587	-2.520
95th percentile	-1.606	-2.056	-2.022
Log_{10} F-ratio for all times < 10,000 years (year/m)			
Mean	5.668	5.590	5.760
Median	**5.692**	**5.645**	**5.882**
Variance	**0.140**	**0.206**	**0.166**
5th percentile	5.000	4.965	5.033
25th percentile	5.454	5.351	5.483
75th percentile	5.924	5.889	6.027
95th percentile	6.203	6.208	6.287
Percent of stream tubes failing to exit	0.000	0.000	0.000

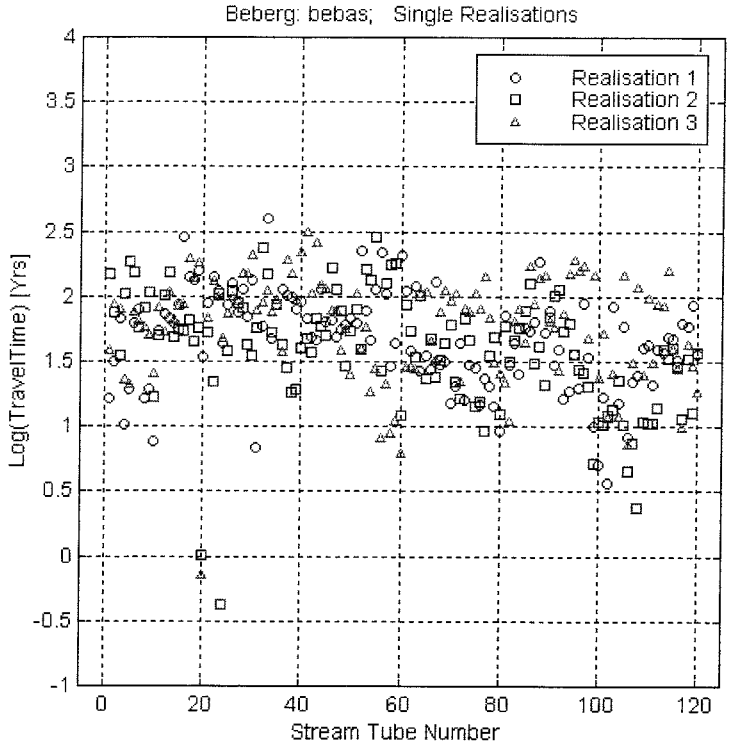

Figure 4.4-4. Log_{10} travel time versus starting position number for three realisations of the Beberg Base Case. Results for a flow porosity of $\varepsilon_f = 1x10^{-4}$.

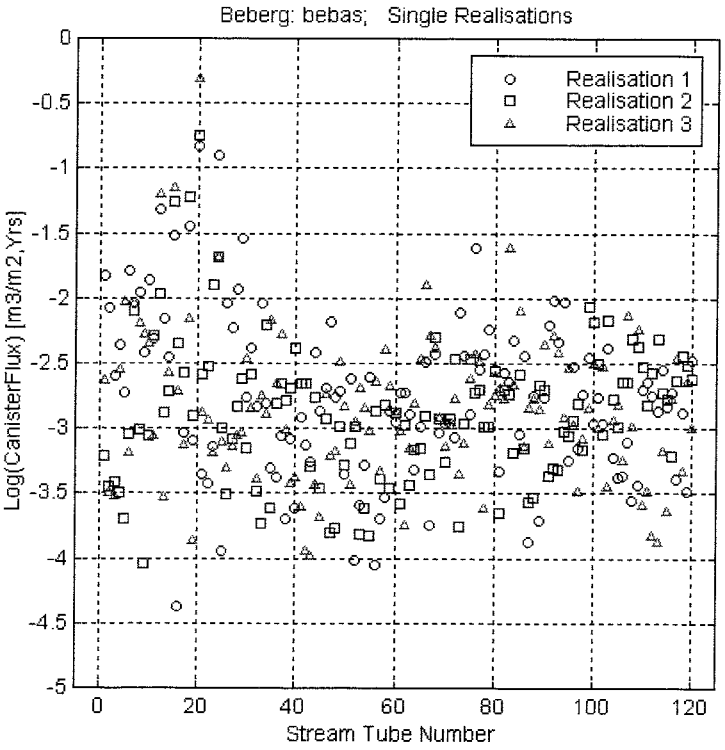

Figure 4.4-5. Log_{10} canister flux versus starting position number for three realisations of the Beberg Base Case.

4.5 Individual Starting Positions

This study examines three individual stream tube starting positions to illustrate the performance of specific repository areas and the variability within realisations. Starting position number 8 represents the repository in the southern rock block, and positions 22 and 66 represent the southern and northern extremes, respectively, of the hypothetical repository lying in the Northern Rock Block. For each of these starting positions, histograms and summary statistics are compiled over all realisations.

Table 4.5-1, Figure 4.5-1 and Figure 4.5-2 present these statistics and associated histograms for the performance measures at these starting positions. Starting position 8 has the shortest median travel time of 33 years, and position 22 has the longest travel time of 77 years. The canister fluxes at positions 8 and 22 have the largest and smallest median canister flux, respectively, suggesting that the $\log_{10}$ travel time is inversely correlated to $\log_{10}$ canister flux, as was discussed in Section 4.3 (see also Figure 4.3-6). Figure 4.5-3 indicates that the travel time at any of these positions can vary over 2 orders of magnitude, and Figure 4.5-4 indicates that the canister flux can vary over more than 2.5 orders of magnitude.

Because median performance measures for individual starting positions may exhibit greater variability than the median over the full set of starting positions, it is important to evaluate the stability of the statistics versus the number of Monte Carlo realisations. Figure 4.5-5 presents a plot of the median of $\log_{10}$ travel time versus realisation number for these three starting positions. Starting position 22 appears to stabilise after 15 realisations, while starting position 8 appears to require more than 50 realisations to stabilise. In either case, 100 realisations appear to be adequate for reliable estimates of the median of $\log_{10}$ travel time.

Figure 4.5-6 presents the stream tubes from these three starting positions for the first 50 realisations. As suggested by the ensemble results for the Southern Rock Block, the stream tubes from starting position 8 are consistently toward the northeast, exiting in the Imundbo zone. Stream tubes from position 22 are much more variable; though many realisations tend to follow Zone 1 to Imundbo, many stream tubes cross through Zone 1 to travel slowly through the rock mass. Stream tubes from position 66 have a similar variability, with as many stream tubes travelling through the rock mass as there are travelling through Zone 1. In spite of this variability, the exit zones for these locations are consistently located near the intersection of Zone 1 and Imundbo.

Table 4.5-1 Summary statistics for three starting positions in the Beberg Base Case. Results for 100 realisations, a flow porosity of $\varepsilon_f = 1x10^{-4}$ and flow-wetted surface $a_r = 1.0\ m^2/(m^3\ rock)$. No stream tubes fail to exit the upper model surface. Statistics in bold are discussed in text.

	Starting Position Number		
Log_{10} Travel Time for times < 10,000 years (years)	**8**	**22**	**66**
Mean	1.540	1.906	1.811
Median	**1.517**	**1.887**	**1.802**
Variance	**0.084**	**0.075**	**0.162**
5th percentile	1.126	1.428	1.122
25th percentile	1.297	1.738	1.507
75th percentile	1.707	2.069	2.085
95 percentile	2.073	2.389	2.463
Log_{10} Canister Flux for all times (m/year)			
Mean	-2.707	-3.142	-3.027
Median	**-2.711**	**-3.026**	**-3.002**
Variance	**0.229**	**0.323**	**0.345**
5th percentile	-3.562	-4.224	-4.191
5th percentile	-3.012	-3.479	-3.440
75th percentile	-2.377	-2.723	-2.610
95th percentile	-1.983	-2.357	-2.131
Log_{10} F-ratio for times < 10,000 years (year/m)			
Mean	5.540	5.906	5.811
Median	**5.517**	**5.887**	**5.802**
Variance	**0.084**	**0.075**	**0.162**
5th percentile	5.126	5.428	5.122
25th percentile	5.297	5.738	5.507
75th percentile	5.707	6.069	6.085
95th percentile	6.073	6.389	6.463

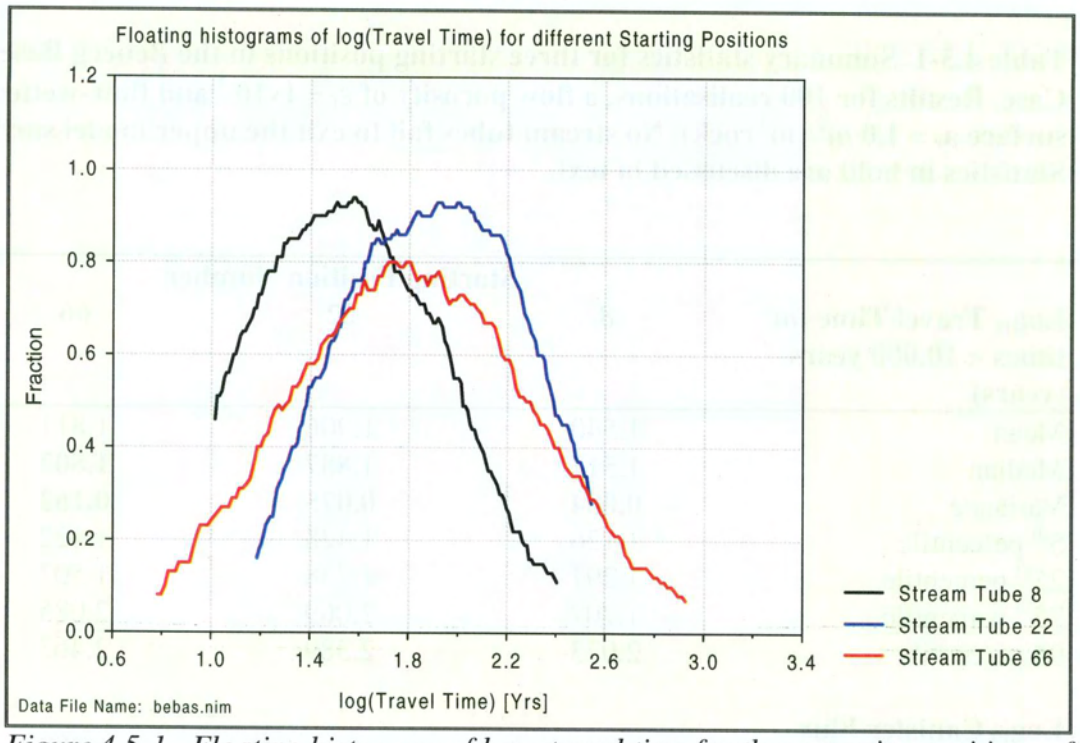

Figure 4.5-1. Floating histogram of $\log_{10}$ travel time for three starting positions of the Beberg Base Case. Results for 100 realisations and a flow porosity of $\varepsilon_f = 1x10^{-4}$.

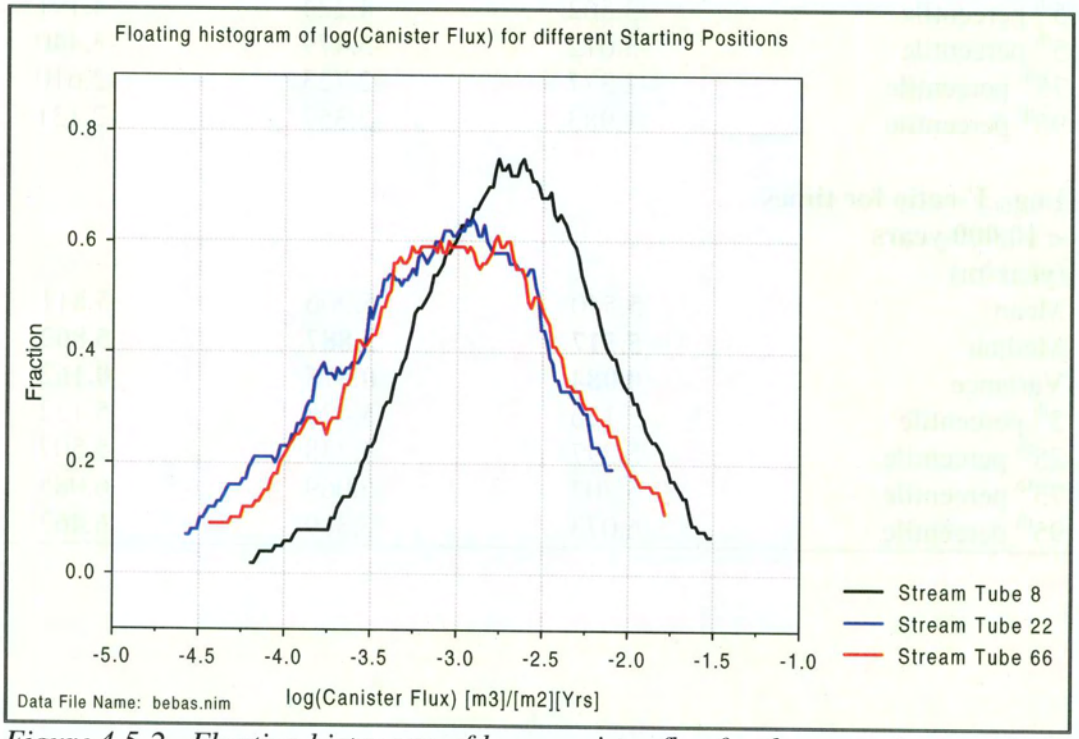

Figure 4.5-2. Floating histogram of $\log_{10}$ canister flux for three starting positions of the Beberg Base Case. Results for 100 realisations

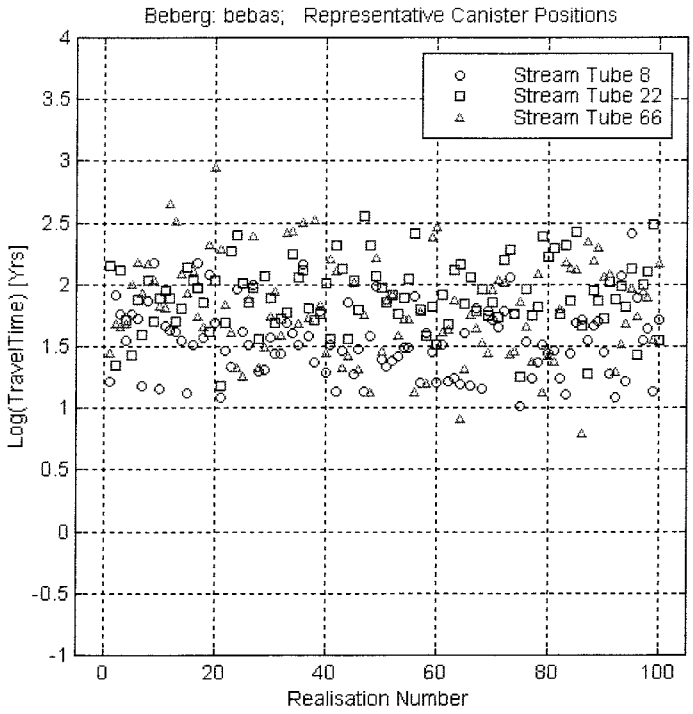

Figure 4.5-3. Log_{10} travel time versus realisation number for three starting positions of the Beberg Base Case. Results for 100 realisations and a flow porosity of $\varepsilon_f = 1x10^{-4}$.

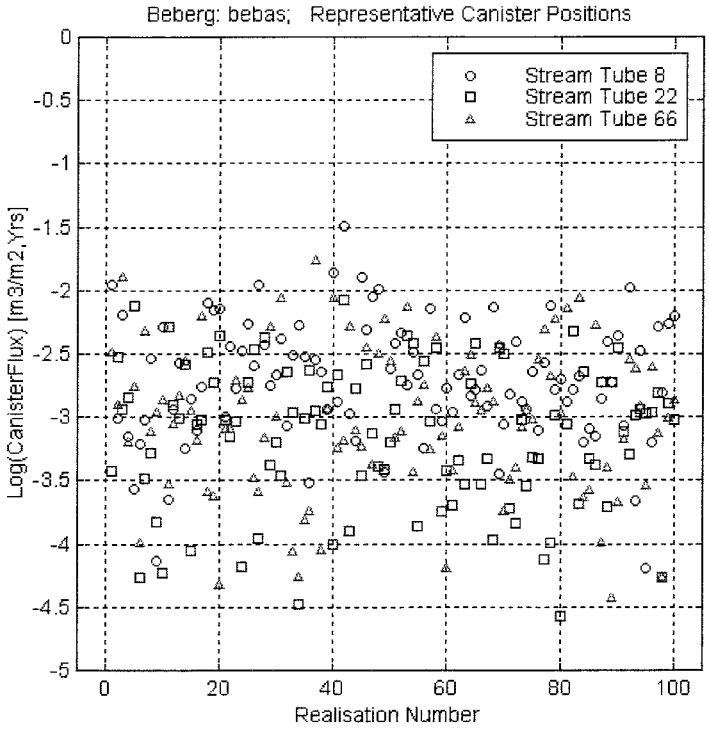

Figure 4.5-4. Log_{10} canister flux versus realisation number for three starting positions of the Beberg Base Case. Results for 100 realisations.

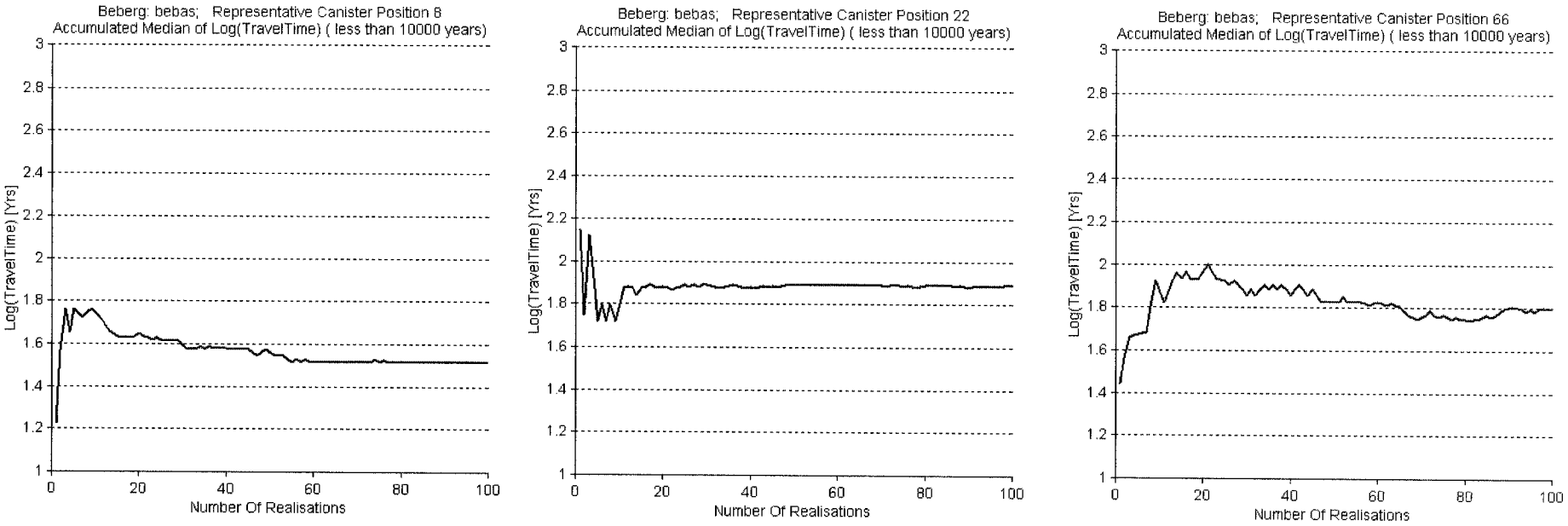

Figure 4.5-5. Monte Carlo stability at starting positions 8, 22 and 66 in the Beberg Base Case. Cumulative median log_{10} travel time versus number of realisations. Results for a flow porosity of $\varepsilon_f = 1 \times 10^{-4}$.

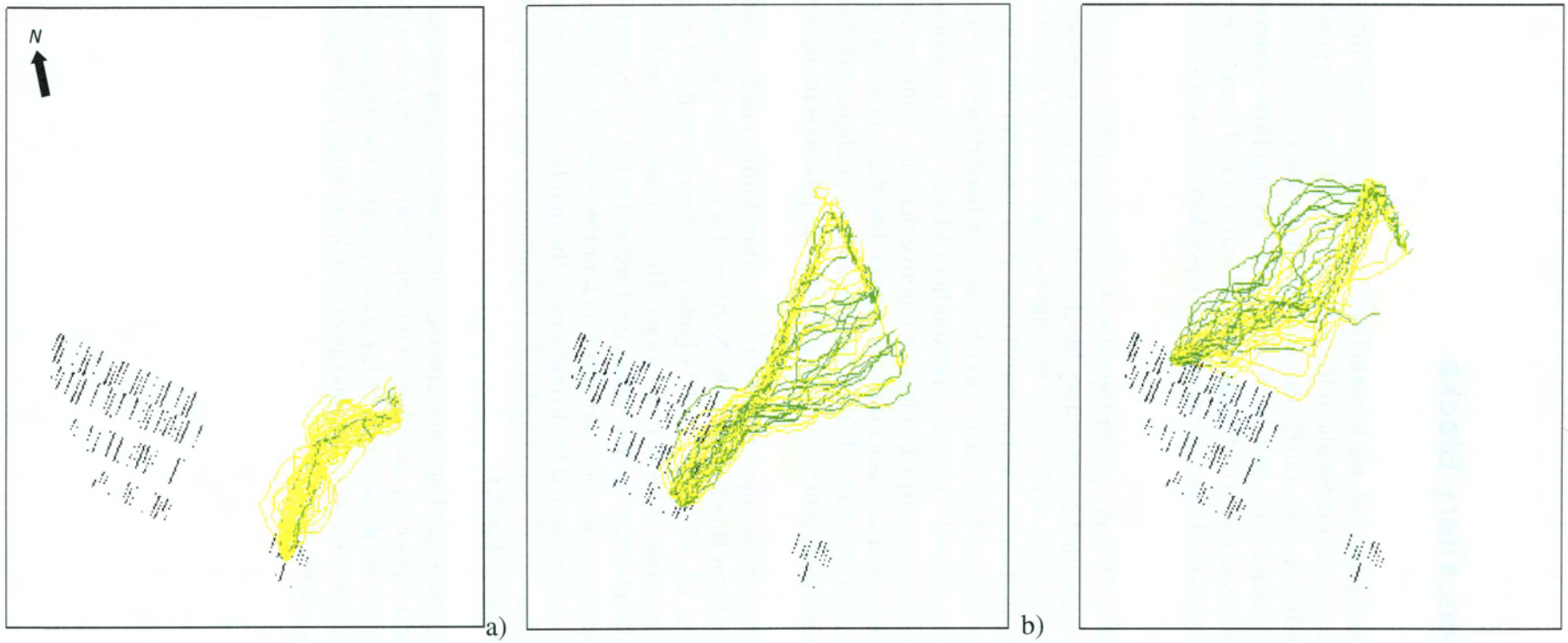

Figure 4.5-6. Stream tubes in the Beberg Base Case from starting position numbers a) 8, b) 22, and c) 66. Results for a flow porosity of $\varepsilon_f = 1 \times 10^{-4}$ *in the first 50 realisations.*

4.6 Repository Blocks

As discussed in Section 3.4, the hypothetical repository is divided into two blocks, with 11 starting positions in the Southern Rock Block and 109 starting positions in the Northern Rock Block. One much-discussed feature of the Beberg site is Zone 2, a subhorisontal fracture zone, and its effects on salinity and flow patterns in the Northern Rock Block. Because it is possible that Zone 2 may affect the repository performance, this study separates the Base Case results by repository block to see if any pattern can be observed.

Figures 4.6-1 and 4.6-2 present histograms of the $\log_{10}$ travel time and $\log_{10}$ canister flux, respectively, sorted by repository block. Table 4.6-1 presents the summary statistics for each block, which show that the median travel time for the Northern Block is 61 years, longer than the median travel time of 31 years for the Southern Block. The median canister flux of 1.13×10^{-3} m/yr for the Northern Block is lower than the median canister flux of 2.03×10^{-3} m/yr for the Southern Block. Although these differences suggest that the Northern Block is less conductive than the Southern Block, the Northern Block hydraulic conductivity is greater than that of the Southern Block. (Section 3.5.3). This indicates that the combination of gradient and Zone 2 reduce the canister flux and increase the travel time for starting positions in the Northern Block.

Table 4.6-1 indicates that the variances of $\log_{10}$ travel time and $\log_{10}$ canister flux are lower in the Southern Block than in the Northern Block. This may be a consequence of starting positions 12, 15, 18, 20, and 24 lying near Zone 8, so that they are effectively inside the fracture zone in some realisations. These create a few extreme values in the distribution and thus increase the variance estimates (note the long upper tail of the $\log_{10}$ canister flux histogram for the Northern Block in Figure 4.6-2). However, interpreting these statistics is complicated by differences in the numbers of stream tubes used to estimate the variances for each block (i.e., 11 starting positions in the Southern Block and 109 the Northern Block).

These results suggest that hydraulic conductivity alone may not be a sufficient criterion for the siting of a repository, and that favourable conditions may also depend on the hydraulic gradient and the location of highly conductive fracture zones. On the other hand, the differences in results by repository block are relatively small in the context of performance assessment.

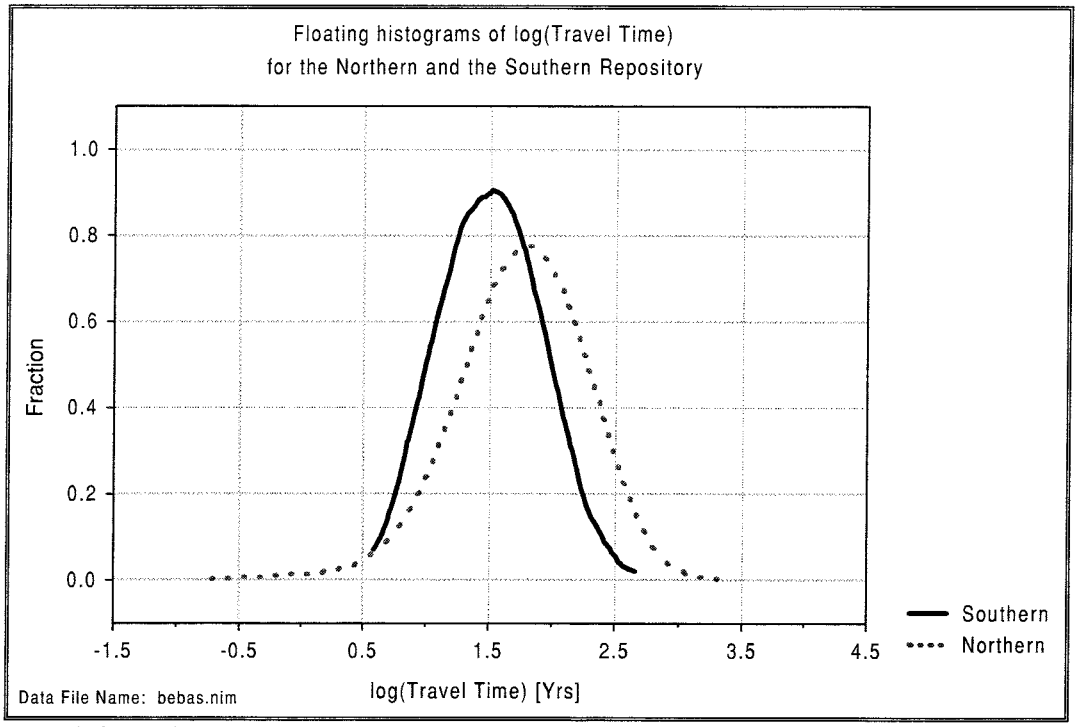

Figure 4.6-1. Floating histogram of $\log_{10}$ travel time for the Beberg Base Case, by repository block. Results for 100 realisations of 120 starting positions and a flow porosity of $\varepsilon_f = 10^{-4}$.

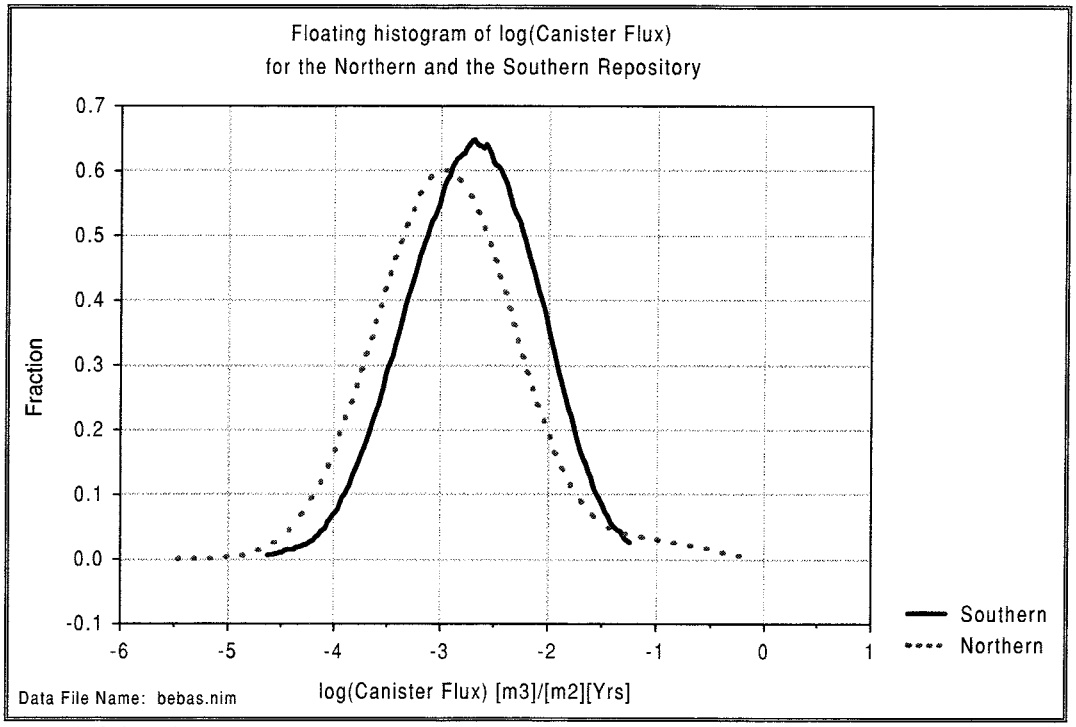

Figure 4.6-2. Floating histogram of $\log_{10}$ canister flux for the Beberg Base Case, by repository block. Results for 100 realisations of 120 starting positions.

Table 4.6-1. Summary statistics by repository block in the Base Case. Results for 100 realisations, a flow porosity of $\varepsilon_f = 1x10^{-4}$ and flow-wetted surface $a_r = 1.0\ m^2/(m^3\ rock)$. Approximately 0.7% of the stream tubes fail to exit the upper surface. Statistics in bold are discussed in text.

	Repository Block	
Log_{10} Travel Time for times < 10,000 years (years)	**Southern**	**Northern**
Mean	1.506	1.740
Median	**1.493**	**1.783**
Variance	**0.091**	**0.209**
5th percentile	1.029	0.973
25th percentile	1.297	1.491
75th percentile	1.704	2.040
95th percentile	2.015	2.380
Log_{10} Canister Flux for all times (years)		
Mean	-2.715	-2.913
Median	**-2.693**	**-2.947**
Variance	**0.284**	**0.434**
5th percentile	-3.588	-3.900
25th percentile	-3.080	-3.341
75th percentile	-2.338	-2.545
95th percentile	-1.883	-1.814
Log_{10} F-ratio for times < 10,000 years (year/m)		
Mean	5.506	5.740
Median	**5.493**	**5.783**
Variance	**0.091**	**0.209**
5th percentile	5.029	4.973
25th percentile	5.297	5.491
75th percentile	5.704	6.040
95th percentile	6.015	6.380

5 Variant Cases

Table 5-1 summarises the Base Case (the reference case for comparison) and the five variant cases evaluated for this study. Each variant corresponds to a possible interpretation of site hydrogeology, and is evaluated to address the acknowledged uncertainties. These are summarised as:

- Base Case (presented in Section 4.0, this represents the expected site conditions);
- Variant 1: Boundary conditions from a salinity dependent regional model via environmental heads;
- Variant 2: Alternative conductive features;
- Variant 3: Alternative hydrogeologic interpretation; and
- Variant 4: Simulation with a deterministic hydraulic conductivity field.

The Base Case is discussed thoroughly in Section 4. The motivation and reasoning for each case is provided in the introduction of the sections corresponding to each case. The results of each variant are briefly compared to the Base Case in terms of the median and interquartile ranges of the performance measures. A simple nonparametric hypotheses test determines the statistical significance of the similarity of the performance measure distributions (Appendix A.2).

Table 5-1. Summary of Base Case and Variant Cases analysed in Beberg site-scale modelling study.

Case	Boundary conditions	Cell size	Hydraulic conductivity field				Conditioning on K	Remarks
	Obtained from		Scaling rule	Geostatistical model	Hydraulic units	EDZ/Backfill	on heads	
Base Case	**Freshwater, AltK case (Appendix B.1)**	**35 m**	**Walker et al.**	**Exponential isotropic Variance 0.69 Practical range 247 m**	**Regional AltK case rescaled to 35 m (both SRD and SCD with depth dependence**	**No/10^{-10} m/s**	**No**	
Variant 1 Alternative Boundary Conditions	Salinity Dependent as Environmental Head, AltK case (Appendix B.2)				Same as Base Case			Same as Base Case
Variant 2 Alternative Conductive Features	Freshwater, AltK + additional zones (Appendix B.3)				Same as Base Case + 11 Additional structures			Additional zones suggested by Saksa and Nummela, 1998.
Variant 3 Alternative Hydrogeologic Interpretation	Salinity Dependent as Environmental Head, Regional Base Case (Appendix B.2)				Regional Base Case of Hartley et al. (1998)			
Variant 4 Deterministic	Same as Base Case			Variance=0	Upscaled from Base Case			Deterministic case

5.1 Alternative Boundary Conditions

As was noted in Section 3.0, this study uses a nested modelling approach, with a regional model providing the site-scale boundary conditions. Hartley et al. (1998) originally included the salinity dependence in the simulations, and found that the effects of salinity could be dramatic. However, HYDRASTAR is unable to simulate salinity, and therefore the Hartley et al. (1998) regional model cannot be used directly to provide boundary heads for the site-scale model. For the purposes of this study, the Base Case uses boundary conditions derived from a supplemental simulation of the regional model case AltK with freshwater conditions (Appendix B.1).

Hartley et al. (1998) found that the flow field is markedly different under salinity-dependent versus freshwater conditions. In the salinity-dependent regional model, the groundwater flow field is oriented downward near the repository, resulting in longer travel paths and travel times. This suggests that it is important to evaluate the sensitivity of the results to alternative boundary conditions. One alternative method for calculating boundary heads is to use the regional model of Hartley et al. (1998) under salinity dependent conditions, converting the resulting boundary pressures and salinities to environmental heads.

This variant uses the same structural model and representation of stochastic hydraulic conductivities as the Base Case. The boundary conditions are taken directly from the Hartley et al. (1998) regional modelling case named AltK, which provides the salinity-dependent heads that are then converted to environmental heads. The details of the conversion to environmental heads are given in Appendix B.2.

Figure 5.1-1 presents the stream tubes from the first realisation of this variant, illustrating the consequences of changing to boundary conditions derived from a salinity-dependent regional model. Similar to the Hartley et al. (1998) regional model (case AltK), the groundwater flow pattern around the repository is generally downward, resulting in 92.2% of the stream tubes exiting the bottom boundary of the model. A small percentage of the stream tubes (7.4%) exits the upper model surface, most of which originate from the starting positions in the Southern Rock Block. As discussed in the Base Case, stream tubes that fail to exit the upper model surface are assigned the default maximum travel time of 10,000 years. Thus, although Table 5.1-1 indicates that the median travel time is decreased to 35 years in this variant from 56 years in the Base Case, this statistic is somewhat misleading, because 92.2% of the results are censored by the default maximum (Figure 5.1-2).

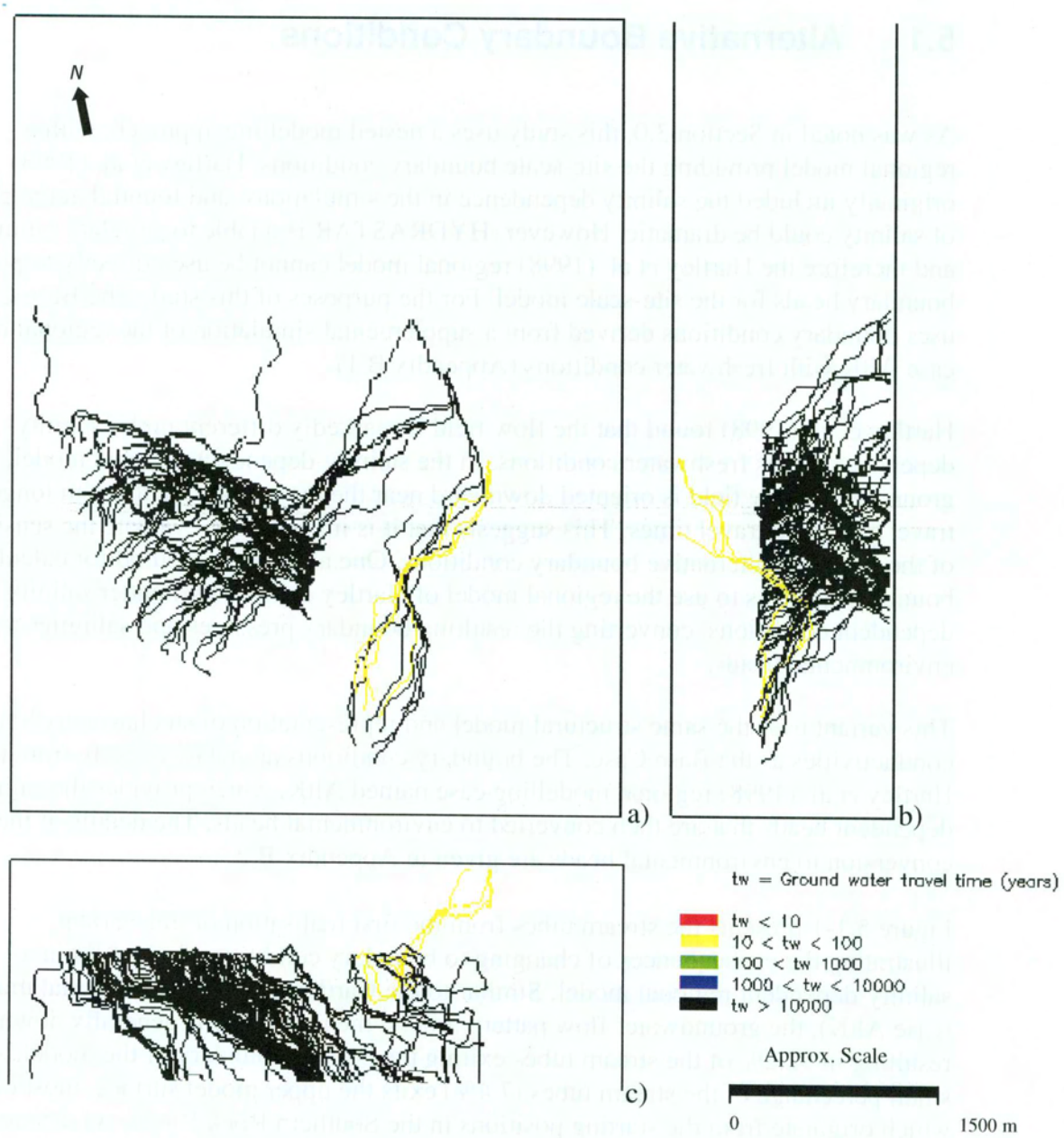

Figure 5.1-1. Stream tubes in realisation 1 of Beberg Variant 1 (alternative boundary conditions), in a) plan view (looking downward), b) elevation view from east and c) elevation view from south. Results for 120 starting position and a flow porosity of $\varepsilon_f = 1x10^{-4}$.

The travel time for the stream tubes failing to exit the upper model surface can be post-processed from the HYDRASTAR output files, as are presented in Table 5.1-1. For the stream tube escaping the bottom boundary, the median travel time is 37 years. For stream tubes escaping the western boundary, the median travel time is 16 years. With respect to the site-scale model, the fate of these escaping stream tubes is unknown. However, the supplemental regional model used to create the boundary conditions for this study indicated that the range of travel times to the limits of the regional model domain would be from 30 to 760 years (Appendix B.5).

Figure 5.1-3 presents the distribution of $\log_{10}$ canister flux, which has statistically significant differences from the distribution of $\log_{10}$ canister flux of the Base Case (Appendix A.2). The median canister flux of this variant is 1.8×10^{-3} m/yr, slightly increased relative to the Base Case. Figure 5.1-4 presents a plot of $\log_{10}$ canister flux versus $\log_{10}$ travel time, which suggests that they are inversely correlated.

Table 5.1-1. Summary statistics for Beberg Variant 1 (alternative boundary conditions). Results for 100 realisations, 120 starting positions, a flow porosity of $\varepsilon_f = 1x10^{-4}$ and flow-wetted surface $a_r = 1.0$ m^2/(m^3 rock). Approximately 92.2% of the stream tubes fail to exit the upper surface. Statistics in bold are discussed in text.

	Stream tubes exiting upper surface			Stream tubes failing to exit upper surface	
	$\log_{10} t_w$ Travel Times < 10,000 yr	**$\log_{10} q_c$**	**$\log_{10}$ F-ratio Travel Times < 10,000 yr**	**$\log_{10} t_w$ (to bottom boundary)**	**$\log_{10} t_w$ (to West boundary)**
Mean	1.491	-2.730	5.491	1.561	1.269
Median	**1.544**	**-2.744**	**5.544**	1.569	1.209
Variance	**0.259**	**0.397**	**0.259**	0.191	0.157
5th percentile	0.526	-3.722	4.526	0.839	0.669
25th percentile	1.279	-3.147	5.279	1.260	1.049
75th percentile	1.794	-2.349	5.794	1.860	1.481
95th percentile	2.162	-1.697	6.162	2.274	2.004

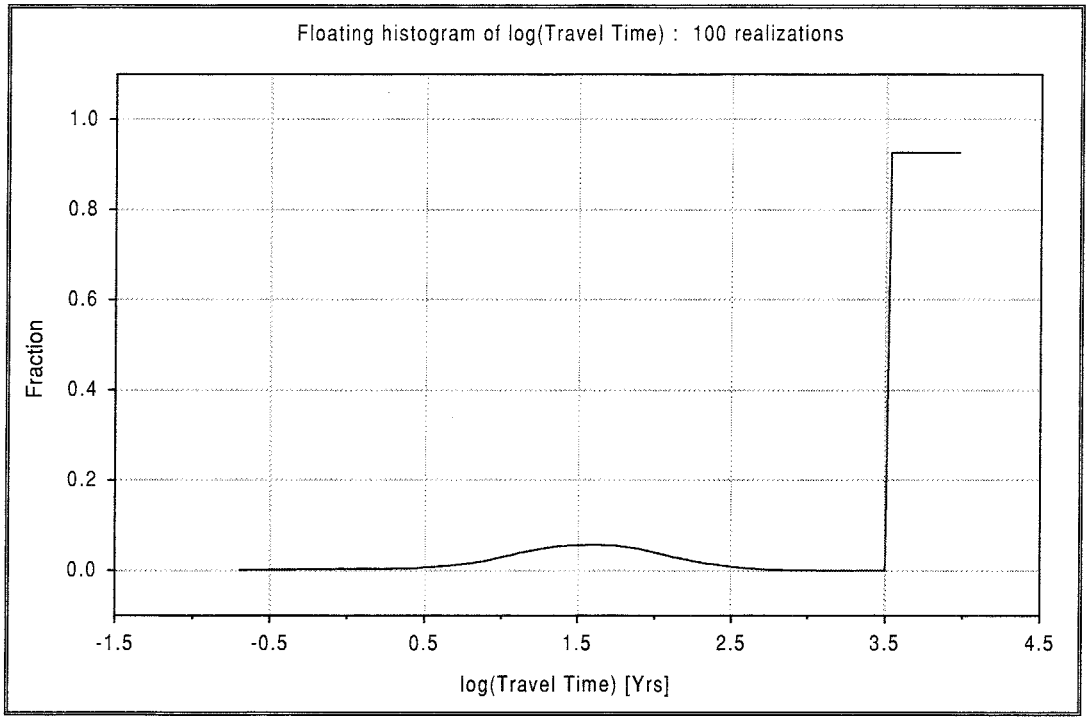

Figure 5.1-2. Floating histogram of log_{10} travel time for Beberg Variant 1 (alternative boundary conditions). Results for 100 realisations of 120 starting positions and a flow porosity of $\varepsilon_f = 1x10^{-4}$.

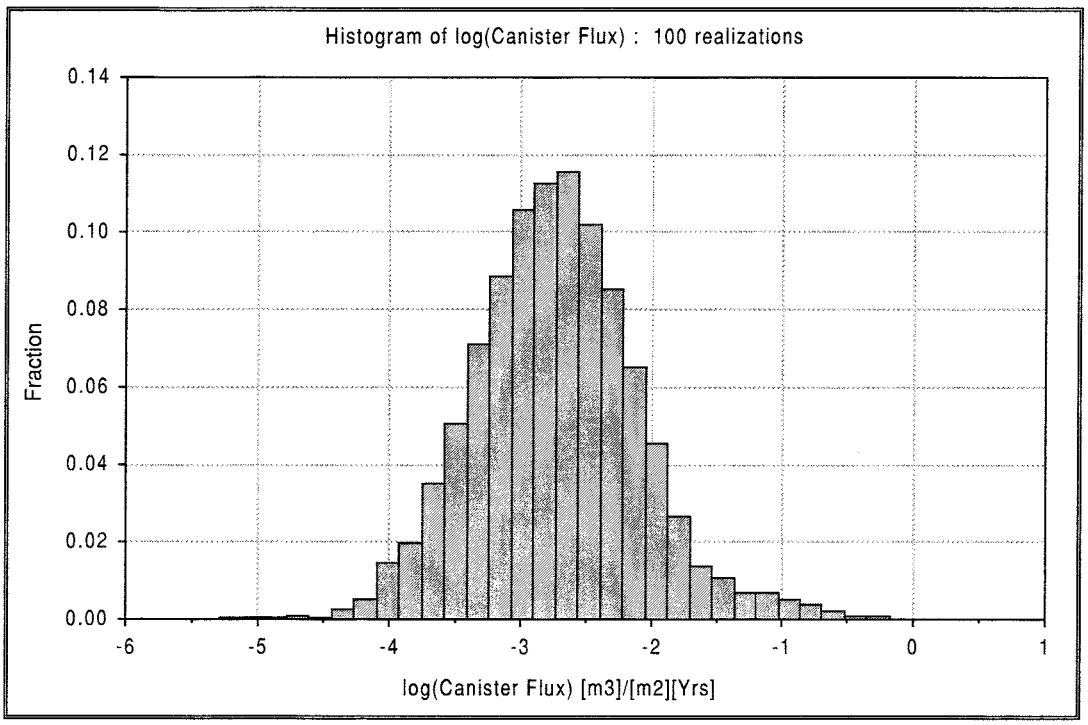

Figure 5.1-3. Relative frequency histogram of log_{10} canister flux for Beberg Variant 1 (alternative boundary conditions). Results for 100 realisations of 120 starting positions.

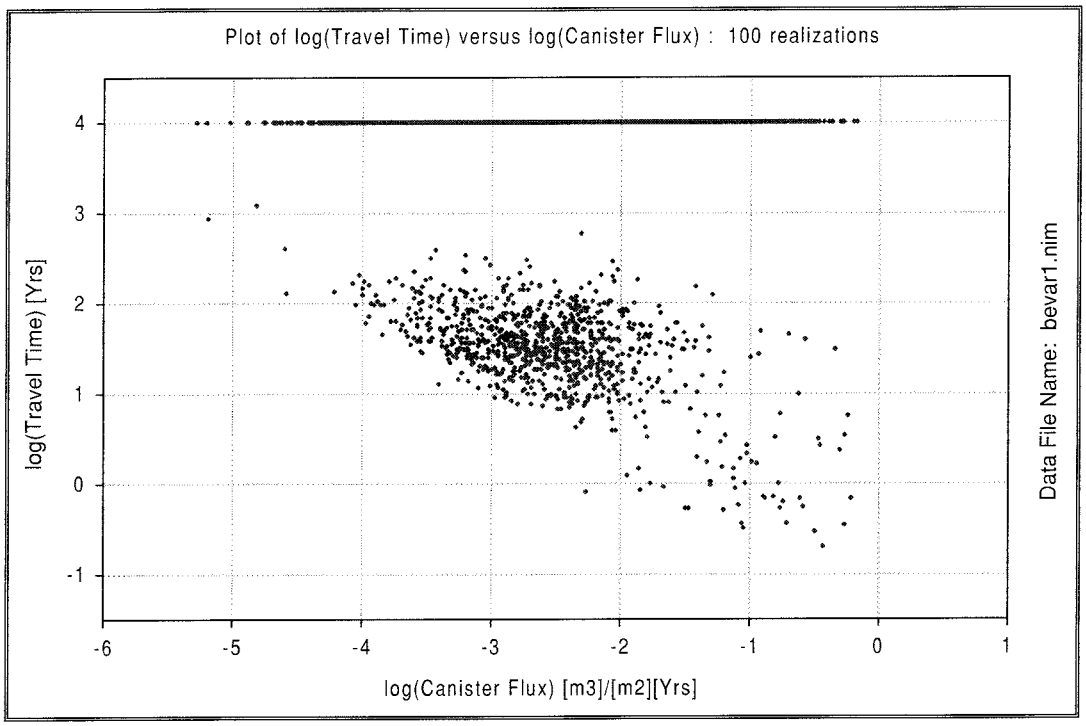

Figure 5.1-4. Log_{10} travel time versus log_{10} canister flux for Beberg Variant 1 (alternative boundary conditions). Results for 100 realisations of 120 starting positions and a flow porosity of $\varepsilon_f = 1x10^{-4}$.

Table 5.1-2 summarises the boundary flows for this variant. Similar to the Base Case, there is a regional mass balance residual of approximately 50%, and the site-scale model tends to overpredict the flows of the regional model by 50%. Although the regional residual is relatively large, limiting further comparison, the results suggest that the nested modelling and possibly also the upscaling of hydraulic conductivity may be valid only in the most general sense (see discussion in Sections 4.2 and 4.3.5).

Table 5.1-2. Boundary flow consistency for Beberg Variant 1 (alternative boundary conditions), regional model versus site-scale model.

Model Surface	Net Flow Through Site Model Surfaces ($m^3/s \times 10^{-3}$) Regional (AltK+env. head)	Variant 1 (5 realisations)	Base Case (5 realisations)
West	6.87 (in)	9.385 (in)	8.602 (in)
East	4.13 (out)	3.363 (out)	2.870 (out)
South	2.31 (in)	2.926 (in)	3.600 (in)
North	3.61 (out)	5.279 (out)	4.154 (out)
Bottom	0.17 (out)	3.094 (in)	4.967 (in)
Top	2.32 (in)	6.732 (out)	10.130 (out)
Total Inflow	11.50	15.404	17.169
Total Outflow	7.91	15.374	17.154
Mass Balance (In – Out)	3.59	0.0298	0.0156

Figure 5.1-5 shows the exit locations for all starting positions in the single realisation of the site-scale model. As discussed previously, most of the stream tubes exit the lower surface of the model. Zone 1 and the Imundbo Zone are major travel paths, organising the exit locations.

Although the large number of lost particles is at first disappointing, Hartley et al. (1998) found that the present-day salinity at the site is a transient phenomenon, slowly evolving toward freshwater conditions (Section 3.3). Thus, although this variant is believed to be representative of present-day conditions, the long-term flow field at the site is thought to be most like that of the Base Case.

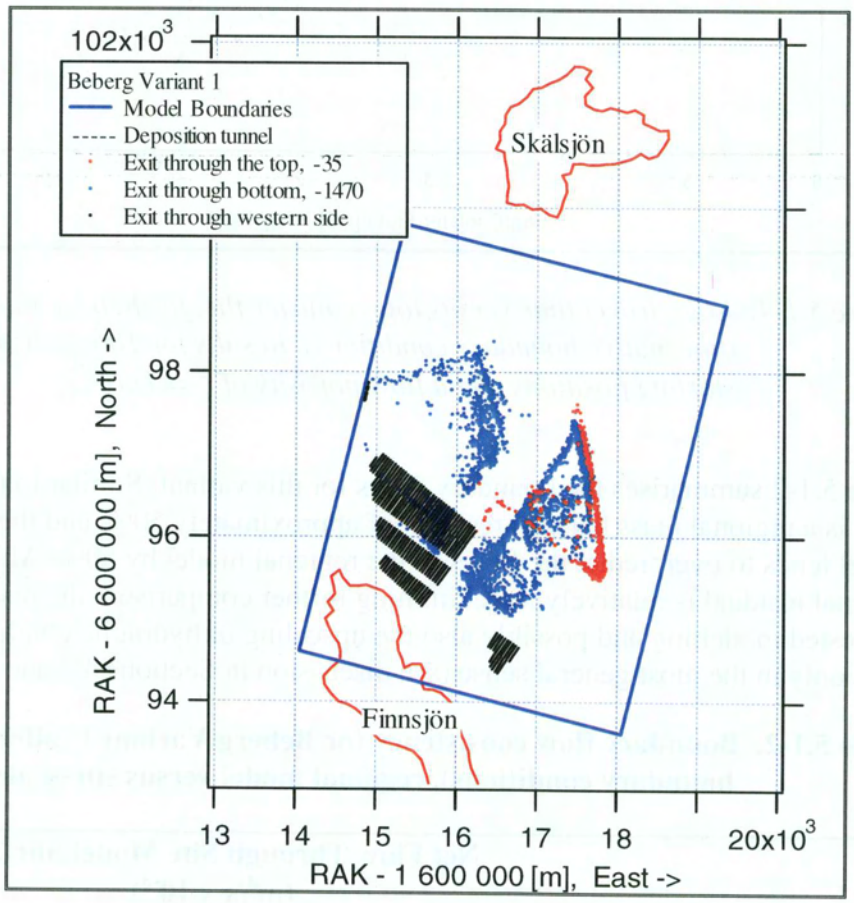

Figure 5.1-5. Exit locations for Beberg Variant 1 (alternative boundary conditions). Results for 100 realisations of 120 starting positions (offset RAK coordinates in metres).

5.2 Alternative Conductive Features

The site characterisation report of Andersson et al. (1992) presented lineament maps that indicated several possible fracture zones in addition to the zones used in the Base Case structural model of this study. Also, Zones 6, 9 and 10 have inferred conductivities equal to or lower than the conductivities of the rock mass and are consequently omitted from the Base Case (Section 3.5.4). In addition to zones suggested as possible by Andersson et al. (1992), Saksa and Nummela (1998) suggested that several additional features might reasonably be interpreted as conductive fracture zones. The structural model and the inferred properties of fracture zones are uncertain, and it is reasonable to examine the effects of hypothetical additional conductive features.

This variant case evaluates the possibility that Zones 6, 9 and 10, and the zones suggested by Saksa and Nummela (1998) are conductive fracture zones, similar to the deterministic zones (SCD) of the Base Case. All of these eleven additional features are assumed to have a hydraulic conductivity equal to the average of the conductive features of the Base Case, with locations and orientations taken from Saksa and Nummela (1998). Because the additional conductive features might change the boundary fluxes and heads, this variant requires a slightly different regional model than that used by the Base Case. The regional model of Hartley et al. (1998) was rerun under freshwater conditions with the additional features to provide site-scale boundary conditions for this variant (Appendix B.3). The variant is otherwise unchanged from the Base Case, and uses 100 realisations.

Zones A through G are included as suggested by Saksa and Nummela (1998), modelled as vertical zones with the widths inferred as in Table 5.2-1. Zone H is assumed to be most similar to Zone 2, inferred as a sub-horisontal feature of 10 m thickness, limited to the Southern Rock Block (i.e., delimited by Zones 3, 1, 5, 14 and 13). It is inferred to have the same strike/dip as Zone 2 and is located below the deepest borehole in the Southern Rock Block (i.e., approximately 250 m below the plane defined by the extention of Zone 2 to the Southern Block). The conductivity of Zones A-G is taken as the average of the values from the borehole measurements. Since Zone H is a hypothetical subhorisontal zone, it is suggested to take its properties from Zone 2.

Table 5.2-1. Widths and conductivities features inferred from Saksa and Nummela (1998) for Beberg Variant 2 (alternative conductive features). Conductivities are given for the zones when modelled as 35 m wide features.

Zone	Width (m)	Arithmetic Mean of Log_{10} K (m/s) at 35 m	
		0 to –100 m depth	Below –100 m
A	5	-6.09	-7.18
B	5	-6.09	-7.18
D	5	-6.09	-7.18
F	5	-6.09	-7.18
C	5	-6.09	-7.18
E	5	-6.09	-7.18
G	25	-6.09	-7.18
H	10	-4.30	-5.39

Figure 5.2-1 presents the HYDRASTAR representation of the additional fracture zones used in this variant, and the additional zones together with the fracture zones used in the Base Case. These figures illustrate that the additional features are very close to the hypothetical repository, with two zones running directly through the repository block. The utility program TRAZON (Appendix E) found that starting position numbers 23, 44, and 120 fall into the additional zones of this variant (Figure 3.4-2). Figure 5.2-2 presents one realisation of the resulting hydraulic conductivity field.

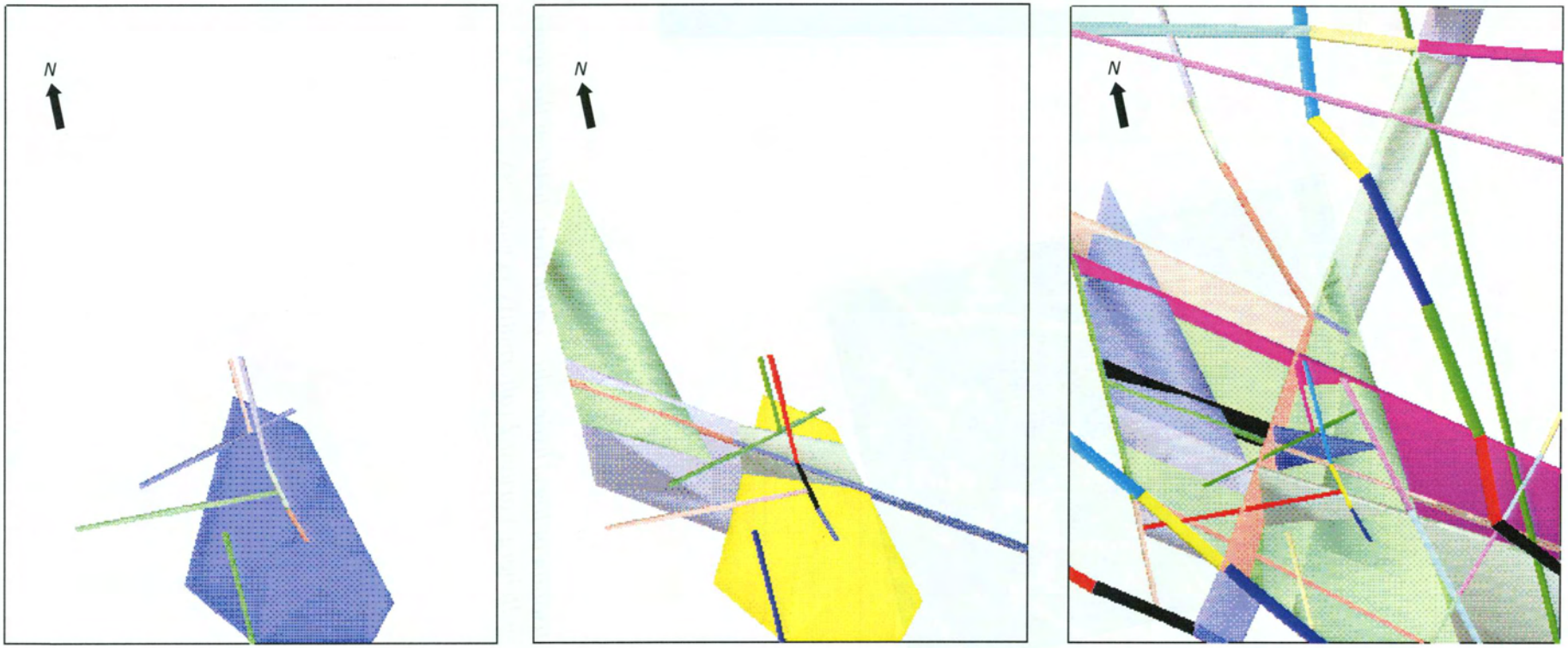

Figure 5.2-1. Schematic illustration of conductive zones used in Beberg Variant 2 (alternative conductors). Plan views of a) zones suggested by Saksa and Nummela (1998), b) Saksa and Nummela (1998) and Zones 6, 9, and 10; and c) all zones used in this variant.

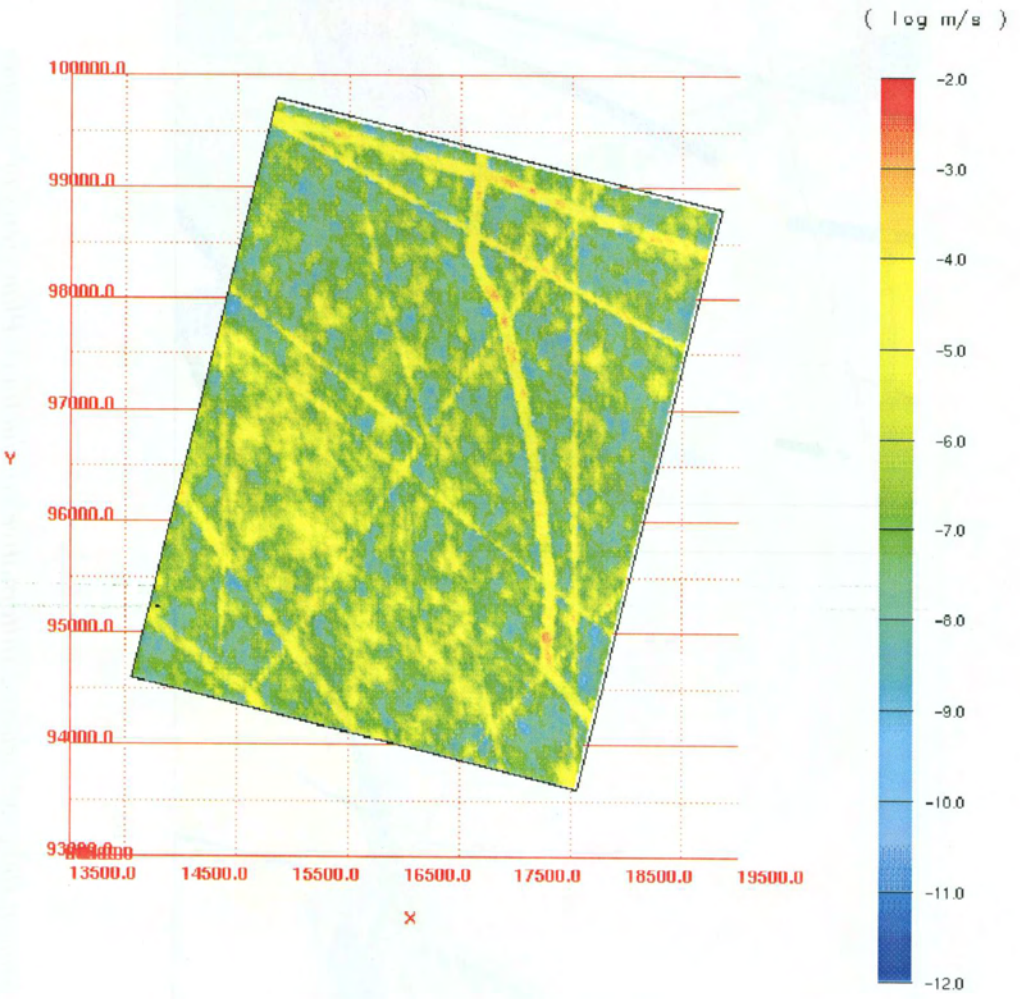

Figure 5.2-2. One realisation of $\log_{10}$ hydraulic conductivity field on the upper model surface of Beberg Variant 2 (alternative conductors)

Table 5.2-2 summarises the effects of including the additional conductive zones. In comparison to the Base Case, the median travel time is slightly reduced from 56 to 53 years, and the variance of $\log_{10}$ travel time is slightly increased from 0.203 to 0.216. These results suggest that some of the stream tubes are intercepted by conductive features, decreasing the median of travel time while increasing the variance of $\log_{10}$ travel time. The resulting $\log_{10}$ travel time distribution for this variant is markedly skewed and has statistically significant differences from the comparable Base Case distribution (Figures 5.2-3 and 5.2-4; see also Appendix A.2). Only 0.42% of the stream tubes fail to exit the upper surface of the model.

Table 5.2-2 also summarises the results with respect to the canister fluxes. The median canister flux is slightly decreased from 1.2×10^{-3} to 1.1×10^{-3} m/year. (See also Section 3.4). This results in the $\log_{10}$ canister flux distribution having statistically significant differences from that of the Base Case or the remaining variants (Figure 5.2-5, Appendix A.2). Figure 5.2-6 shows that the travel times and canister fluxes are slightly correlated in this variant.

Table 5.2-2. Summary statistics for Beberg Variant 2 (alternative conductive features). Results for 100 realisations, of 120 starting positions, a flow porosity of $\varepsilon_f = 1x10^{-4}$ and flow-wetted surface $a_r = 1.0$ m^2/(m^3 rock). Approximately 0.42% of the stream tubes fail to exit the upper surface. Statistics in bold are discussed in text.

	All values			**Travel Times > 10,000 years deleted**		
	$\text{Log}_{10}\ t_w$	**$\text{Log}_{10}\ q_c$**	**Log_{10} F-ratio**	**$\text{Log}_{10}\ t_w$**	**$\text{Log}_{10}\ q_c$**	**Log_{10} F-ratio**
Mean	1.692	-2.920	5.692	1.682	-2.918	5.682
Median	1.726	**-2.952**	5.726	**1.725**	-2.951	**5.725**
Variance	0.237	**0.425**	0.237	**0.216**	0.426	**0.216**
5th percentile	0.905	-3.914	4.905	0.903	-3.911	4.903
25th percentile	1.421	-3.344	5.421	1.419	-3.344	5.419
75th percentile	1.993	-2.547	5.993	1.990	-2.546	5.990
95th percentile	2.363	-1.850	6.363	2.349	-1.846	6.349

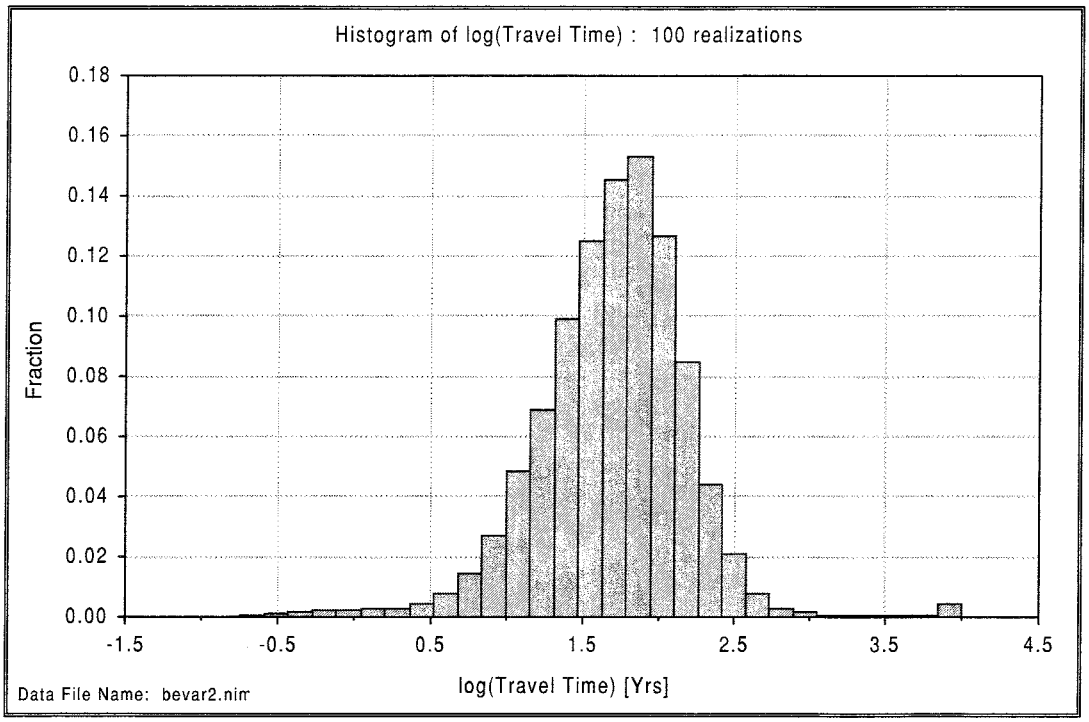

Figure 5.2-3. Relative frequency histogram of log_{10} travel time for Beberg Variant 2 (alternative conductors). Results for 100 realisations of 120 starting positions and a flow porosity of $\varepsilon_f = 1x10^{-4}$.

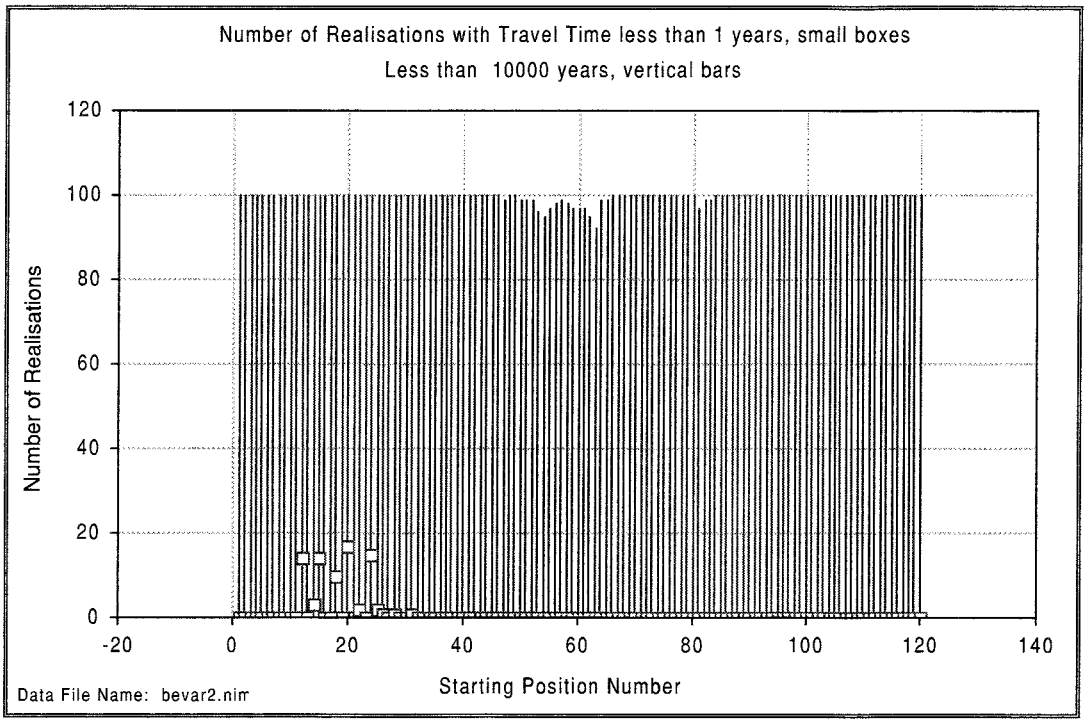

Figure 5.2-4. Number of realisations with travel times less than 1 year (squares) and 10,000 years (lines) by stream tube number for Beberg Variant 2 (alternative conductors). Results for 100 realisations and a flow porosity of $\varepsilon_f = 1x10^{-4}$

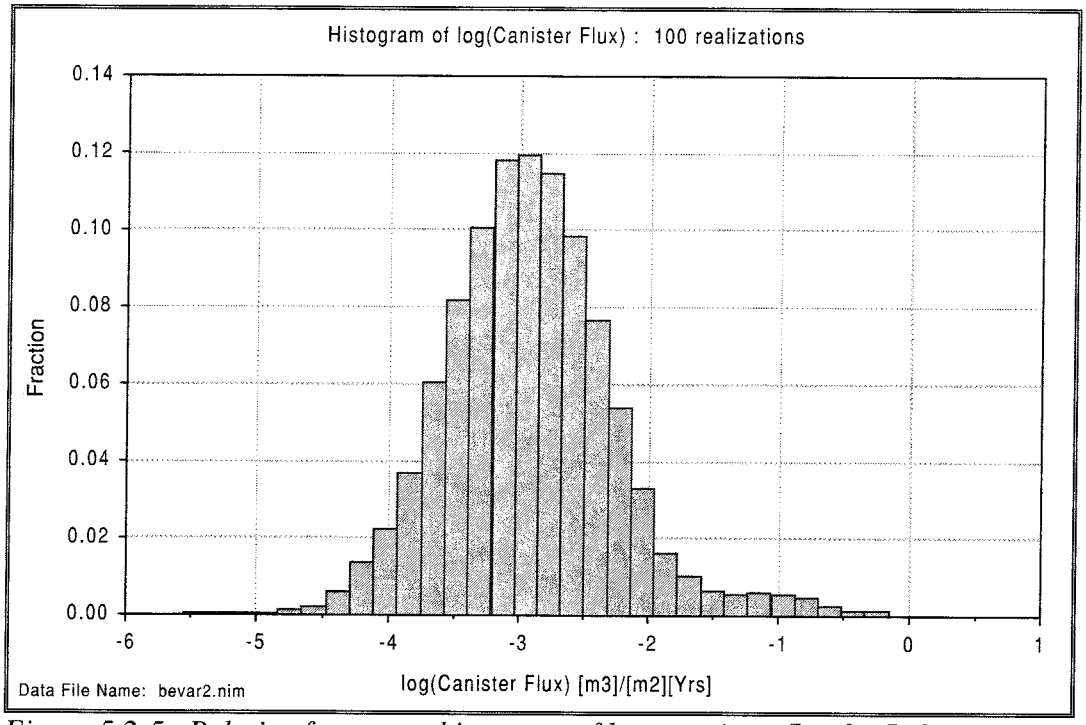

Figure 5.2-5. Relative frequency histogram of log_{10} canister flux for Beberg Variant 2 (alternative conductors). Results for 100 realisations of 120 starting positions.

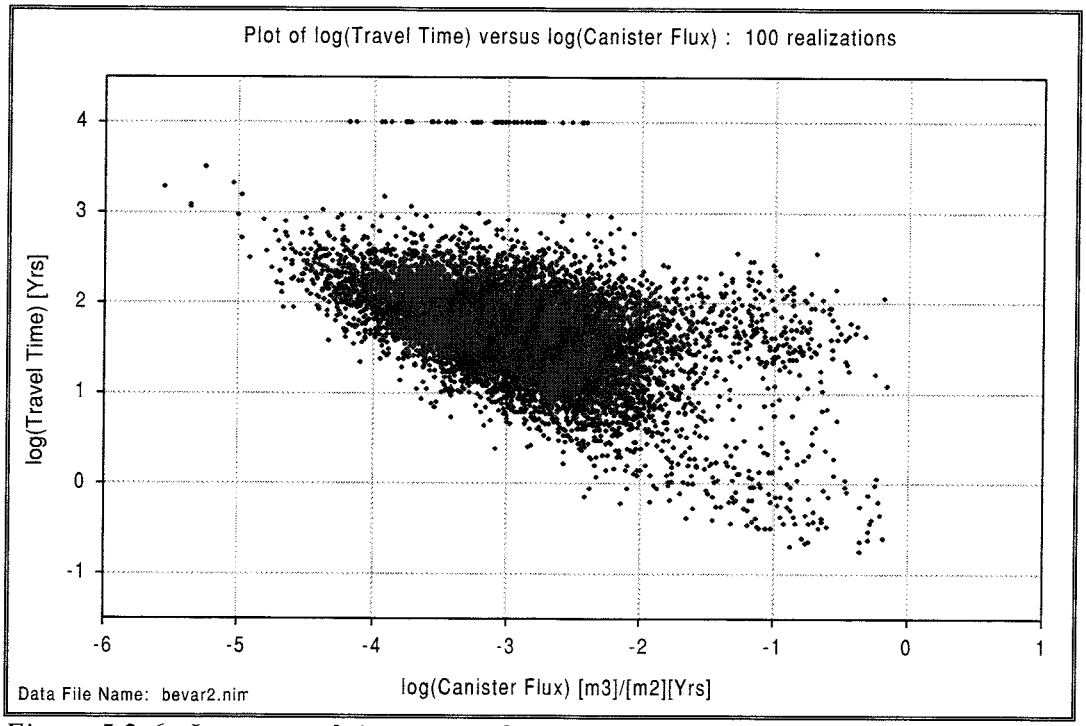

Figure 5.2-6. Log_{10} travel time versus log_{10} canister flux for Beberg Variant 2 (alternative conductors). Results for 100 realisations of 120 starting positions and a flow porosity of $\varepsilon_f = 1x10^{-4}$.

Table 5.2-3 summarises the boundary flows for this variant. Similar to the Base Case, there is a regional mass balance residual of approximately 50%, and the site-scale model tends to overpredict the flows of the regional model by 50%. The regional residual is approximately equal to the net flow over any of the regional model surfaces, limiting further comparison of the nested models. However, this comparison suggests that the nested modelling and upscaling are valid only in the most general sense. Some of this discrepancy between the models may be attributable to mismatches in zone geometries or to the upscaling of hydraulic conductivities (see Sections 4.2 and 5.4).

Table 5.2-3. Boundary flow consistency for Beberg Variant 2 (alternative conductive features), regional model versus site-scale model.

Model Surface	Net Flow Through Site Model Surfaces ($m^3/s \times 10^{-3}$)		
	Regional (AltK + Saksa + freshwater)	**Variant 2 (5 realisations)**	**Base Case (5 realisations)**
West	6.24 (in)	8.602 (in)	8.602 (in)
East	3.51 (out)	2.972 (out)	2.870 (out)
South	2.63 (in)	4.057 (in)	3.600 (in)
North	3.44 (out)	4.214 (out)	4.154 (out)
Bottom	0.17 (in)	5.817 (in)	4.967 (in)
Top	1.23 (in)	11.263 (out)	10.130 (out)
Total Inflow	10.27	18.476	17.169
Total Outflow	6.95	18.449	17.154
Mass Balance (In – Out)	3.32	0.0277	0.0156

Figure 5.2-7 presents the exit locations. In contrast to the Base Case, a number of stream tubes from the south repository block travel almost vertically to exit at the ground surface (Figure 5.2-8). That is, under the influence of the additional fracture zones, the exit locations for the south repository block have shifted dramatically to the area immediately north of the south block. Although the discharge areas change appreciably, the number of stream tubes failing to exit the upper model surface is 0.42%, little different from the Base Case. Thus, although the $\log_{10}$ travel time and $\log_{10}$ canister flux distributions have statistically significant differences from the comparable Base Case distributions (Appendix A.2), there is little practical difference in the median performance measures as a result of including additional fracture zones.

While this variant has explored the uncertainty of the existence of certain fracture zones, it has not specifically examined the properties of the fracture zones. As discussed in Section 3.5.1 the inference of hydraulic conductivity, width and extent are uncertain for the SCD representation. Variant 3 in part evaluates such uncertainties.

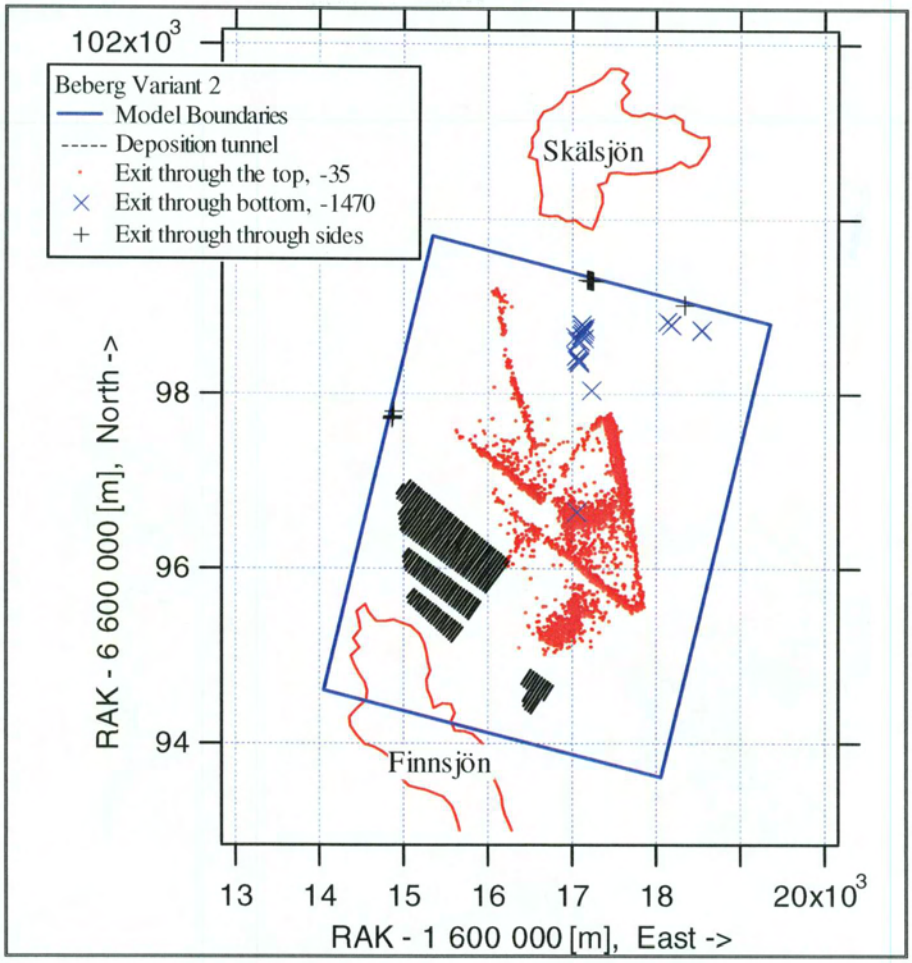

Figure 5.2-7. Exit locations in Beberg Variant 2 (alternative conductors). Results for 100 realisations of 120 starting positions (offset RAK coordinates in metres).

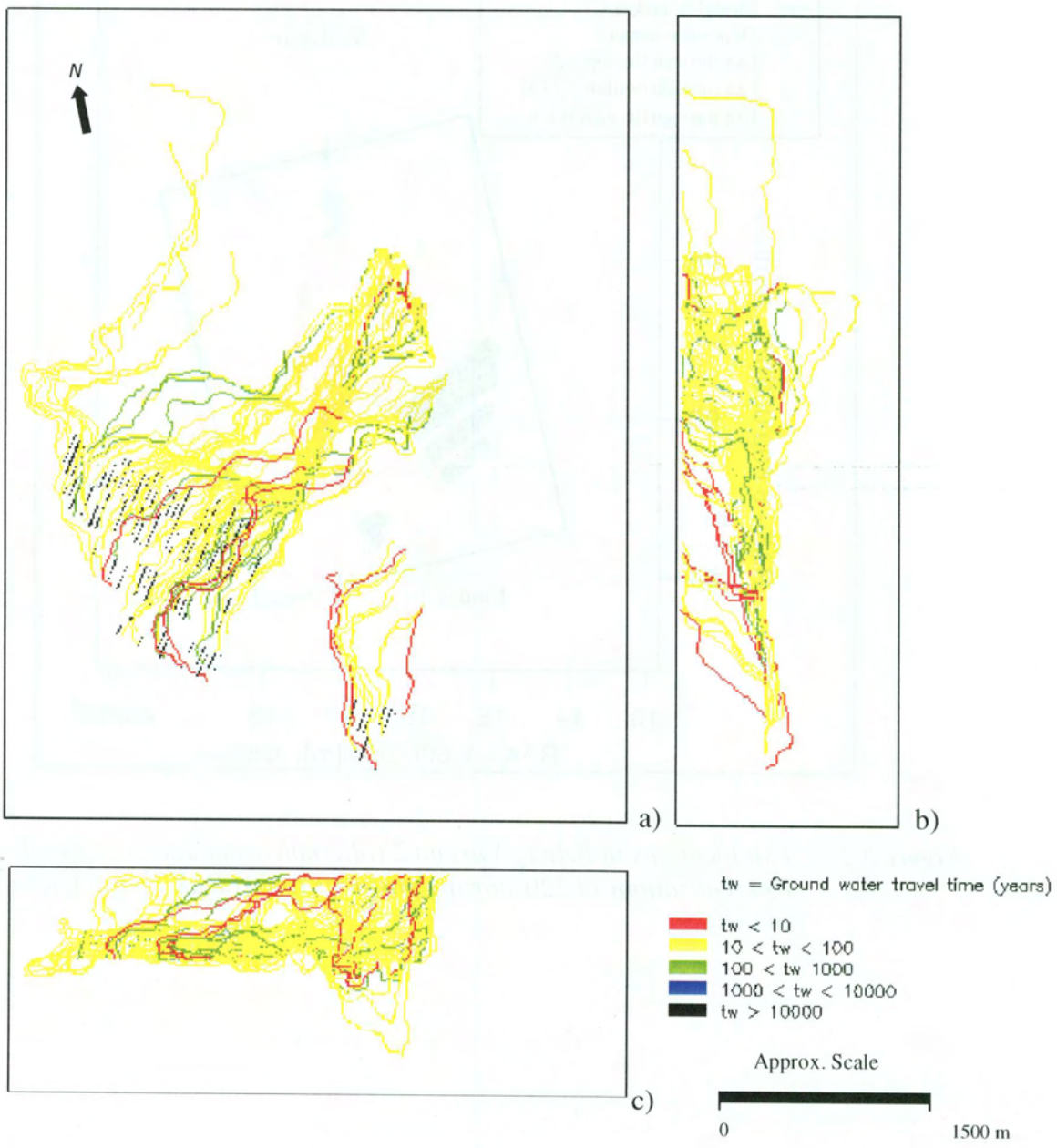

Figure 5.2-8. Stream tubes in realisation 1 of Beberg Variant 2 (additional conductors) in a) plan view (looking downward), b) elevation view from east and c) elevation view from south. Results for 120 starting positions and a flow porosity of $\varepsilon_f = 1x10^{-4}$.

5.3 Alternative Hydrogeologic Interpretation

As discussed in Section 3.5, the preliminary representation of the conductive fracture zones (SCD) given by Walker et al. (1997) results in excessive freshwater recharge at great depths. Several alternative representations of the fracture zones could be used to limit the recharge, such as the depth-dependent representation of fracture zone hydraulic conductivity used in the Base Case of this study (Section 3.5.1). This representation corresponds to the regional case AltK of Hartley et al. (1998). However, Hartley et al. (1998) found that the AltK regional case was only one of the possible cases that could reproduce the observed salinity at the site. For example, Hartley et al. (1998), used a qualitative calibration approach, trying to match the broad features of the measured salinity pattern and found that terminating certain vertical fractures before they penetrate Zone 2 could also reproduce the observed salinities at the site. This latter representation formed the basis of the regional base case in the Hartley et al. (1998) study. It is important to note that the regional base case did not necessarily use the expected values estimated from the hydraulic test data, but rather was the result of a qualitative calibration exercise to obtain the best fit of observations. The calibration was by no means unique, however, and thus there may be several other combinations of parameters that give as good or a better match to observed conditions.

This variant investigates the consequences of using the Hartley et al. (1998) regional base case with salinity dependence to calculate the boundary heads for the site-scale model. On the site scale, this variant uses the regional base case properties rescaled to 35 m. The pressures and salinities of the regional model are transferred to the site-scale model as environmental heads (Appendix B.4).

In the regional base case model, three zones (Zones 4, 12, and 14, the zones that delimit Zone 2 to the north, south and east) were truncated below Zone 2. In this site-scale variant, more detail is necessary, and therefore five zones are truncated below Zone 2 (Zone 5, 12, 14, 7W and 8). Zone 5 is the local zone that defines zone 2 to the north, instead of Zone 4 in the regional model. Zone 7W and Zone 8 are local zones that cross Zone 2 in the base case, and since there are no zones that cross Zone 2 in the regional model, they have to be terminated to avoid lateral transport in the area of Zone 2.

Similar to the regional base case representation, Zone 2 is split into three vertical layers with upper and lower layers of 25 m thickness and a relatively high hydraulic conductivity. The middle layer is 50 m thick and has a relatively low hydraulic conductivity, so that Zone 2 is effectively anisotropic in this variant (Figure 5.3-1). Note that the layer thickness is adjusted to the cell size, and hence all three layers were made 35 m thick.

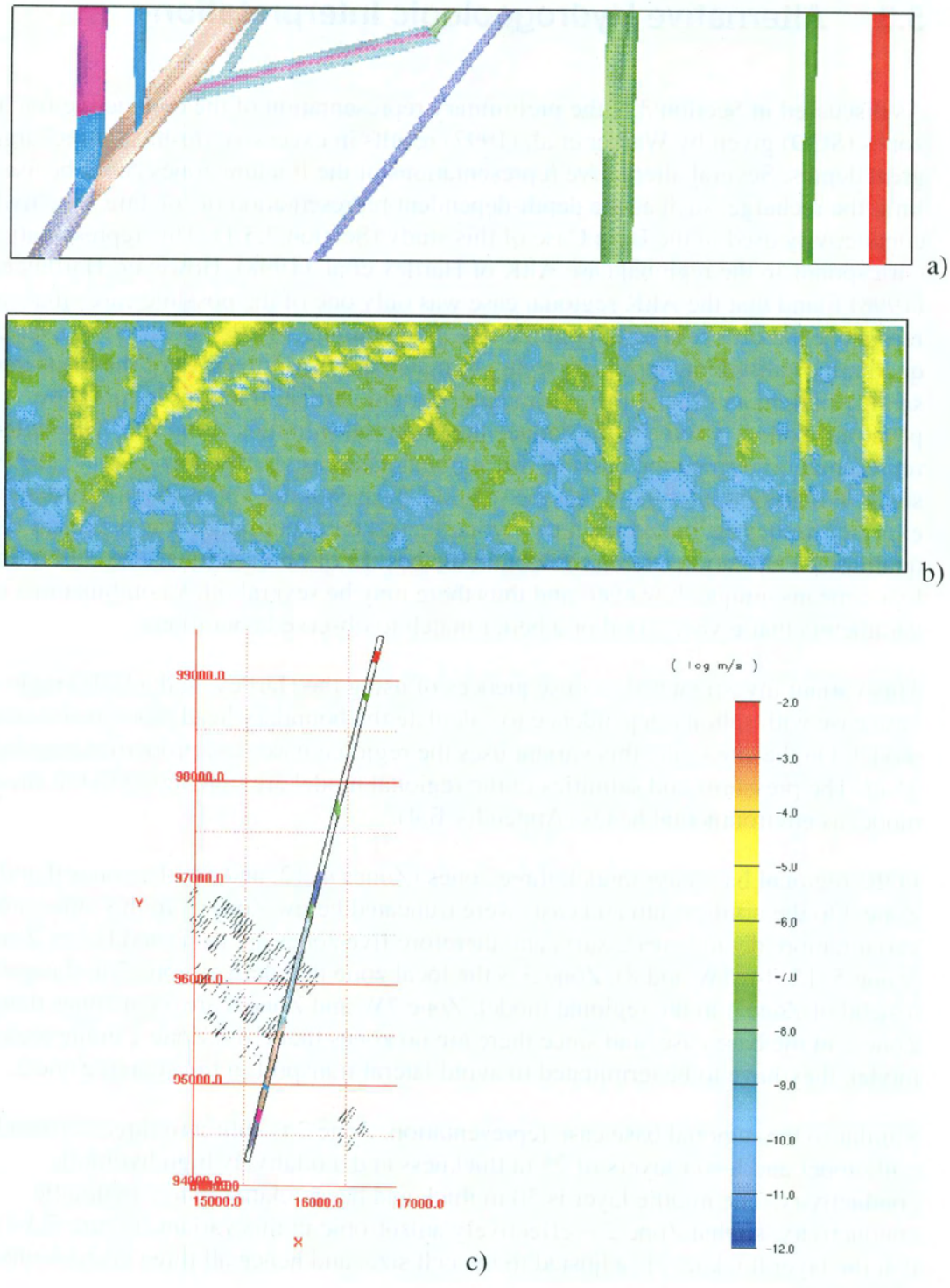

Figure 5.3-1. Conductive zones used in Beberg Variant 3 (alternative hydrogeologic interpretation) in a) a slice running approximately south - north, b) the corresponding conductivity field, and c), the location of the slice. (offset RAK coordinates in metres, hydraulic conductivity in m/s).

Figure 5.3-2 presents a schematic illustration of the depth dependence of hydraulic conductivity used in Variant 3. The fracture zones have a simple step decrease of –1.48 in the mean $\log_{10}$ K-values below –850 masl. The rock domain is divided into three layers: above –70 masl, -70 to -850 masl, and below –850 masl, with mean $\log_{10}$ K-values of –7.17, -8.20 and –8.58, respectively. Note that Hartley et al. (1998) divided the rock mass into four layers in the corresponding regional base case model. This is simplified to three layers in this variant, since the conductivities in the two middle layers are approximately the same. Thus, the level below -850 masl in this variant is an average of the bottom layers in the regional base case model. Table 5.3-1 summarises the hydraulic conductivities used in this site-scale variant and compares them to the site-scale Base Case.

In summary, in contrast to the Base Case of this study, Variant 3 assumes that:

- Zone 2 is modelled as a three-layered structure, i.e., a conductive fracture zone with a less permeable core.
- Five fracture zones are terminated at the level of Zone 2.
- A different model of depth dependence is used for the hydraulic conductivity in the rock domain.
- Similar to Variant 1, the boundary conditions are taken from a salinity-dependent regional model, whose boundary salinities and pressures are then converted to environmental heads. The regional model corresponds to the regional base case of Hartley et al. (1998; see also Appendix B.4).

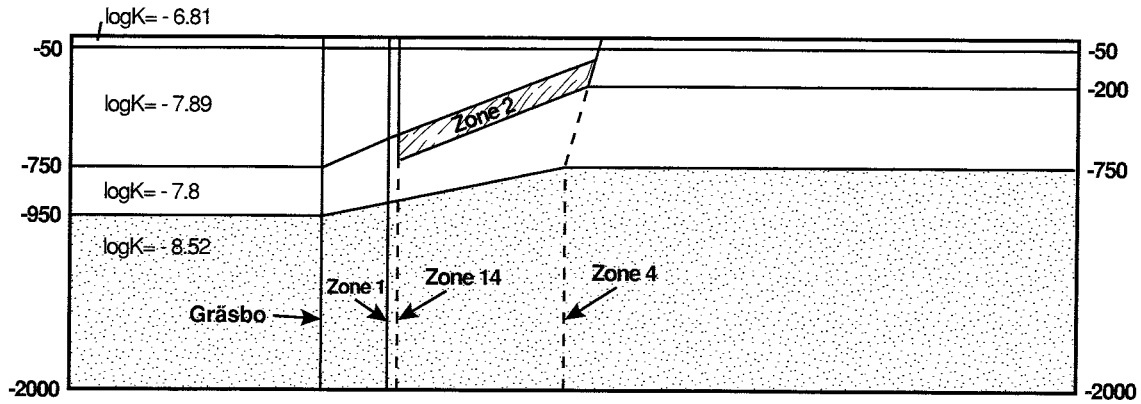

Figure 5.3-2. Schematic illustration of the rock mass depth dependence in the regional model that provides boundary conditions for Beberg Variant 3 (alternative hydrogeologic interpretation). View from east on a slice at X = 15,400 m.

Table 5.3-1. Comparison of Base Case and Variant 3 (alternative hydrogeologic interpretation) representations of hydraulic conductivity (35 m scale).

Zone	Log_{10} K (m/s) upper layer		Log_{10} K (m/s) middle layer	Log_{10} K (m/s) bottom layer	
	Variant 3 (>-70 masl)	Base Case (>-100 masl)	Variant 3 (-70<z<-850 masl)	Variant 3 (<-850 masl)	Base Case (<-100 masl)
1	-4.69	-4.68	-4.69	-6.17	-5.77
2 middle*			-9.36	-10.84	-4.85
2 high*			-5.20	-6.68	-4.85
3	-5.99	-5.99	-5.99	-7.47	-7.08
4	-5.52	-4.26	-5.52	-7.00	-5.35
12	-5.27	-5.27	-5.27	-6.75	-6.36
13	-4.69	-4.68	-4.69	-6.17	-5.77
14	-5.84	-5.27	-5.84	-7.32	-6.36
Imundbo	-5.52	-4.26	-5.52	-7.00	-5.35
Gräsbo	-5.84	-5.27	-5.84	-7.32	-6.36
Skogsbo	-5.52	-4.26	-5.52	-7.00	-5.35
Giboda	-5.52	-4.26	-5.52	-7.00	-5.35
Giboda S	-5.52	-4.26	-5.52	-7.00	-5.35
5	-5.52	-4.26	-5.52	-7.00	-5.35
7	-5.84	-5.30	-5.84	-7.32	-6.39
8	-5.84	-5.30	-5.84	-7.32	-6.39
11	-6.6	-6.38	-6.6	-8.08	-7.47
SRD North	-7.17	-6.42	-8.20	-8.58	-7.51
SRD South	-7.17	-6.78	-8.20	-8.58	-7.87
SRD Other	-7.17	-7.16	-8.20	-8.58	-8.25

* Zone 2 is modelled as a three layered structure in Variant 3, a high conductive zone with a less permeable core.

Figure 5.3-3 presents the stream tubes from the first realisation of this variant, illustrating the consequences of changing to boundary conditions derived from a salinity-dependent regional model. Similar to the results of the Hartley et al. (1998) regional base case model, the groundwater flow pattern around the repository is generally downward. Consequently, 71% of the stream tubes exit the bottom boundary of the model (Figure 5.3-4). Approximately 29% of the stream tubes exit the upper model surface, most of which originate from the starting positions in the Southern Rock Block. As discussed in the Base Case, stream tubes that fail to exit the upper surface of the model are assigned the default maximum travel time of 10,000 years. Thus, although Table 5.3-2 indicates that the median travel time is increased from 56 years in the Base Case to 86 years in this variant, this statistic is somewhat misleading, because 71% of the results are censored by the default maximum, as indicated in Figure 5.3-5.

The flow pattern of this variant is similar to that of Variant 1, but a large number of stream tubes exits the bottom of the model domain immediately to the north of the North Block. This suggests that the flow pattern of this variant may be oriented even more vertically than the flow pattern in Variant 1. Despite this difference, Zone 1 and the Imundbo Zone are still the major pathways for this variant.

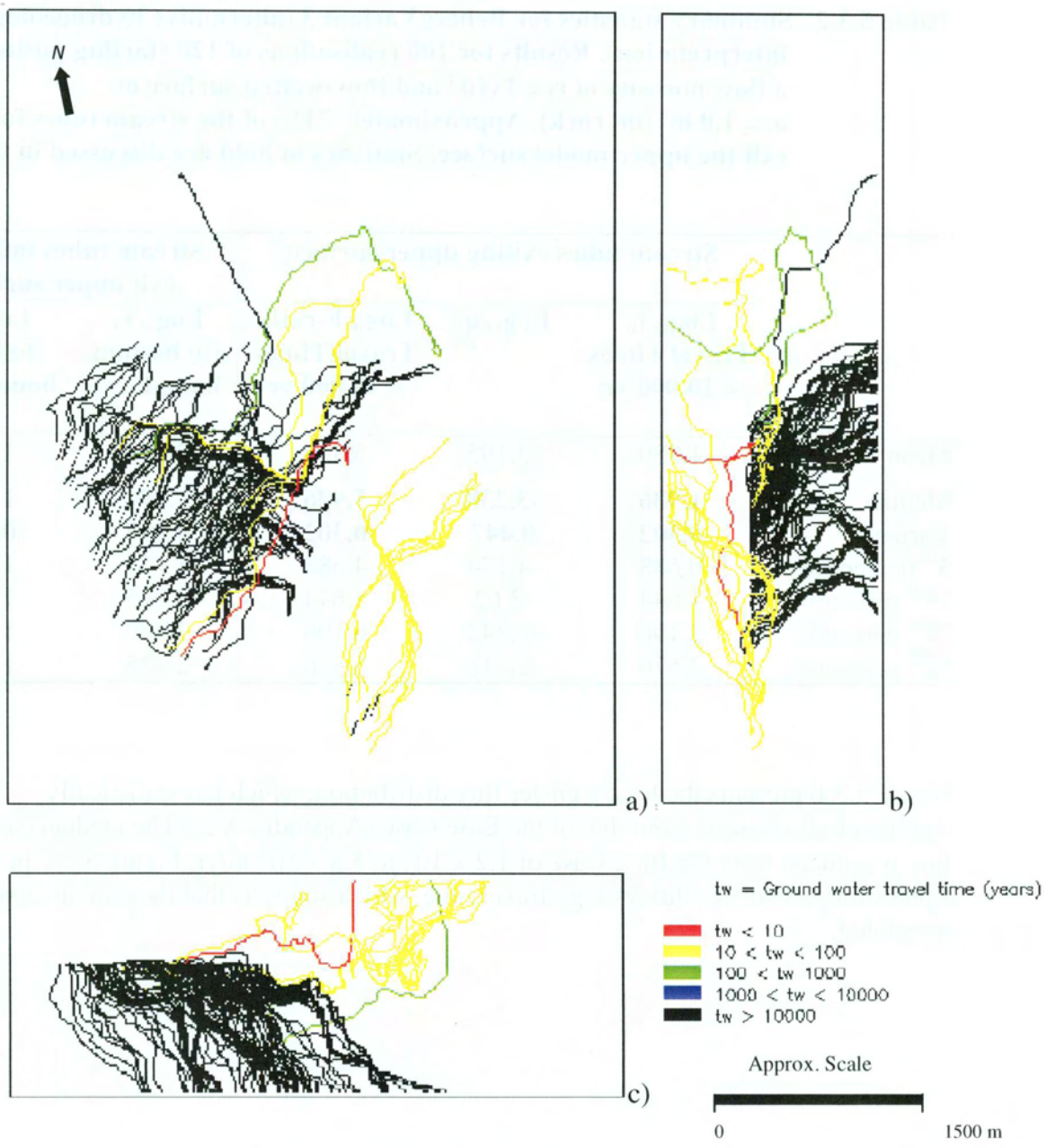

Figure 5.3-3. Stream tubes in realisation 1 of Beberg Variant 3 (alternative hydrogeologic interpretation) in a) plan view (looking downward), b) elevation view from east and c) elevation view from south. Results for 120 starting positions and a flow porosity of $\varepsilon_f = 1x10^{-4}$.

Table 5.3-2. Summary statistics for BebergVariant 3 (alternative hydrogeologic interpretation). Results for 100 realisations of 120 starting positions, a flow porosity of $\varepsilon_f = 1x10^{-4}$ and flow-wetted surface of $a_r = 1.0\ m^2/(m^3\ rock)$. Approximately 71% of the stream tubes fail to exit the upper model surface. Statistics in bold are discussed in text.

	Stream tubes exiting upper surface			Stream tubes failing to exit upper surface	
	$Log_{10}\ t_w$ Travel Times < 10,000 yr	**$Log_{10}\ q_c$**	**Log_{10} F-ratio Travel Times < 10,000 yr**	**$Log_{10}\ t_w$ (to bottom boundary)**	**$Log_{10}\ t_w$ (to lateral boundaries)**
Mean	1.859	-3.195	5.859	2.288	1.545
Median	**1.936**	**-3.238**	**5.936**	**2.294**	**1.587**
Variance	**0.302**	**0.447**	**0.302**	**0.097**	**0.090**
5th percentile	0.688	-4.174	4.688	1.777	1.044
25th percentile	1.644	-3.62	5.644	2.085	1.519
75th percentile	2.196	-2.842	6.196	2.499	1.671
95th percentile	2.576	-2.118	6.576	2.775	1.917

Figure 5.3-6 presents the log_{10} canister flux distribution, which has statistically significant differences from that of the Base Case (Appendix A.2). The median canister flux is reduced from the Base Case of 1.2×10^{-3} to 5.8×10^{-4} m/yr. Figure 5.3-7 presents a plot of log_{10} canister flux vs log_{10} travel time, which suggests that they are inversely correlated.

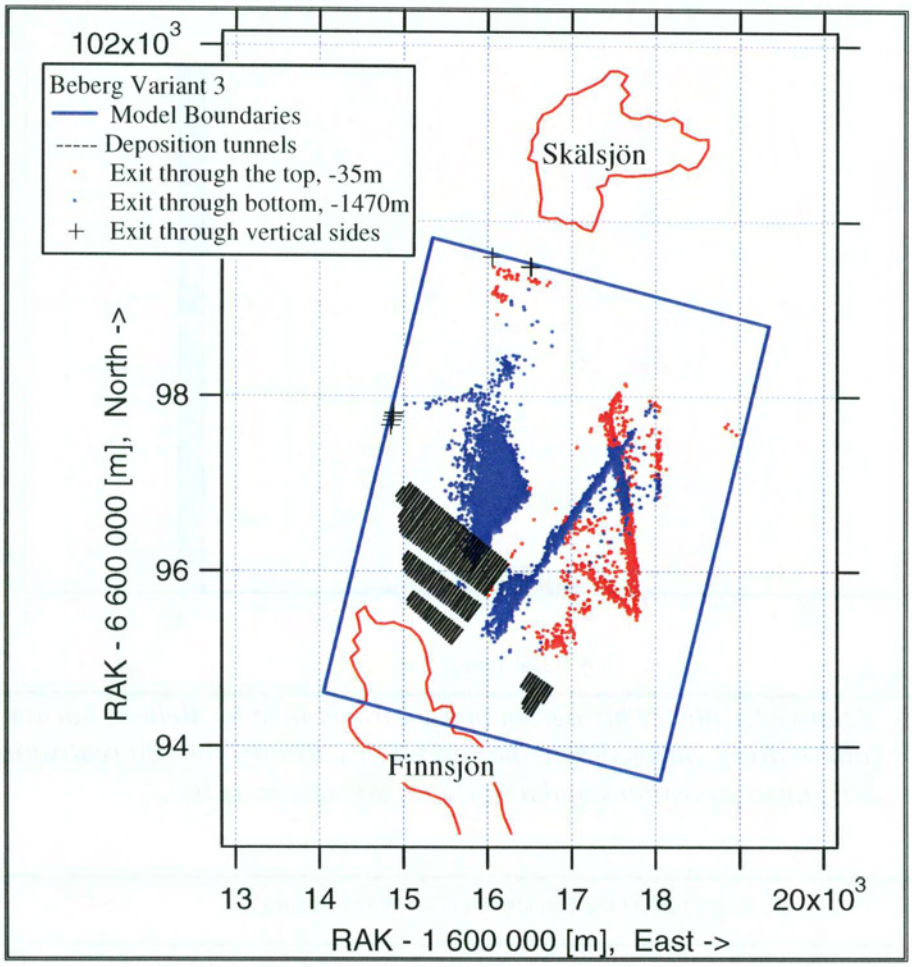

Figure 5.3-4. Exit locations Beberg Variant 3 (alternative hydrogeologic interpretation). Results for 100 realisations of 120 starting positions (offset RAK coordinates in metres).

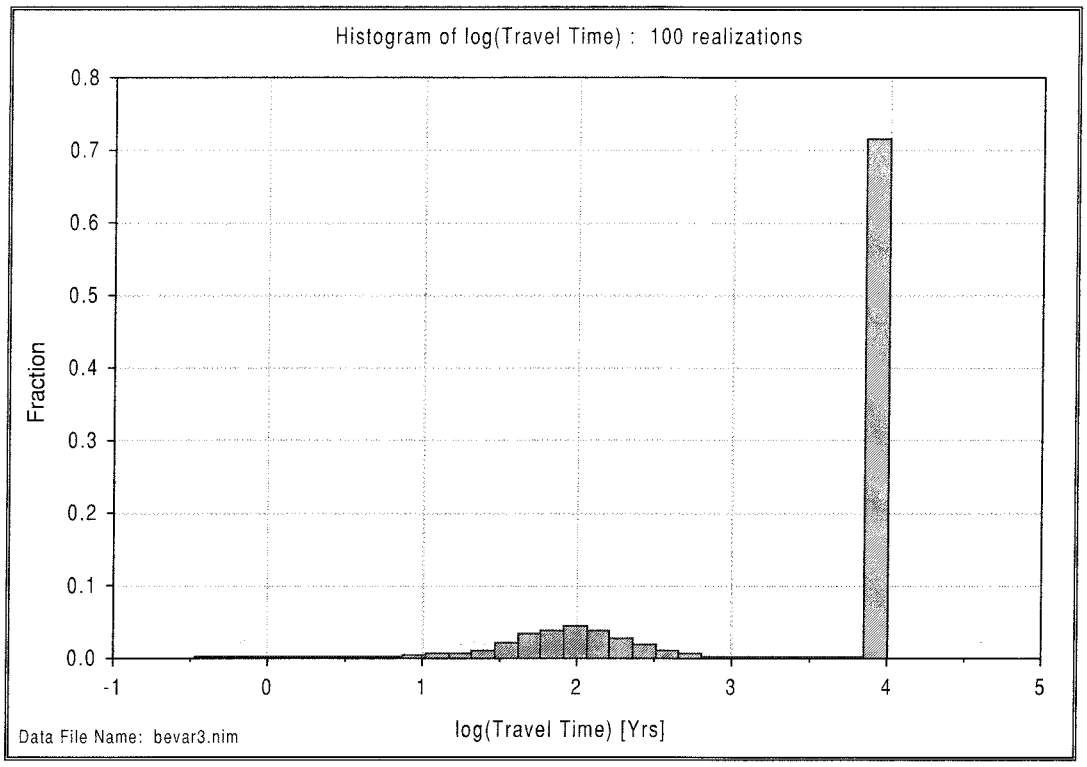

Figure 5.3-5. Relative frequency histogram of log_{10} travel time for Beberg Variant 3 (alternative hydrogeologic interpretation). Results for 100 realisations of 120 starting positions and a flow porosity of $\varepsilon_f = 1x10^{-4}$.

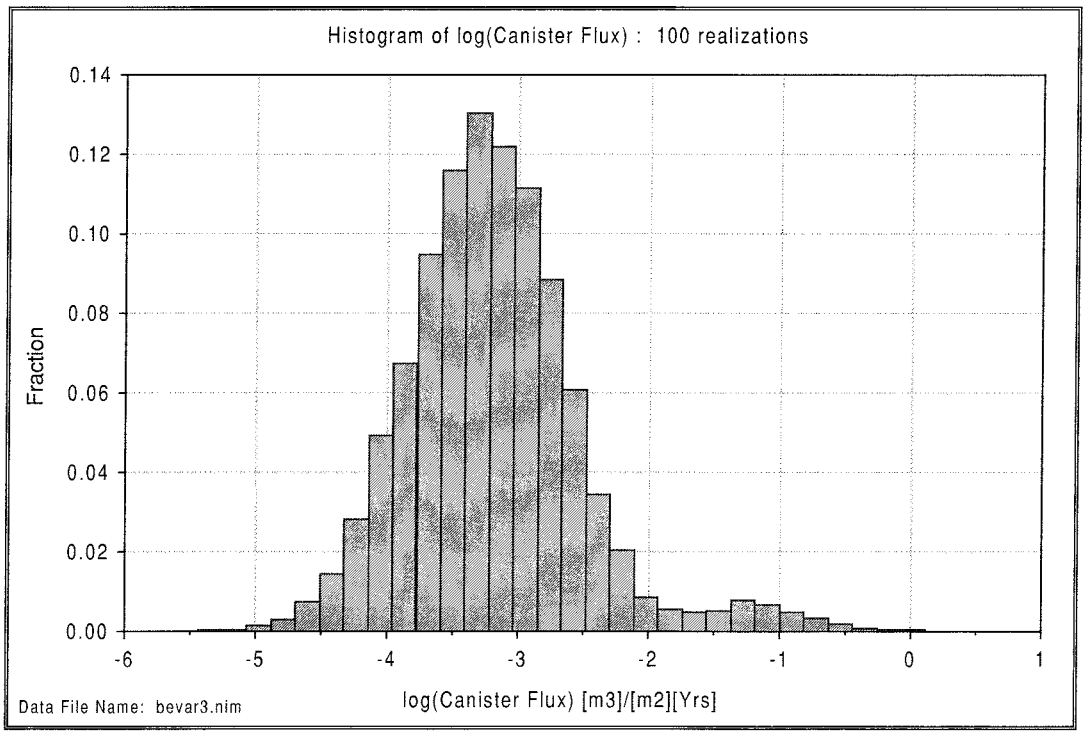

Figure 5.3-6. Relative frequency histogram of log_{10} canister flux for Beberg Variant 3 (alternative hydrogeologic interpretation). Results for 100 realisations of 120 starting positions.

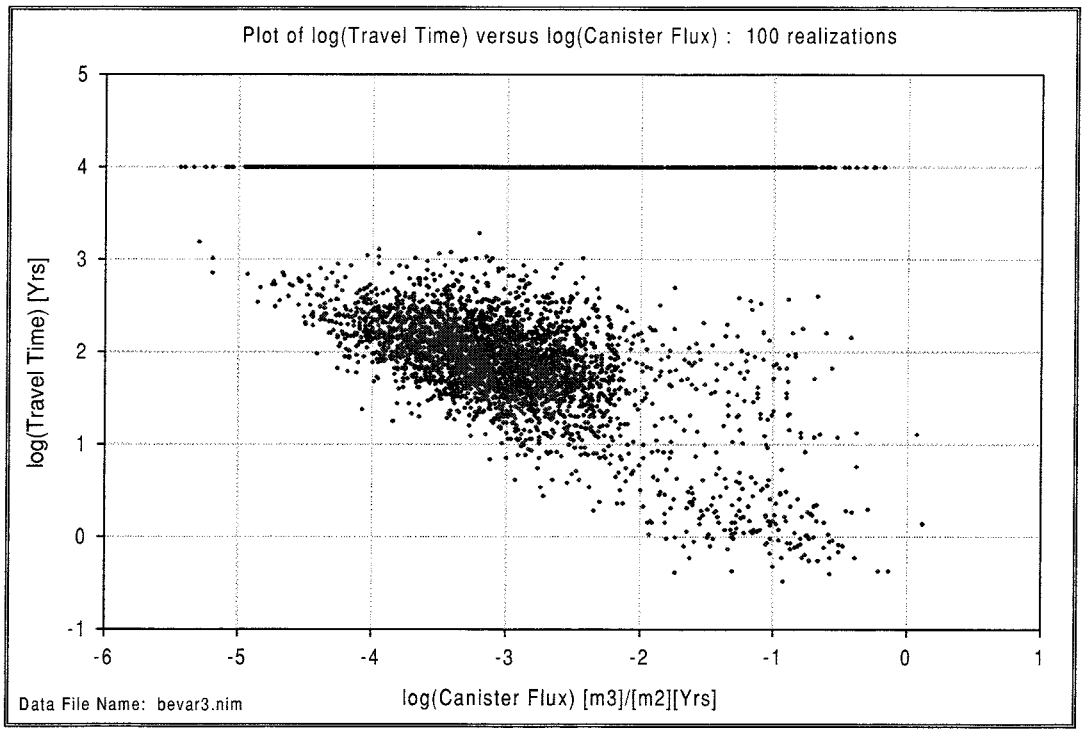

Figure 5.3-7. Log_{10} travel time versus log_{10} canister flux for Beberg Variant 3 (alternative hydrogeologic interpretation). Results for 100 realisations, of 120 starting positions and a flow porosity of $\varepsilon_f = 1x10^{-4}$.

The travel time for the stream tubes failing to exit the upper model surface can be post-processed from the HYDRASTAR output files, as are presented in Table 5.3-2. For the stream tubes escaping the bottom boundary, the median travel time is 197 years. For stream tubes escaping the western boundary, the median travel time is 39 years. With respect to the site-scale model, the fate of these escaping stream tubes is unknown. However, the regional model base case estimated that the advective travel times to the limits of the regional model domain would be on the order of 10 to 890 years (Appendix B.5).

It is important to note that the salinity-dependent conditions represented by this variant are believed to be a transient phenomenon, slowly evolving toward freshwater conditions (Section 3.3; Hartley et al.,1998). Thus, although this variant is a possible interpretation of present-day conditions, the long-term flow field at the site is thought to be most like that of the Base Case.

Table 5.3-3 summarises the boundary flows for this variant. The regional mass balance residual is approximately 10%, and the site-scale model tends to overpredict the fluxes of the regional model by a factor of 2. The overprediction suggests that the upscaling of hydraulic conductivities is only approximately self-consistent. In comparison to the Base Case, the regional mass balance residual is greatly reduced, and confirms that the nested modelling preserves the flow direction on the upper surface. This suggests that the nested modelling and upscaling are valid in the general sense (see discussion in Sections 4.2 and 4.3.5).

Table 5.3-3. Boundary flow consistency for Beberg Variant 3 (alternative hydrogeologic interpretation), regional model versus site-scale model.

Model Surface	Regional (Hartley et al., 1998)	Net Flow Through Site Model Surfaces ($m^3/s \times 10^{-3}$) Variant 3 (5 realisations)	Base Case (5 realisations)
West	2.59 (in)	2.776 (in)	8.602 (in)
East	1.16 (out)	4.168 (out)	2.870 (out)
South	3.48 (in)	7.284 (in)	3.600 (in)
North	3.36 (out)	2.974 (out)	4.154 (out)
Bottom	0.02 (out)	0.036 (in)	4.967 (in)
Top	1.14 (out)	2.963 (out)	10.130 (out)
Total Inflow	4.93	10.096	17.169
Total Outflow	4.54	10.105	17.154
Mass Balance (In – Out)	0.39	-0.0091	0.0156

5.4 Deterministic Simulation

This variant is a simplified simulation of the site using a deterministic representation of the hydraulic conductivity field (i.e., the field has no random component and thus needs only one 'realisation'). The objectives of this simulation are to further evaluate the empirical upscaling and nested modelling, and to examine the effects of the large-scale heterogeneity (e.g., the fracture zones and rock blocks). As discussed in Sections 3.5 and Appendix C.2, choosing the appropriate hydraulic conductivities is complicated by the apparent scale dependence of hydraulic conductivity. As a compromise, this study uses the empirical upscaling rule (Appendix C.2) to determine the effective conductivity, K_e, for each rock unit. If the nested modelling and upscaling are consistent, the boundary flows should be approximately the same for both the Base Case and this Deterministic Variant.

This variant also examines the effects of the large-scale structures without the small-scale variability of the geostatistical simulation. Tables 5.4-1 and 5.4-2 present the effective conductivities of each unit; note that for this variant, there is no block-scale variability (zero variance).

Table 5.4-1. Site-scale conductor domain properties (SCD) based on 3 m tests, Base Case versus Variant 4 (deterministic). Below 100 masl, K is reduced by a factor of 12.3 (i.e., [Log_{10}K below -100 masl] = [Log_{10}K above -100 masl] - 1.09).

Zone	Width	Median Log_{10} K (m/s)		K_e
		3 m	35 m	(100 m)
1*	20	-5.66	-4.68	-4.33
2	100		-4.86**	-4.50**
3	50	-6.82	-5.99	-5.63
4	10	-6.35	-4.26	-3.90
5	5	-6.35	-4.26	-3.90
6	5	-8.39	-6.56	-6.20
7	5	-7.39	-5.30	-4.94
8	5	-7.39	-5.30	-4.94
9	50	-7.94	-7.10	-6.74
10	5	-8.34	-7.51	-7.15
11	100	-7.22	-6.38	-6.02
12	25	-6.10	-5.27	-4.91
13	20	-5.66	-4.68	-4.33
14	100	-6.10	-5.27	-4.91

** Zone 2 is modelled without depth dependence. Value is for –100 masl.

Table 5.4-2. Site-scale rock mass domain (SRD) based on 3 m tests, Beberg Base Case versus Variant 4 (deterministic). Below - 100 masl, K is reduced by a factor of 12.3 (i.e., [Log_{10}K below - 100 masl] = [Log_{10}K above - 100 masl] - 1.09).

SRD	Arithmetic mean Log_{10} K (m/s)		K_e
	3 m	35 ms	(100 m)
SRD North	-7.35	-6.42	-6.06
SRD South	-7.51	-6.78	-6.42
SRD other	-6.95*	-7.16	-6.81

* SGU mean at approximately 67 m scale

Table 5.4-3 summarises the results of this deterministic simulation in terms of the travel time, canister flux and F-ratio averaged over all the starting positions. In comparison to the Base Case, the median travel time is decreased from 56 to 27 years and the median canister flux is increased from 1.2×10^{-3} to 1.9×10^{-3} m/yr, suggesting that the upscaling to effective conductivity has been excessive, resulting in an approximate factor of 2.0 increase of the Darcy velocity. Figure 5.4-1 presents the exit locations for this variant. The discharge areas are clearly organised around fracture zones. Figure 5.4-2, which presents the stream tubes for this variant, shows the influence of the fracture zones. Note that these fracture zones are deterministic in this model, but are uncertain in reality (section 3.5). This suggests a possible model enhancement of representing these zones stochastically.

Table 5.4-3. Summary statistics for Beberg Variant 4 (deterministic). Results for 100 realisations, of 120 starting positions, a flow porosity of $\varepsilon_f = 1x10^{-4}$ and flow-wetted surface $a_r = 1.0\ m^2/(m^3\ rock)$. None of the stream tubes fail to exit the upper model surface.

	All values		
	$Log_{10}\ t_w$	$Log_{10}\ q_c$	Log_{10} F-ratio
Mean	1.393	-2.623	5.393
Median	**1.433**	**-2.732**	**5.433**
Variance	**0.108**	**0.162**	**0.108**
5th Percentile	0.746	-2.974	4.746
25th Percentile	1.230	-2.817	5.230
75th Percentile	1.631	-2.529	5.631
95th Percentile	1.820	-2.312	5.820

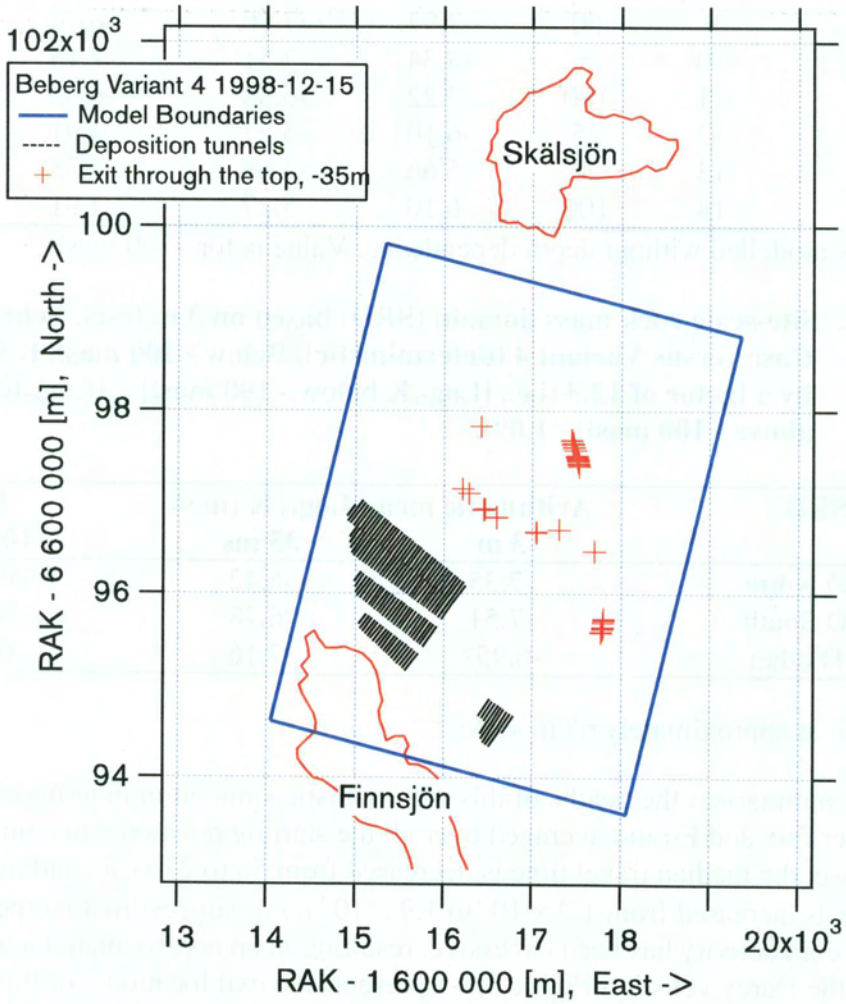

Figure 5.4-1. Exit locations for Beberg Variant 4 (deterministic). Results for 100 realisations of 120 starting positions (offset RAK coordinates in metres).

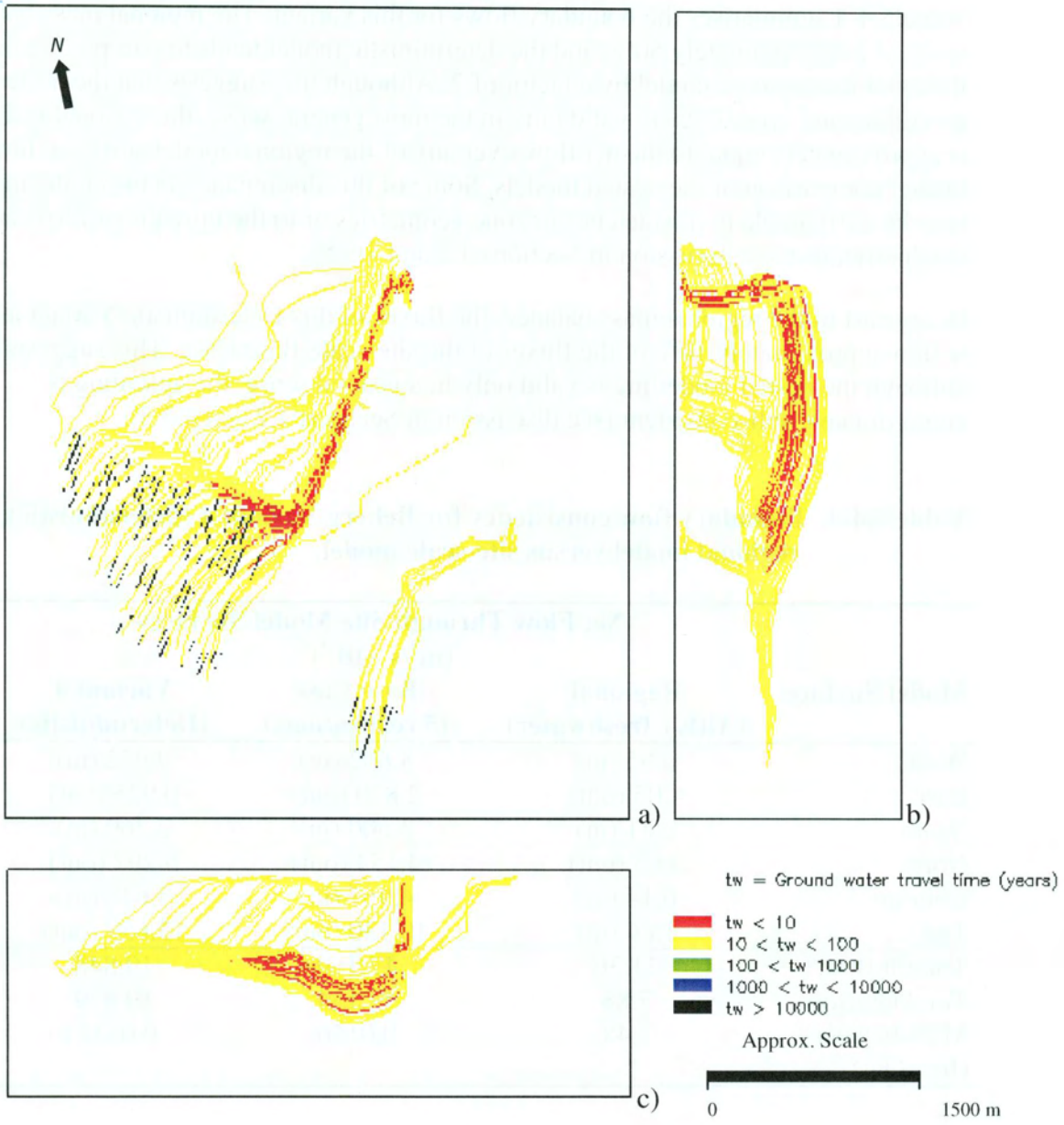

Figure 5.4-2. Stream tubes in Beberg Variant 4 (deterministic) in a) plan view (looking downward), b) elevation view from east and c) elevation view from south. Results for 120 starting positions and a flow porosity of $\varepsilon_f = 1x10^{-4}$.

Table 5.4-4 summarises the boundary flows for this variant. The regional mass balance residual is approximately 50%, and the deterministic model tends to overpredict the fluxes of the regional model by a factor of 2. Although this suggests that the nested modelling and upscaling are valid only in the most general sense, the regional residual is approximately equal to the net flow over any of the regional model surfaces, limiting further comparison of the nested models. Some of this discrepancy between the models may be attributable to mismatches in zone geometries or to the upscaling of hydraulic conductivities (see discussion in Sections 4.2 and 4.3.5).

In contrast to the regional mass balance, the fluxes of this Deterministic Variant are within approximately 10% of the fluxes of the site-scale Base Case. This suggests that although the nested modelling is valid only in a general sense, the upscaling is approximately self-consistent (see discussion in Sections 4.2 and 4.3.5).

Table 5.4-4. Boundary flow consistency for Beberg Variant 4 (deterministic), regional model versus site-scale model.

	Net Flow Through Site Model Surfaces ($m^3/s \times 10^{-3}$)		
Model Surface	**Regional (AltK+ freshwater)**	**Base Case (5 realisations)**	**Variant 4 (Deterministic)**
West	6.95 (in)	8.602 (in)	9.932 (in)
East	4.05 (out)	2.870 (out)	0.923 (out)
South	2.41 (in)	3.600 (in)	2.269 (in)
North	3.83 (out)	4.154 (out)	5.297 (out)
Bottom	0.14 (in)	4.967 (in)	7.647 (in)
Top	1.86 (in)	10.130 (out)	13.659 (out)
Total Inflow	11.36	17.169	19.848
Total Outflow	7.88	17.154	19.879
Mass balance (In – Out)	3.48	0.0156	-0.03111

6 Discussion and Summary

The SKB SR 97 study is a comprehensive performance assessment illustrating the results for three hypothetical repositories in Sweden. This study addresses the hydrogeologic modelling of Beberg, one of the three SR 97 sites. The study uses HYDRASTAR, a stochastic continuum groundwater flow and transport modelling program developed by SKB. This section of the report summarises the modelled cases and discusses the main results of the study in terms of statistics for travel time, F-ratio and canister flux. It also summarises the findings of the study with regard to model parameter uncertainty. Table 6.1-1 summarises the statistical results of all cases examined in this study, and Figures 6.1-1 and 6.1-2 present floating histograms of the results for intercomparison of the Base Case and Variants 1 through 4.

Input data for the model is a combination of the fracture zone descriptions and parameter values given by Walker et al. (1997b) and a series of modifications based on the findings of the regional modelling study of Hartley et al. (1998; see also Appendix B). The major modification to the parameter values given by Walker et al. (1997b) is the inclusion of depth dependence in the hydraulic conductivity of the fracture zones. An additional modification of the input data was the rescaling of hydraulic conductivities as suggested by Walker et al. (1997b). The SKB geostatistical analysis code INFERENS is used to infer a regularised variogram model based on the 3 m interpreted hydraulic conductivities taken from SICADA.

The boundary conditions for this model are constant head boundaries, derived from a deterministic, regional scale model modified from that of Hartley et al. (1998). The overall flow pattern of the regional model is typical of northeastern Uppland: low relief and consequently low gradients, driving groundwater from topographic highs to topographic lows. The transfer of regional heads via constant head boundaries generally preserves this pattern in the site-scale model. Adjustment of the scaling of hydraulic conductivity to fine-tune the boundary flow consistency between the regional and site-scale models is not pursued.

6.1 Base Case

The Base Case uses 100 realisations of the hydraulic conductivity field with 120 starting positions to evaluate the canister fluxes, travel times, and F-ratios for the proposed repository. As discussed in Section 4.0, the median travel times and median canister fluxes of the Base Case appear to be stable with respect to the number of simulations and are reasonably consistent with the regional model fluxes. All statistics are calculated with respect to the common logarithm transforms of the travel times, canister fluxes, and F-ratios to facilitate summary and display.

Table 6.1-1. Summary of Beberg flow modelling results.

Performance Measure	Statistic	Base Case	Variant 1 (Alt. Boundary)	Variant 2 (Alt. Conductors)	Variant 3 (Alt. Interp.)	Variant 4 (Deterministic)
Log_{10} Travel Time	Median	**1.752**	1.544	1.725	1.936	1.433
(years, for travel times less than 10,000 years)	Variance	**0.203**	0.259	0.216	0.302	0.108
Log_{10} Canister Flux	Median	**-2.923**	-2.744	-2.952	-3.238	-2.732
(m/yr, for all travel times)	Variance	**0.423**	0.397	0.425	0.447	0.162
Log_{10} F-ratio	Median	**5.752**	5.544	5.725	5.936	5.433
(yr/m, for travel times less than 10,000 years)	Variance	**0.203**	0.259	0.216	0.302	0.108

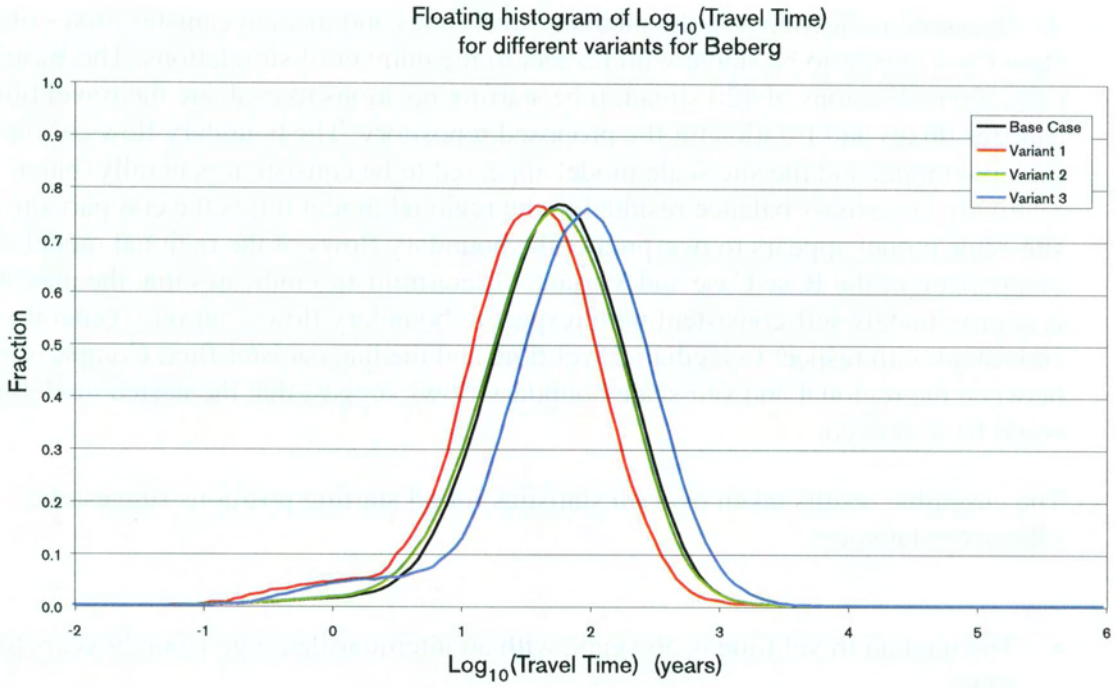

Figure 6.1-1. Floating histograms of log_{10} travel time for the Base Case, Variants 1, 2, and 3, each normalised to the number of stream tubes with $t_w < 10{,}000$ years. Results for 120 starting positions and a flow porosity of $\varepsilon_f = 1x10^{-4}$.

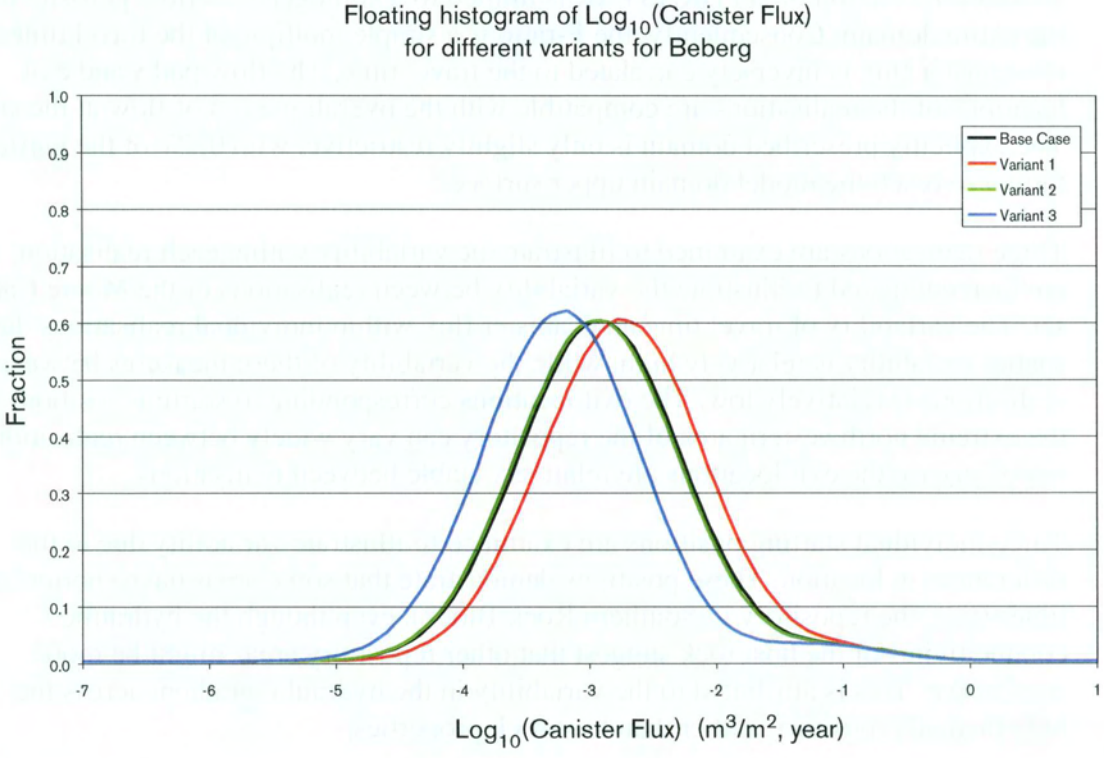

Figure 6.1-2. Floating histograms of log_{10} canister flux for the Base Case, Variants 1, 2, 3 and 4, each normalised to total number of streamtubes. Results for 120 starting positions.

As discussed in Section 4.0, the median travel times and median canister fluxes of the Base Case appear to be stable with respect to the number of simulations. The Base Case uses 100 realisations of 120 stream tube starting positions to evaluate the travel times, canister fluxes and F-ratios for the proposed repository. The boundary flows of the regional model and the site scale model appeared to be consistent generally, but a relatively large mass balance residual in the regional model limits the comparison. The site-scale model appears to overpredict the boundary flows of the regional model. A comparison of the Base Case and Variant 4 (deterministic) indicates that the upscaling is approximately self-consistent with respect to boundary flows, but only generally consistent with respect to median travel time and median canister flux. Comparisons between the regional and site-scale boundary flows suggest that the nested modelling could be improved.

The ensemble results taken over all statistics for all starting positions suggest the following statistics:

- The median travel time is 56 years, with an interquartile range from 29 years to 104 years.
- The median canister flux is 1.2×10^{-3} m/year with an interquartile range from 4.8×10^{-4} m/year to 3.0×10^{-3} m/year.
- The median F-ratio is 5.6×10^{5} year/m, with an interquartile range from 2.9×10^{5} year/m to 1.0×10^{6} year/m.

The current version of HYDRASTAR is limited to a homogeneous flow porosity over the entire domain. Consequently, the F-ratio is a simple multiple of the travel time, and the canister flux is inversely correlated to the travel time. The flow paths and exit locations of the realisations are compatible with the overall pattern of flow at the site. The explicitly prescribed domain is only slightly restrictive, with 0.7% of the particles failing to reach the model domain upper surface.

Three realisations are examined to illustrate the variability within each realisation, and are then compared to illustrate the variability between realisations of the Monte Carlo set. The variability of travel time and canister flux within individual realisations due to spatial variability is relatively high, while the variability of these measures between realisations is relatively low. The exit locations corresponding to starting positions in the extreme northwestern area of the repository can vary widely between realisations, but otherwise the exit locations are relatively stable between realisations.

Three individual starting positions are examined to illustrate variability due to the differences in location. These positions demonstrate that some areas have shorter travel times (e.g., the repository in Southern Rock Block), even though the hydraulic conducitivites of the host rock suggest that other repository areas might be more conductive. This is attributed to the variability in the hydraulic gradient across the hypothetical repository, rather than host rock properties.

6.2 Variant Cases

6.2.1 Alternative Boundary Conditions

The regional modelling study of Hartley et al. (1998) found that the flow field is markedly different under salinity dependent versus freshwater conditions, which suggests that it is important to evaluate the sensitivity of the results to alternative methods of generating boundary conditions. This variant uses the same structural model and representation of stochastic hydraulic conductivities as the Base Case (i.e., the AltK case of the Hartley et al. (1998) regional model, scaled to 35 m). In contrast to the Base Case (AltK and freshwater), this variant takes its boundary conditions from the salinity-dependent AltK case of the regional model, which are then converted to environmental heads.

Relative to the Base Case, the median travel time is decreased to 33 years and the canister flux is increased to 1.8×10^{-3} m/yr. The travel time statistics are somewhat misleading, however, since the flow field in this variant is directed downward, resulting in 92% of the stream tubes failing to reach the surface. In the long term, Hartley et al. (1998) found that the present-day salinity at the site is a transient phenomenon, slowly evolving toward freshwater conditions (Section 3.3). Consequently, the salinity dependent conditions represented by this variant will eventually be reduced to freshwater conditions. Thus, although this variant is representative of present-day conditions, the long term flow field at the site is thought to be most like that in the Base Case. This variant demonstrates that the flow direction is generally downward at the repository under present-day conditions and agrees with the regional modelling study.

6.2.2 Alternative Conductive Features

This variant case evaluates the possibility that all of the fracture zones and several possible zones are all relatively conductive features, similar to the set of deterministic zones used for the Base Case. This variant includes all of these additional features using a hydraulic conductivity equal to the average of the conductive features identified by Andersson et al. (1992). Positions of these zones are taken from Saksa and Nummela (1998).

In comparison to the Base Case, the median travel time is slightly reduced to 53 years and the variance of $\log_{10}$ travel time is slightly increased to 0.216, suggesting that some of the stream tubes are intercepted by conductive features, decreasing the median of travel time while increasing the variance of $\log_{10}$ travel time. The median canister flux is slightly decreased to 1.1×10^{-3} m/yr, and the variance of $\log_{10}$ canister flux is 0.425, approximately the same as the Base Case. The exit locations for starting positions in the Southern Rock Block are shifted, and the performance measure distributions have statistically significant differences from those of the Base Case. However, the performance measure statistics show little change and the differences are believed to be minor in the context of perfomance assessment.

6.2.3 Alternative Hydrogeologic Interpretation

The Hartley et al. (1998) base case regional model consisted of a deterministic hydraulic conductivity field under salinity dependent conditions, whose structural model and hydraulic properties were determined via calibration. This variant is a comparable site-scale simulation, using the regional base case model of Hartley et al. (1998) to calculate the boundary heads for the site-scale model. Because the regional base case model was salinity dependent, the hydraulic heads are transferred to the site-scale model as depth-integrated environmental heads.

In comparison to the Base Case, the median travel time is increased to 86 years while the median canister flux is reduced to 5.8×10^{-4} m/yr. Similar to Variant 1 the travel time statistics are somewhat misleading because 71% of the stream tubes fail to exit the upper model surface. The results of this variant are quite similar to those of Variant 1, in that the flow pattern at the repository is predominantly downward. It also confirms the importance of salinity in the present-day conditions.

6.2.4 Deterministic Simulation

This variant is a simplified simulation of the site using a deterministic representation of the hydraulic conductivity field (i.e., the field has no random component and thus needs only one 'realisation'). The objectives of this simulation are to further evaluate the empirical upscaling and nested modelling, and to examine the effects of the large-scale heterogeneity (e.g., the fracture zones and rock blocks). If the nested modelling and upscaling are consistent, the boundary flows should be approximately the same for both the Base Case and this deterministic variant.

This variant has a median travel time of 27 years, which is shorter than that of the Base Case. The median canister flux of 1.9×10^{-3} m/yr is greater than that of the Base Case. These results suggest that the upscaling of hydraulic conductivities is only approximately correct. In contrast, the boundary flow comparison between this variant and the Base Case model indicates that the upscaling is self-consistent. The importance of the fracture zones is clearly seen in this variant, and suggests that both the uncertainties in zone properties and occurrence be further evaluated.

6.3 Possible Model Refinements

This modelling study evaluates the groundwater flow system at the Beberg site, using a model that incorporates the processes believed to dominate the site groundwater system. This includes simulations of the Base Case, representing the expected site conditions, and several Variant Cases that evaluate uncertainties. Although the study is considered adequate for performance assessment, there are additional variant cases which may be of interest.

It is possible to examine several additional variants and model refinements within the current features of HYDRASTAR. For example, this study finds that the fracture zones

are the dominant pathways at the site, while the data compilation report (Walker et al., 1997) indicates that the fracture zone properties are uncertain. Variant 3 (alternative hydrogeologic interpretation) addresses the uncertainties regarding the fracture zones, but it is possible that other fracture zone property combinations may yield different results. The results of the Base Case also indicate that, because the model grid is relatively coarse, several starting positions may be effectively connected to a fracture zone. Although the overall performance of the hypothetical repository might not be affected, this does suggest a variant with an increased model grid density to isolate the effects of the exclusion zone width from the grid density. Finally, the comparison of the boundary flows in the Base Case and Variant 4 indicates that the nested modelling could be improved, and that the upscaling method could be investigated further.

Other model refinements are possible but are outside of the current features of HYDRASTAR. These include experimentation with alternative upscaling methods and the use of alternative methods of representing the hydraulic conductivities (e.g., nonparametric geostatistical simulation, discrete feature networks upscaled to numerical block conductivities, stochastic fracture zones, etc.). Ultimately, because of the dominating effect of the boundary conditions, such refinements may not have a profound impact on the performance measures. The relative importance of the boundary conditions, however, suggests a variant case to investigate the effects of using constant flux (Neuman) or third-type boundaries instead of the present constant head (Dirichlet) boundaries. The apparent mass balance residual of the regional model, attributed to interpolation errors, suggests refining the regional model flow balance so that the flow balance becomes a more powerful modelling tool. Lastly, although the Base Case addresses what is believed to be the long-term salinity conditions, Variants 1 and 3 indicate that salinity can result in dramatic changes in the groundwater flow pattern. While Variants 1 and 3 are generally consistent with the flow patterns of the salinity-dependent regional model, the salinity effects do suggest a follow-up study with a modelling code that is capable of including the density-dependent effects of salinity.

6.4 Summary of Findings

The findings of this study may be summarised as follows. With regard to the usage of data and consistency with the regional model, the representation of fracture zone hydraulic conductivities has been modified from that originally proposed by Walker et al. (1997) in order to better represent the salinity distribution in the regional model. Apart from this modification, the parameters are unchanged from those inferred directly from the field data except for the rescaling of hydraulic conductivities inherent to stochastic continuum modelling. The boundary flows of the regional and site-scale models suggest that the nested modelling could be improved and that the upscaling of conductivities is approximately self-consistent.

The variability between realisations for median travel time and median canister flux is relatively low, although exit locations corresponding to a some starting positions can vary widely between realisations. Some areas of the hypothetical repository appear to have shorter travel times (e.g., the repository in Southern Rock Block), which is attributed to the differences in the hydraulic gradient across the hypothetical repository.

The results for 100 realisation of 120 starting positions, a flow porosity of $\varepsilon_f = 1x10^{-4}$ and a flow-wetted surface of $a_r = 1.0\ m^2/(m^3\ rock)$ suggest the following results for the Base Case:

- The median travel time is 56 years, with an interquartile range from 29 years to 104 years.
- The median canister flux is 1.2×10^{-3} m/year with an interquartile range from 4.8×10^{-4} m/year to 3.0×10^{-3} m/year.
- The median F-ratio is 5.6×10^5 year/m, with an interquartile range from 2.9×10^5 year/m to 1.0×10^6 year/m.
- The common logarithm of canister flux appears to be inversely correlated to the common logarithm of travel time.
- The flow paths and exit locations were compatible with the pattern of flow at the site.

The uncertainties of this study are addressed by a series of variant cases that evaluate the sensitivity of the results to changes in assumptions regarding the boundary conditions and the hydraulic conductivities. The results are most sensitive to the use of boundary conditions derived from a salinity-dependent regional model, transferred to the site-scale model as environmental heads. Although the approach to upscaling appears to be approximately self-consistent, the nested modelling approach and the regional model mass balance could be re-examined.

Acknowledgements

The authors of this report would like to acknowledge the support and guidance of Anders Ström and Jan-Olof Selroos of the Swedish Nuclear Fuel and Waste Management Company (SKB). This study has benefited enormously from the comments of Johan Andersson and Sven Follin of Golder Grundteknik, Ingvar Rhén, of VBB VIAK. Raymond Munier of Scandia Consult, Jan-Erik Ludvigson and Rune Nordqvist of GeoSigma contributed data, ideas and useful comments throughout this study. Lydia Biggs (DE&S) contributed a number of illustrations and formatting suggestions to this report. The final text has benefited enormously from the careful editing of Marcie Summerlin (DE&S).

At the end of a long study, it is tempting to list all of modelling team members as coauthors of the final report, but this would be a practical impossibility for this report. The efforts of the following contributors are appreciated and are hereby acknowledged:

- Maria Lindgren and Sara Södergren (Kemakta) implemented the structural model and assisted in setting up the HYDRASTAR model for this study.
- Niko Marsic (Kemakta) postprocessed the model output to provide the statistical summaries of results, and Lars Lovius (Hellström and Lovius Data) provided general support for the HYDRASTAR simulations and postprocessing of results.
- Magdalena Ericsson and Håkan Svensson (Kemakta) assisted in illustrating and computer visualisation of the results.
- Björn Bergman (DE&S) performed the scoping calculations for travel time, and along with Cecilia Andersson (DE&S) assisted in preparing the preliminary sections of the report.
- Gregory Ruskauff (DE&S) assisted in the geostatistical analysis and helped review and summarise the study.

This study was funded by The Swedish Nuclear Fuel and Waste Management Company (SKB).

References

Andersson J., Nordqvist R, Nyberg G, Smellie J, and Tirén S, 1991. Hydrogeological conditions in the Finnsjön area. Compilation of data and conceptual model. Swedish Nuclear Fuel and Waste Management Co., SKB Technical Report TR 91-24, Stockholm, Sweden.

Andersson J., 1999. SR 97 – Data and data uncertainties: Compilation of data and evaluation of data uncertainties for radionuclide transport calculations, Swedish Nuclear Fuel and Waste Management Co., SKB Technical Report TR-99-09, Stockholm, Sweden.

Boghammar A., and Marsic N., 1997. Using Statistica when evaluating results from HYDRASTAR 1.5+. Swedish Nuclear Fuel and Waste Management Co., SKB Progress Report PR U-97-18, Stockholm, Sweden.

Dagan G., 1986. Statistical theory of groundwater flow and transport: pore to laboratory, laboratory to formation, and formation to regional scale. Water Resources Research, 22(9), p 1205-1345.

de Marsily G., Lavedan C., Boucher M., and Fasanino G., 1984. Interpretation of interference tests in a well field using geostatistical techniques to fit the permeability distribution in a reservoir model, in geostatistics for natural resources characterization. Second NATO Advanced Study Institute, GEOSTAT 1983, Tahoe City, California. Edited by G. Verly, M. David, A.G. Journel, and A. Marachal, p 831-849, D. Reidel, Hingham, MA.

Geier J., 1993. Verification of the geostatistical inference code INFERENS, Version 1.1, and demonstration using data from Finnsjön. Swedish Nuclear Fuel and Waste Management Co., SKB Technical Report TR 93-09, Stockholm, Sweden.

Gylling B., Lindgren M., and Widén H., 1999. Preparatory hydrogeological calculations for site scale models of Aberg, Beberg, and Ceberg. Swedish Nuclear Fuel and Waste Management Co., SKB Report R-99-06, Stockholm, Sweden.

Hartley, L., Boghammar, A., Grundfelt, B., 1998. Investigation of the large scale regional hydrogeological situation at Beberg. Swedish Nuclear Fuel and Waste Management Co., SKB Technical Report TR-98-24, Stockholm, Sweden.

Hammersley J.M., and Handscomb D.C., 1975. Monte Carlo Methods. Methuen, London.

Hodgkinson D.P., and Barker J., 1985. Specification of a Test Problem for HYDROCOIN Level 1 Case1: Transient Flow from a Borehole in a Fractured Permeable Medium. Report AERE R-11574, UK Atomic Energy Authority, Harwell Laboratories, UK.

Journel A.G., and Huijbregts Ch J., 1978. Mining Geostatistics. Academic Press.

Larsen, R.J., and Marx, M.L., 1986. An Introduction to Mathematical Statistics and Its Applications. Prentice-Hall, London.

Lovius L., 1998. Calculation of flux through boundaries in HYDRASTAR. Swedish Nuclear Fuel and Waste Management Co., SKB Progress Report PR U-98-08, Stockholm, Sweden.

Lovius L., and Eriksson L., 1993. Verification of HYDRASTAR version 1.4. Swedish Nuclear Fuel and Waste Management Co., SKB Working Report AR 93-46, Stockholm, Sweden.

Lovius L., and Eriksson L., 1994. Development of a transient version of HYDRASTAR. Swedish Nuclear Fuel and Waste Management Co., SKB Working Report AR 94-12, Stockholm, Sweden.

Lusczynski N.J., 1961. Head and flow of ground water of variable density. Journal of Geophysical Research, 66(12), p 4247-4256.

Marsic N., 1999. Using STATISTICA and MATLAB when evaluating results from HYDRASTAR 1.5+. Swedish Nuclear Fuel and Waste Management Co., SKB Progress Report TS-99-04, Stockholm, Sweden.

Morris S.T., and Cliffe K.A, 1994. Verification of HYDRASTAR: Analysis of hydraulic conductivity fields and dispersion. Swedish Nuclear Fuel and Waste Management Co., SKB Technical Report TR 94-21, Stockholm, Sweden.

Munier R., Sandstedt H., and Niland L., 1997. Förslag till principiella utformningar av förvar enligt KBS-3 för Aberg, Beberg och Ceberg. Swedish Nuclear Fuel and Waste Management Co., SKB Report R-97-09, Stockholm, Sweden.

Neuman S., and Jacobsen E., 1984. Analysis of nonintrinsic spatial variability by residual kriging with application to regional groundwater levels. Mathematical Geology, 16(5), p 499-521.

Neuman S., 1988. A proposed conceptual framework and methodology for investigating flow and transport in Swedish crystalline rocks. Swedish Nuclear Fuel and Waste Management Co., SKB Working Report AR 88-37, Stockholm, Sweden.

Norman S., 1991. Verification of HYDRASTAR - A code for stochastic continuum simulation of groundwater flow. Swedish Nuclear Fuel and Waste Management Co., SKB Technical Report TR 91-27, Stockholm, Sweden.

Norman S., 1992a. Statistical inference and comparison of stochastic models for the hydraulic conductivity at the Finnsjön-site. Swedish Nuclear Fuel and Waste Management Co., SKB Technical Report TR 92-08, Stockholm, Sweden.

Norman S., 1992b. HYDRASTAR - A code for stochastic simulation of groundwater flow. Swedish Nuclear Fuel and Waste Management Co., SKB Technical Report TR 92-12, Stockholm, Sweden.

OECD, 1983. The International HYDROCOIN Project: Groundwater hydrology modelling strategies for performance assessment of nuclear waste disposal. Level: Code verification.

Rhén I., Gustafson G., Stanfors R., and Wikberg P. 1997. Äspö Hard Rock Laboratory – Geoscientific Evaluation 1997/5. Models based on site characterisation 1986-1995. Swedish Nuclear Fuel and Waste Management Co., SKB Technical Report TR 97-06, Stockholm, Sweden.

Rubin Y., and Gómez-Hernández J.J., 1990. A stochastic approach to the problem of upscaling of conductivity in disordered media: Theory and unconditional numerical simulations. Water Resources Research, 26(4), p 691-701.

SKB, 1992. SKB 91: Final disposal of spent nuclear fuel. Importance of bedrock for safety. Swedish Nuclear Fuel and Waste Management Co., SKB Technical Report TR 92-20, Stockholm, Sweden.

SKB, 1996a. Template for safety reports with descriptive example. Swedish Nuclear Fuel and Waste Management Co., SKB Technical Report TR 96-05, Stockholm, Sweden.

SKB, 1996b. User's Guide to HYDRASTAR 1.5. Swedish Nuclear Fuel and Waste Management Co., SKB Progress Report PR U-96-15, Stockholm, Sweden.

SKI, 1997. SKI Site-94 Deep repository performance assessment project. Swedish Nuclear Power Inspectorate, SKI Report 97:5, Stockholm, Sweden.

Walker D., and Bergman B., 1998. Verification of HYDRASTAR v.1.7: Transient simulation and pilot point calibration. Swedish Nuclear Fuel and Waste Management Co., SKB Progress Report in preparation, Stockholm Sweden.

Walker D., Lovius L., and Eriksson L., 1997a. Verification of HYDRASTAR 1.7: Nugget effect in geostatistical simulations. Swedish Nuclear Fuel and Waste Management Co., SKB Progress Report PR U-97-22, Stockholm, Sweden.

Walker D., Rhén I., and Gurban I., 1997b. Summary of Hydrogeologic Conditions at Aberg, Beberg and Ceberg. Swedish Nuclear Fuel and Waste Management Co., SKB Technical Report TR 97-23, Stockholm, Sweden.

Walker, D., and Gylling, B., 1998. Site-scale groundwater flow modelling of Aberg. Swedish Nuclear Fuel and Waste Management Co., SKB Technical Report TR-98-23, Stockholm, Sweden.

Walker, D., and Gylling, B., 1999. Site-scale groundwater flow modelling of Ceberg. Swedish Nuclear Fuel and Waste Management Co., SKB Technical Report TR-99-13, Stockholm, Sweden.

Ward D., Buss D., and Mercer J., and Hughes S., 1987. Evaluation of a groundwater corrective action at the Chem-Dyne hazardous waste site using a telescopic mesh refinement modeling approach. Water Resources Research, 23(4), p 603-617.

APPENDIX A. Definition of Statistical Measures

A.1 Floating Histograms

This study generally uses binned histograms to display the frequency distributions of the performance measures. The bin width of such histograms is determined by the default algorithms of Statistica. Although the bin width is somewhat subjective, binned histograms do provide a relatively unprocessed image of the data. However, binned histograms are not well suited to graphical comparisons (e.g. overlaying multiple binned histograms is confusing to the eye).

An alternative method of constructing a frequency distribution histogram is to use a floating histogram. Floating histograms are single curved line representations of the frequency of the data. Although floating histograms are smoothed representations of the data, they are more legible when superimposed for the comparison of multiple histograms. Depending on the format and type of data being processed, several software packages (Appendix F) are used to calculate the floating histograms using a moving window as a filter passing over the ordered sequence of the data. For each datum value centred in the window, the smoothed frequency is calculated as the fraction of the data falling within the window. The width of the window is somewhat arbitrarily set to $\pm$ ½ an order of magnitude around the datum value in the centre of the window, and the frequency of each window is normalised by dividing by the total number of data. Generally, Statistica is used to calculate the moving window statistics and plot the resulting histograms. The exceptions to this are Figures 6.1-1 and 6.1-2, where MATLAB is used to calculate the moving window statistics, and the histograms displayed in Excel. The floating histograms of Variant 4, the Deterministic Case, are omitted, since the low performance measure variances result in virtually the entire distribution falling within the smoothing window.

A.2 Statistical Significance of the Comparison of Distributions

Section 5 makes a number of comparisons of variant cases versus the Base Case or versus other variants, concluding that 'there are statistically significant differences'. This statement of significance is quantitatively supported by a statistical comparison of the distributions, testing the null hypothesis:

H_0: the distributions are the same

The significance of this test, or p-value, is the probability of rejecting H_0 when it is in fact true (a so-called Type I error). Thus, a small p-value indicates that we can safely reject the hypothesis that the distributions are the same (Larsen and Marx, 1986). Because the distributions to be compared in this study are skewed, they are not suited to

test statistics that assume normally (Gaussian) distributed data. This study therefore uses nonparametric (distribution-free) test statistics to compute the p-value of the above test. The Kolmogorov-Smirnov test (K-S) is a nonparametric test used to compare distributional shapes (i.e., skewness, variability, and location), as documented in the Statistica manual. The p-value of a K-S test of H_0 is computed for the various combinations of the Base and variant cases (Tables A-1, and A-2).
Note: When computing the p-value for the comparisons of $\log_{10}$ travel time distributions, times greater than the default maximum travel time of 10,000 years are deleted from the distributions prior to the comparison. The resulting K-S p-value therefore ignores the flow paths failing to exit the upper surface of the model.

Table A-1 Test for similarity of travel time distributions (Kolmogorov-Smirnov 2-sample).

Case	Base Case	Variant 1	Variant 2	Variant 3
Base Case	-	Reject (p<0.001)	Reject (p<0.001)	Reject (p<0.001)
Variant 1	Reject (p<0.001)	-	Reject (p<0.001)	Reject (p<0.001)
Variant 2	Reject (p<0.001)	Reject (p<0.001)	-	Reject (p<0.001)
Variant 3	Reject (p<0.001)	Reject (p<0.001)	Reject (p<0.001)	-

Table A-2 Test for similarity of canister flux distributions (Kolmogorov-Smirnov 2-sample).

Case	Base Case	Variant 1	Variant 2	Variant 3
Base Case	-	Reject (p<0.001)	Reject (p<0.05)	Reject (p<0.001)
Variant 1	Reject (p<0.001)	-	Reject (p<0.001)	Reject (p<0.001)
Variant 2	Reject (p<0.05)	Reject (p<0.001)	-	Reject (p<0.001)
Variant 3	Reject (p<0.001)	Reject (p<0.001)	Reject (p<0.001)	-

APPENDIX B. Supplemental Regional Simulations

This appendix documents supplemental regional simulations based on the Beberg regional groundwater model of Hartley et al. (1998). These simulations are performed to supply the site scale modelling with appropriate boundary conditions. The following supplemental regional scale simulations are generated:

- Case AltK with steady-state freshwater flow boundary conditions, and transferring the freshwater head to the site-scale model (equivalent to the site-scale Base Case); and
- Case AltK with additional 'Saksa' site-scale zones, steady-state freshwater conditions, and transferring the freshwater head to the site-scale model (equivalent to site-scale Variant 2).

Notes on the transfer of heads between regional and site-scale models are provided for Variants 1, 3 and 4.

Note that Variant 1 (alternative boundary conditions) takes its boundary conditions directly from the regional case AltK transferring the pressures and salinities via environmental head to the site-scale model. Variant 3 (alternative hydrogeologic interpretation) takes its boundary conditions directly from the regional base case transferring the pressures and salinities via environmental head to the site-scale model.

Performance measures for these regional simulations are summarised in Appendix B.5.

B.1 Base Case

The original regional model AltK case calculated the evolution of groundwater flow and salinity from 4,000 years BP to the present day. This gave a prediction of the current groundwater head and salinity distribution. In the site-scale modelling it was necessary to use steady-state constant density models. This conceptual difference necessitates an approximate method in deriving site-scale boundary conditions from the larger regional scale model. Two approximation methods are considered. The first (Base Case) is to recalculate the AltK variant for a steady-state freshwater flow condition. The second (Variant 1) is to use the environmental (density adjusted) head for the current day variable density flow as predicted by the original AltK regional model.

For the Base Case (AltK + freshwater) the boundary conditions are:

1 topographic head boundary conditions on the top surface;
2 hydrostatic head on the vertical sides;
3 no flow on the base.

Pathline calculations for this variant suggest that the major discharge region for particles starting at the hypothetical repository are in the northeast around the intersect of Zone 1 and Imundbo. Boundary conditions for the site-scale model are calculated by interpolation of the freshwater head in the regional model for the nodes on the surfaces of local-scale model. This regional simulation also provides boundary conditions for Variant 4, the Deterministic Case.

B.2 Variant 1

For Variant 1, the regional model includes the effects of salinity in the regional AltK case. Although no supplemental simulation is necessary, this necessitates an additional step to transfer boundary heads to the site-scale model, since HYDRASTAR does not address salinity dependence. One method for converting from saline water head to freshwater head is to calculate the environmental head (or density adjusted head). The environmental head h_e at any point in the model domain is equal to the residual head at that point h_r, less the excess weight (relative to fresh water) of the column of saline water above it (Lusczynski, 1961), calculated as:

$$h_e = h_r - \int_z^{z_0} \left(\frac{\rho(z)}{\rho_0} - 1\right) dz$$

where ρ is the density of saline water, ρ_0 is the density of fresh water, and z is the elevation (z-positive upward) relative to the reference datum z_0. Using the environmental head gives the correct vertical gradient for predicting vertical flow velocities. In fact, for a stratified salinity distribution, the environmental head is the appropriate potential function for predicting variable density flows (Lusczynski, 1961).

B.3 Variant 2

In Variant 2 additional site-scale zones are incorporated into the site-scale model based on the re-evaluated structural model of Saksa and Nummela (1998). In order to maintain consistency in the nested modelling approach, a supplemental regional-scale simulation is required that includes these additional features in the AltK simulation with freshwater. The site-scale zones are typically 5 m wide, much smaller than the regional scale mesh spacing of about 100 m near the site domain. Hence, it is not practical to represent the site-scale zones explicitly in the regional model.

Instead, an implicit treatment of the site-scale zones is used to ensure consistency of the bulk flows between the regional and site-scale models. This is achieved by calculating the effective hydraulic conductivity for the Finnsjön northern and southern rock blocks based on the combined properties of each fracture zone and the rock mass. For example, the effective hydraulic conductivity parallel to the local zones (NW-SE and vertical) is calculated as an arithmetic mean of the hydraulic conductivity for the zones and rock mass, with weights proportional to the relative thickness of the zones and rock mass. In the direction orthogonal to the zones, a weighted harmonic mean is used. This results in an anisotropic effective hydraulic conductivity for the northern and southern blocks.

For the northern block, the site-scale zones 5, 6, 7, 8 and Saksa C and E are included implicitly. For the southern block, zones 5, 6, 7, 8 Saksa A, B, C, D, E, F, and G are included. The resulting effective hydraulic conductivities are summarised in the following table.

Table B-1. Hydraulic conductivities for supplemental regional simulation corresponding to Variant 2.

SRD	Hydraulic Conductivity (m/s)			
	KXX	KXY	KYY	KZZ
northern block (z>-100 masl)	2.57E-7	1.39E-8	1.69E-7	2.70E-7
northern block (z<-100 masl)	2.09E-8	1.13E-9	1.37E-8	2.20E-8
southern block (z>-100 masl)	2.57E-7	1.39E-8	3.00E-7	4.02E-7
southern block (z<-100 masl)	2.09E-8	1.13E-9	2.44E-8	3.27E-8

The hypothesised 'Saksa H' subhorizontal zone is represented explicitly by an extra 10 m subhorizontal layer of finite-elements with a hydraulic conductivity of 3.26×10^{-5} m/s. Steady-state freshwater boundary conditions were specified for this variant, as detailed in Appendix B.1.

B.4 Variant 3

Variant 3 is an alternative hydrogeologic model based on the calibrated base case of the regional modelling study (Hartley et al., 1998). No supplemental simulation is required for this study, but the variable density and pressures are converted to environmental heads to provide boundary conditions for the site-scale model (Appendix B.2).

B.5 Regional Pathline Results

Table B-2 summarises statistics for the travel time (t_w) and initial Darcy velocity (q_c) for each of the regional models corresponding to the site-scale variants. These statistics are based on a small sample (16) of start locations distributed uniformly in the Northern Rock block. Hence, the results presented are approximate, and intended for broad comparison with the more detailed site-scale transport study.

Table B-2. Summary of Beberg regional flow modelling results.

	Base Case		Variant 1		Variant 2		Variant 3	
	Log_{10} t_w years	Log_{10} q_c m/year	Log_{10} t_w years	Log_{10} q_c m/year	Log_{10} t_w years	Log_{10} q_c m/year	Log_{10} t_w years	Log_{10} q_c m/year
Mean	2.06	-3.01	2.28	-3.01	1.86	-2.89	2.07	-2.83
Variance	0.21	0.59	0.16	0.43	0.40	0.52	0.46	0.50
Min.	1.09	-3.50	1.43	-3.67	0.39	-3.35	1.01	-3.47
Max.	2.67	-0.24	2.88	-0.69	2.54	-0.27	2.95	-0.33

For the Base Case, the results compare favourably with those in Table 4.3-1. Mean travel times and initial Darcy velocities of the regional model are within one standard deviation of the site-scale model. The regional minimum and maximum values also compare well with the 5th and 95th percentile, respectively, of the site-scale models. The high maximum velocity for the regional scale is due to one of the start points being just within Zone 2. The regional scale results also show that travel times are greatest for Variant 1 and least for Variant 2, as for the site-scale results. For the variants where salinity is included, Variants 1 and 3, the regional scale results predict shorter travel times.

In the regional model, the travel time is taken as the time at which the pathline exits the regional model domain and whether it is on the top or vertical surface; i.e., no default maximum travel time is used.

B.6 Regional Model Mass Balance Calculations

Several sections of this report discuss the mass balance of the regional model and the boundary flows across the site-scale domain, but Hartley et al. (1998) did not document these quantities. The regional flows discussed in this study are determined concurrently with the supplemental regional simulations discussed in preceeding sections of this Appendix. This section outlines the approximation method used to determine the subdomain boundary fluxes and the resulting regional model mass balance calculations.

The mass balance computations use the small-scale regional NAMMU model for Finnsjön to determine the volumetric flows (m^3/s) through the six planar faces of a cube coincident with the boundaries of the site-scale model. The NAMMU code uses the finite element method of solving the governing equations for groundwater flow, a numerical method that inherently conserves mass over the element faces. In addition, NAMMU uses a direct solver, so that the solution to the system of equations is exact within the accuracy of the host platform. That is, regardless of the mass balance residual over arbitrary subdomains, the finite element method and NAMMU's direct solver conserve mass and that the resulting simulated heads are correct (Cliffe et al, 1995).

However, the cube faces of the site-scale model do not necessarily coincide with element faces of the regional model. For this study, the regional flows over the site-scale domain were estimated by sampling the outward normal flux (specific discharge, in m/s) at a regular grid of points on each face of the cube. The spacing of sample points was set at 10 m in the horizontal directions and 3 m in the vertical. The finite elements of the regional model are typically about 100 m on a side, so the sample points are close enough to resolve the variation in permeability and hence velocity with depth. The net flow out of each face was taken as the sum of pointwise flux samples, multiplied by the cross-sectional area (m^2) represented by each sampling point. The sampling grid was refined until the calculated net flows converged to a stable value, and mass balance residuals were computed for all three regional cases. These residuals reflect the sampling errors of this approximating method, and it is expected that a more rigorous approach (e.g., Gaussian quadrature within each element) would reduce this error dramatically.

APPENDIX C. Supplemental Calculations

C.1 AltK and Revisions to Walker et al. (1997)

The preliminary base case model for Beberg conductors of Walker et al. (1997), RCD1, proposed that the hydraulic conductivity of the fracture zones be constant with depth. The Beberg regional modelling study report of Hartley et al. (1998) suggests that the hydraulic connection to the subsurface is badly over-predicted if the subvertical fracture zones have a constant hydraulic conductivity with depth. Hartley et al. (1998) found that, if several of the subvertical fracture zones were terminated before connecting with Zone 2, then realistic salinity levels could be predicted in Zone 2.

Rather than terminate the fractures, their hydraulic conductivity may decrease with depth similar to the rock mass, as suggested in the alternative model RCD2. This may have the same effect of reducing freshwater recharge into Zone 2, without implying that the vertical fractures terminate abruptly. Such a conclusion is similar to that of Andersson et al. (1991), who reduced the conductivity of Zone 1 in order to model pumping tests of Zone 2.

The median hydraulic conductivity of each fracture, constant with depth was presented in SCD1 of Walker et al. (1997). Because each of the medians is generally from a single borehole intercept, the median reported in Walker et al. (1997) represents a single depth. To apply the stepwise relative change in hydraulic conductivity, the measurements were indexed to their median depth then increased or decreased as necessary. That is, measurements taken near the surface are decreased to produce a decrease with depth, while measurements taken at depth are increased with increasing elevation. This is particularly important in the case of Zone 1, since the data used to infer the properties of Zone 1 are from relatively shallow depths. If K decreases with depth, then the K value for Zone 1 provided in Walker et al. (1997) represents the conductivity above –100 masl. Finally, we note that there is little difference between the means inferred for the lower three depth intervals, which suggests that both SRD1 and SCD2 may be simplified to a single change at –100 masl. It should be noted that there is insufficient test data in the fracture zones to infer a change with depth, consequently the interpreted hydraulic conductivities falling in the rock domain are used to infer the change at –100 masl. This is accomplished by taking the arithmetic mean of the conductivities in the zone below –100 masl. This results in a uniform change in Log10K of –1.09 below -100 masl.

Walker et al. (1997) suggested a hydraulic conductivity for Zone 2 based on the 3 m packer tests upscaled to 100 m. However, it would be more consistent with the Aberg model to use the interference test data for Zone 2. The result is an increase in the horizontal conductivity, from LogK = -5.14 to –4.5 m/s. If Zone 2 is modelled in greater detail as an anisotropic feature, then the interference test data suggested that the conductivity perpendicular to the plane of Zone 2 is LogK = -6 (log m/s).

Andersson et al. (TR 91-24 and Lindbom et al (TR 91-12) suggested that Zone 4 should take its properties from Zone 5. Subsequent reports (e.g. TR 92-20) may have taken the properties of Zone 4 from Singö. This study uses the hydraulic conductivities of Zone 5 for Zone 4; the difference is approximately one order of magnitude.

In summary, the revised site-scale representation of the rock domain and conductor domain consists of:

- input mean log10 K values for the three SRD (Northern Block, the Southern block, and outside the Finnsjön rock block);
- input log10 K values for each of the fracture zones in the SCD; and
- a uniform –1.09 decrease in Log10 K at –100 masl in both the SRD and SCD.

On the regional scale, the model is most similar to the AltK case of Hartley et al. (1998), except for rescaling to 35 m and with additional detail.

C.2 Upscaling of Hydraulic Conductivity Model

C.2.1 Approach

The injection and pumping tests performed in the cored boreholes and tunnel probeholes are the principal source of hydraulic conductivity data. These tests were interpreted and the measurements reported for various depths, rock types, etc. as described by Rhén et al. (1997). The interpreted hydraulic conductivities for the 3 m packer tests were taken directly from the SKB SICADA database and analysed with the SKB geostatistical inference code INFERENS.

The scale of these measurements (as inferred from the packer length) is much different from the proposed model grid scale. As discussed in Walker et al. (1997b), hydraulic conductivity is a scale-dependent parameter, which requires that the measured hydraulic conductivities be upscaled to the finite difference grid scale of the model. Thus, HYDRASTAR requires that the geometric means of interpreted hydraulic conductivities found in SICADA must be rescaled. This study uses the scaling relationship provided in Rhén et al. (1997), which assumes that the geometric mean of hydraulic conductivity at the measurement scale, L_m, may be adjusted for scale using the regression equation:

$$Log_{10}K_{gu} = Log_{10}K_{gm} + 0.782(Log_{10}L_u - Log_{10}L_m)$$

where:

K_g = geometric mean of hydraulic conductivity (m/s)

L = length scale (m), assumed equal to the packer interval.

The subscripts m and u refer to the measurement and upscaled values, respectively. Rhén et al. (1997) developed this empirical scaling relationship using the 3 m, 30 m, 100 m packer tests and full-length tests in the same cored boreholes.

C.2.2 Upscaling and Inference for 35 m Scale

This inference of spatial correlation models for Beberg site-scale hydraulic conductivity begins by dividing the data in the rock domain (SRD) into northern and southern rock blocks, with a break between upper and lower levels at –100 masl. The elevation zones and rock blocks are treated as step changes in the mean of $\log_{10}$ conductivities, and a single variogram model is inferred for the entire domain (i.e., the same variogram for SRD and SCD). As discussed in Walker et al. (1997b), the correct approach to the upscaling of hydraulic conductivities to the numerical grid block is not known. As an interim approach, this study uses the Äspö scaling relationships of Rhén et al. (1997) to determine the geometric mean of hydraulic conductivity in each SRD and depth zone (Appendix C.2.1). The effect of upscaling on the variogram is determined by applying the Moye's formula-based regularisation algorithm and fitting a variogram–trend model via iterative generalised least squares estimation (IGLSE; see Neuman and Jacobsen, 1984) to the regularised data. The SKB program INFERENS, which includes the Moye's formula-based regularisation, automates the IGLSE fitting algorithm. Program restrictions of HYDRASTAR and INFERENS limit the geostatistical model to one variogram model for both domains. Because the majority of the 3 m packer tests fall in the SRDs and this data yields a clearer variogram, the geostatistical model will be developed from the interpreted hydraulic conductivities in the SRDs.

Walker et al. (1997b) explores the data and fits a model for the 24 m scale. This study merely repeats the INFERENS fitting using a 35 m regularisation scale and a single change in log10 K at –100 masl, and applies the Äspö scale relationships to determine the geometric mean (K_g) at the 35 m scale. The resulting experimental and fitted model variograms are shown in Figure 3.5-4, and the upscaled K_g 's are presented in Tables 3.5-1 and 3.5-2. The effect of the upscaling is to decrease the total variance of the experimental variogram and to increase the practical range.

C.3 Scoping Calculation for Approximate Travel Times

The purpose of this section is to provide rough estimations of travel times to be used as check on the model results. It uses Darcy's law applied to a single travel path, with the hydraulic gradient roughly estimated from the observed watertable.

C.3.1 Approach

The approach is to apply Darcy's Law and use the hydraulic gradient (∇h) and hydraulic conductivity (K) from various reports. The apparent velocity (V_a) is found by:

Darcy's Law: $$V_a = K\nabla h \qquad \text{(C.3.1)}$$

The gradient is calculated by using the difference in watertable divided by the horizontal distances between the release and the exit locations.

Hydraulic gradient: $$\nabla h = \frac{h_{exit} - h_{start}}{Distance} \qquad \text{(C.3.2)}$$

The average particle velocity (V_{mean}) is given by dividing the apparent velocity (V_a) by the porosity ρ.

Average particle velocity: $$V_{mean} = \frac{V_a}{\rho} \qquad \text{(C.3.3)}$$

The porosity is given a fixed value of ρ =1e-4 for all calculations. The travel times for the average particle is then given by

Travel times: $$travel\,time = \frac{Travel\,length}{V_{mean}} \qquad \text{(C.3.4)}$$

C.3.2 Application

The gradient is difficult to estimate due to the complexity of the flow pattern. For this scoping calculation, we assumed that the hydraulic head at the starting position could be estimated as the water table elevation immediately above the starting position of interest. The head at the exit location was taken as the groundwater table surface elevation at the exit position. The water table surface elevations are taken from Andersson et al. (1991).

The horizontal distances were measured from the maps provided in Walker et al. (1997) with the block location found in Munier et al. (1997). The values for the effective hydraulic conductivity are taken from Walker et al. (1997) for K at the 100 m scale. The following travel paths are considered:

- Path one: Start point in north west part of block 1 at depth 600 m, through zone 3 to the intersection with Brändan, through Brändan to the exit point in the small stream 17.8 km Northeast of the start point.

- Path two: Start point in north west part of block 1 at depth 600 m, through zone 3 to the intersection with Brändan, through Brändan to the intersection with Imundbo to the exit point in Skälsjön 11.3 km north of the start point.

The conductivities, gradients and resulting travel times are presented in Tables C-1 and C-2.

Table C-1. Path 1.

Hydraulic Gradient		**0.00067416**	
Fractures	**Travel Length**	**$Log_{10}K_{100}$**	**Travel Times**
Zone 3	2500		50.16
<200	0	-5.63	0.00
>200	2500	-6.63	50.16
Brändan	16,000		12.74
<200	3700	-4.33	0.37
>200	12,300	-5.33	12.37
Total	18,500 m		**62.9 yr**

Table C-2. Path 2.

Hydraulic Gradient		**0.00176991**	
Fractures	**Travel Length**	**$Log_{10}K_{100}$**	**Travel Times**
Zone3	2500		19.11
<200	0	-5.63	0.00
>200	2500	-6.63	19.11
Brändan	4000		1.53
<200	0	-4.33	0.00
>200	4000	-5.33	1.53
Imundbo	4900		3.64
<200	3800	-5.16	0.98
>200	1100	-6.13	2.66
Total	11,400 m		**24.3 yr**

APPENDIX D. Summary of Input Parameters

Table D-1 Mechanisms and model parameters considered in this study when modelling groundwater flow at Beberg using HYDRASTAR.

Mechanism	HYDRASTAR model parameter Symbol (unit)	Description	Source
Topographically driven flow	-	Fracture zone and rock domain geometries	Based on the interpreted geologic structural model for the site, TR 91-24, page A22-A24
	T (m^2/s)	Fracture zone transmissivities	Based on the interpreted geohydrological model for the site, TR 97-23 and TR 91-24; see also Appendix C. 100 m interference tests rescaled as described in Section 3.0
	K (m/s)	Rock mass hydraulic conductivity	Based on the interpreted geohydrological model for the site (TR 91-24 and TR 97-23) and single-hole water injection tests on 3 m scale. These tests are the basis for geostatistical analysis. Upscaling as described in Section 3.0. See Appendix C.
	S_s (m^{-1})	Specific storativity. Necessary for transient simulations.	Not used
	-	Top boundary condition	Constant head, as provided by Hartley et al (1998). See Appendix B. Files: tbcaltfhs.bcs
	-	Vertical/lower boundary conditions	Constant head, as provided by Hartley et al (1998). See Appendix B. Files: tbcaltfhs.bcs
	–	Variant cases	1: Pressure , from environmental head File: tbcalteh.bcs 2: Pressure, freshwater File: tbcsksafh.bcs 3. Pressure, from environmental head File: tbcbaseeh.bcs (See Appendix B of this report).
	ε_f (-)	Flow porosity Necessary for travel time calculation, but is poorly known in general	From TR 91-24, uniform throughout model at $\varepsilon_f=1\times10^{-4}$
Thermally and/or salinity driven flow	ρ (kg/m^3)	Groundwater density	Constant density.
Repository	Tunnel Layout		Recommended alternative layout at –600 masl, (for hydraulic structural model) from R 97-09 Figure 6-25. File: b_koord.xls, kapkoord.xls
	Starting Positions		120 starting positions spread uniformly over layout R 97-09
	EDZ / Backfill K (m/s)		No / 10^{-10} m/s, based on SKB AR D-96-011
Model Domain	-	Extent of model required to assess travel times	Premodelling study of Gylling et al., 1998.

APPENDIX E. Data Sources

The data used as input to the calculations consist of coordinates for fracture zones, deposition tunnels, and boundary conditions. These were taken directly from SKB archives or from the authors of the studies, as documented in this section.

E.1 For coordinates and previous interpreted K values

Output to: File

Date :970423 16:25:53

Table(s) :sic_dba.steady_state_inj_cd

Columns: steady_state_inj_cd.idcode, steady_state_inj_cd.start_date, steady_state_inj_cd.seclen, steady_state_inj_cd.secup, steady_state_inj_cd.k, steady_state_inj_cd.comment, steady_state_inj_cd.midpoint,

New column: midpoint=secup+seclen/2

Criteria : steady_state_inj_cd.idcode like'KFI%' AND

(steady_state_inj_cd.seclen =2 OR steady_state_inj_cd.seclen =2.05)

Result : 678 rows written to file.

Coordinate calculations done.

Coordinate system : RT

Coordinate calculation column: secup

Filename : /home/skbee/fi_secup.csv

File format : csv

Output to: File

Date :970423 16:27:11

Table(s) :sic_dba.steady_state_inj_cd

Columns: steady_state_inj_cd.idcode, steady_state_inj_cd.start_date, steady_state_inj_cd.seclen, steady_state_inj_cd.secup, steady_state_inj_cd.k, steady_state_inj_cd.comment, steady_state_inj_cd.midpoint,

New column: midpoint=secup+seclen/2

Criteria: steady_state_inj_cd.idcode like'KFI%' AND

(steady_state_inj_cd.seclen =2 OR steady_state_inj_cd.seclen =2.05)

Result : 678 rows written to file.

Coordinate calculations done.

Coordinate system : RT

Coordinate calculation column: midpoint

Filename : /home/skbee/fi_mid.csv

File format : csv

E.3 Structural data

Coordinates for the fracture zones are based on the interpreted strucutural model given by pages A22 through A24 of Andersson et al. (1992). The hydraulic properties of the SCD and SRD are from Walker et al. (1997), adapted as described in Appendix C.

E.4 Repository lay-out

The layout of the repository is a single-level design specified by Munier et al. (1997, recommended tunnel design). The tunnels of this repository design lie at an elevation of –600 masl, oriented perpendicular to the principal regional stress. The layout is described by tunnel endpoint coordinates in Excel spreadsheets, received directly from Raymond Munier of Scandia Consult. The file b_ koord.xls contains tunnel coordinates for a layout based on hydraulic structures and the file kapkoord.xls contains canister positions. The latter file was used to check that all the positions fall into the designed tunnels.

File	Main contents here	Date received	Source
b_koord.xls	Tunnel coordinates	April 16 1998	Munier, SCC
kapkoord.xls	Canister positions	April 16 1998	Munier, SCC

E.5 Boundary conditions

Four sets of boundary conditions were obtained from Lee Hartley of AEA Technology, Plc. The different sets correspond to the regional AltK case with freshwater, Variant 1 (AltK with saline conditions as environmental head), Variant 2 (AltK with additional fracture zones of Saksa and Nummela, as freshwater) and Variant 3 (the regional Base Case with saline conditions as environmental head). Variant 4 used identical boundary conditions as the base case.

Case	Files	Main Contents	Date Received	Source
Base	tbcaltfhs.bcs	Pressure, freshwater	November 17, 1998	Hartley, AEAT
Variant 1	tbcalteh.bcs	Pressure, from environmental head	December 11, 1998	Hartley, AEAT
Variant 2	tbcsksafh.bcs	Pressure, freshwater	January 15, 1999	Hartley, AEAT
Variant 3	tbcbaseeh.bcs	Pressure, from environmental head	December 18 1998	Hartley, AEAT

E.6 Location of Files

Files are located within the following directories on the SKB Convex or on the SKB SUN machines. The path to the input files and result files on Convex starts with:

/slow/sultan3/kembgtmp/

or on the SUN machines (e.g. sultan):

/net/sultan/export/home3/kembgtmp/

In each directory, there is a file with a short description of the performed simulations in addition to the necessary files for HYDRASTAR and result files:

README.txt Description of the problem

The necessary HYDRASTAR files and result files may be found at:

bebas/ Base case with unconditional stochastic simulations, HYDRABOOT

bevar1/ Variant 1, Boundary condition study, 100 stochastic realisations

bevar2/ Variant 2, Additional fracture zones, 100 stochastic realisations

bevar3/ Variant 3, Alternative hydrogeological interpretation, 100 stochastic realisations

determ/ Variant 4, Deterministic calculations

APPENDIX F. Additional Software Tools

INFERENS (Norman, 1992b; Geier, 1993). INFERENS is a FORTRAN program developed by SKB that incorporates the HYDRASTAR regularisation algorithm and Universal Kriging via iterative generalised least squares estimation (IGLSE). It is necessary in this study because each of the sites in SR 97 divides the model domain into a series of fracture zones, rock masses and depth zones that represent stepwise changes in the hydraulic conductivity. HYDRASTAR represents this complex hydraulic conductivity field as a multivariate lognormal regionalised variable with local trends in $\log_{10}$ hydraulic conductivity. A single variogram model is inferred for the entire domain (i.e., the same variogram for SRD, SCD, etc.). Although not a restriction of HYDRASTAR itself, this study will consider the trends as constants within well-defined volumes in the domain (0 order trends in $\log_{10} K_b$). This complex model of trend and spatial correlation violates the assumptions of ordinary least squares estimation (i.e., fitting trends by simple least squares regression). This study instead uses the more versatile IGLSE for universal kriging suggested by Neuman and Jacobsen (1984). INFERENS is an SKB computer program for geostatistical inference that automates the IGLSE fitting and data exploration (Norman, 1992b). INFERENS is unique in that includes the same regularisation algorithm as HYDRASTAR to upscale the data and apply universal kriging. Thus the resulting model of trends and variogram are compatible with the conditioning data and the chosen grid scale.

A program limitation prohibited using the crossvalidation option in INFERENS for this study. Alternative methods that met QA standards were not readily available during this study; therefore, crossvalidation was omitted.

HYDRAVIS (Hultman, 1997) HYDRAVIS is a graphical post-processor for HYDRASTAR, permitting users to view the repository layout, deterministic zones, hydraulic conductivities, stream tubes, and hydraulic heads. HYDRAVIS is an Advanced Visual Systems (AVS) system 5 application module developed by Cap Gemeni under contract to SKB. HYDRAVIS scans the HYDRASTAR input <casename>.hyd file and the output files for the required information, which is then displayed in a GUI format for the user. The system runs under Sun/OS, and requires a compatible version of AVS to be available. (AVS is a commercial software package for scientific visualisation on Windows NT and UNIX platforms).

IGOR Pro (WaveMetrics) IGOR Pro is a commercial Mac and MS/Windows package used in this study to produce exit location plots and special plots; e.g., for studying single realisations and single starting positions. IGOR Pro is an interactive programmable environment for data analysis and plotting. It handles large data sets (more than 100,000 points) and it includes a wide range of capabilities for analysis and graphing.

MATLAB (MathWorks) MATLAB is a commercial software package for numerical computation, visualisation and programming. It supplies a large number of high-level mathematical operations that are convenient for data analysis and visualisation. In this study, several MATLAB programs are used to interpolate between the regional and site-

scale modelling domains and to post-process HYDRASTAR results. These programs include the following:

GENERAL SCRIPTS FOR PRE-PROCESSING TO THE STATISTICA PACKAGE:

Path: 2170BeSharp\Statistik\StatTools\

`layerabc.m` These files start up and run the GUI in **MATLAB**.

`layfunc.m` Reads the input data files and generates *`casename.nim`*. The definitions of layers and end point areas are also made here as well as the definition of the string variable `'HomeDir'`. This string must be adjusted to match the installation path of the **MATLAB** files.

`perfm.m` Calculates the performance measures for the entire data file as well as for separate canisters (defined here) and layers or end point areas (depending on which model domain is being studied).

`perfmout.m` Generates a text file called *`casename_s.txt`* containing performance measures for the entire data file and the chosen canisters.

`perfplot.m` Draws graphs of accumulated mean and median (including standard deviation) of $\log_{10}$ (TT) and log(CF) for each one of the three canisters selected and also scatter plots for the three canisters.

`b_out.m` Generates text files containing performance measures for the different repository blocks (north and south) in Beberg. They are given names BebergX.txt where X indicates the part of the repository.

Statistica (StatSoft) Statistica is commercial MS/Windows software package that performs general statistical analysis of data. One of its strengths is a macro scripting language that allows users to automate a series of sorting, analysis and plotting operations. Under contract to SKB, Kemakta has developed scripts that translate HYDRASTAR output and compute summary statistics of the simulation results. The first script, statistica.pl, is a Perl script that scans and extracts the raw HYDRASTAR travel time and canister flux files and organises them into a format for Statistica input. A second Perl script, endpoints.pl, extracts the exit locations from the HYDRASTAR travel path files. A Statistica Basic program, Hydrast_.STB, is a Statistica Basic program that acts as a macro for the Statistica GUI. Optional outputs include tables of summary statistics, histograms, and box plots of canister fluxes, travel time and F-ratio. This study uses Statistica version 5.1 and the scripts documented in Boghammar and Marsic (1997). Marsic (1999) updated the script Hydrast_.STB for use in this study. Additional statistical post-processing was provided by MATLAB.

TRAZON

This program is a modification of HYDRASTAR 1.7.2 that helps identify the canister locations versus the deterministic zones. It reads the HYDRASTAR input <casename>.hyd file and compares the stream tube starting position versus the ZONE and XALFA definitions. If the starting position falls within a defined ZONE or XALFA, a comment is written to the logfile. This feature is intended to be included as an option in future versions of HYDRASTAR.

APPENDIX G. Base Case HYDRASTAR Input File

```
#  AVS
#----------------------------------------
------------------
#
#   NAME: bebas.hyd
#   DESC: BASE CASE HYDRASTAR LOCAL
BEBERG MODEL
#   DATE: 981124
#   USER: BJORN GYLLING, KEMAKTA
#
#   VERSION: HS 1.7.3
#
#----------------------------------------
------------------
#
SYSTEM SAVE_SCRATCH_FILES
SYSTEM IGNORE_ERRORS
#SYSTEM SKIP_USER_INTERFACE
#SYSTEM VERBOSE
#
#
BEGIN_BLOCK COVARIANCE
#  DETERMINISTIC    YES
#SPHERIVAL MODEL
#EXPONENTIAL MODEL
  VARIANCE         0.69
#
#  RANGE           -247.0
  RANGE            -82.33
BEGIN_DEF    ANISOTROPY
     KXX          1.0
     KXY          0.0
     KXZ          0.0
     KYY          1.0
     KYZ          0.0
     KZZ          1.0
  END_DEF
  RELATIVE_TOL     1.0E-02
  NUM_ICOSAHEDRON 40
  NUM_LINES        0
  ORIGIN           0.0 0.0 0.0
  MUL_FACTOR       0.2
  TRUNCATION       999.
END_BLOCK
#
BEGIN_BLOCK GEOM
#
# 35 METER BLOCK SCALE
# NAMMU BC
#
  AXISLENGTH       4130. 5355. 1505.
# 35 m block scale
  NUMBER_OF_NODES    119 154  44
  BOUNDARY         NAMMU
#   BOUNDARY         SIMPLE #
[SIMPLE,NOFLOW,NAMMU,HYRV11]
#   GRADIENT         -1.0  0.0  0.0
#   LEVEL            10.0
#
 BEGIN_DEF USER_SYSTEM
   XY_ROTATE  346.0
   ZY_ROTATE  0.0
#Top surface at 60 m above sea level
   TRANSLATE  14050  94610 -1505
   SYSTEM RIGHT
 END_DEF
   BEGIN_DEF WORLD_SYSTEM
     XY_ROTATE   346.0
     ZY_ROTATE  0.0
    TRANSLATE  14050  94610 -1505
   SYSTEM RIGHT
  END_DEF
END_BLOCK
#
#
BEGIN_BLOCK KRGE_NBH
  BEGIN_DEF SECONDARY
     NORMAL        0.  0. 1.
     WIDTH         3000.0
     OVERLAP       50.0
     MEASUREMENTS 16
  END_DEF
END_BLOCK
#
#
BEGIN_BLOCK KRIGE
  NUM_ITERATIONS  60
#  NUM_ITERATIONS  200
  RESIDUAL_TOL     1.0E-02
  METHOD           CG
  RESTART
  PATH             .
END_BLOCK
#
#
BEGIN_BLOCK HYDROLOGY_EQ
  NUM_ITERATIONS  16000
  RESIDUAL_TOL     1.0E-09
  PRECOND          DIAGONAL
END_BLOCK
#
#
BEGIN_BLOCK TRANSPORT
  TRANSPORT_MODEL STREAM
  PLOT_TIMES       1
  BACK_INTERPOL    NOBACKINT
  INTERVALS        FIXED
  DELIMITERS
                   1.0
                   10.0
                   100.0
                   1000.0
END_LIST
#  BEGIN_DEF EXTERNAL
#    NEIGHBOURS 2
#    SCALE      NOSCALING
#    VELIDIST   40.0
#  END_DEF
  LOGON
  TOLERANCE        0.2
  PRESENTATION     0.0
  CELL_SHIFTS      1024
  PLOTTING_MOMENTS 1.0E4
  STREAM_TUBES     120
  DIVISION         SPATIAL
  VIEW             ALL
END_BLOCK
#
BEGIN_BLOCK RESULT_ESTIMATION
   PERIOD           1
   SAVE_TRANSPORT   TRANSPORT
END_BLOCK
```

```
#
BEGIN_BLOCK PRESENTATION
   POST_PROCESSOR    AVS
   VIEW              ZDIR
   PRESENT           ALL
   NUM_REALIZATIONS
     1
   END_LIST
   INTERACTIVE       NO
   MODEL_NAME        FAA
BEGIN_DEF PSLICE
      NORMAL         0. 0. -1.
      DISTANCE      105.
      WIDTH          70.
      C_THRESHOLD   0.
      V_THRESHOLD   0.
   END_DEF
END_BLOCK
BEGIN_BLOCK TRENDS
#
#
  REF_DEPTH   100.0
  ALFA        -7.16
  BETA         0.0
  STORATIVITY  1.0
#
# Structural model 981106
(PLNEQNlarge4.xls, struct_stoc.txt)
#
# Start defining fracture Z01 #ZON2-----
--------------------------------------
BEGIN_DEF PLANE
          NAME P01 #ZON2_U
          EQUATION    -0.162249357   -
0.200896829    0.966082633
       22143.08008
          TYPE UPPER
END_DEF
BEGIN_DEF PLANE
          NAME P02 #ZON2_L
          EQUATION    -0.162249357   -
0.200896829    0.966082633
       22229.08008
          TYPE LOWER
END_DEF
BEGIN_DEF PLANE
          NAME P03 #ZON5_V
          EQUATION    0.497812291
       0.649474313    0.574774773    -
70710.79599
          TYPE UPPER
END_DEF
BEGIN_DEF PLANE
          NAME P04 #ZON12
          EQUATION    -0.999968469   -
0.00794453     0       15637.08105
          TYPE UPPER
END_DEF
       BEGIN_DEF PLANE
          NAME P05 #ZON14
          EQUATION    -0.812103212   -
0.583513796    0       67956.32813
          TYPE UPPER
END_DEF
       BEGIN_DEF PLANE
          NAME P06 #ZON1b
          EQUATION    -0.810993612
       0.524575055    -0.259056687   -
37258.85547
          TYPE LOWER
END_DEF
BEGIN_DEF ZONE
          NAME Z01 #ZON2
          ALFA -3.76
          BETA 0
          TEST_POINT  15443.70679
       96140.69922    -378.8356628
          PLANE P01 #ZON2_U    #
Distance to testpoint =       -
42.99961079
          PLANE P02 #ZON2_L    #
Distance to testpoint =
       43.00038921
          PLANE P03 #ZON5_V    #
Distance to testpoint =       -
799.559533
          PLANE P04 #ZON12     #
Distance to testpoint =       -
569.9314364
          PLANE P05 #ZON14     #
Distance to testpoint =       -
684.980143
          PLANE P06 #ZON1b     #
Distance to testpoint =
       747.5494424
END_DEF
# Start defining fracture Z02 #GibodaS--
--------------------------------------
BEGIN_DEF PLANE
          NAME P07 #GibodaS_U
          EQUATION    -0.479671627   -
0.877448082    0       94707.99219
          TYPE UPPER
END_DEF
BEGIN_DEF PLANE
          NAME P08 #GibodaS_L
          EQUATION    -0.479671627   -
0.877448082    0       94757.99219
          TYPE LOWER
END_DEF
BEGIN_DEF PLANE
          NAME P09 #Giboda1_V
          EQUATION    0.929345933    -
0.369210153    0       22691.70414
          TYPE LOWER
END_DEF
BEGIN_DEF PLANE
          NAME P10 #FE
          EQUATION    -0.970295846
       0.241921455    0       -
5125.530273
          TYPE LOWER
END_DEF
BEGIN_DEF ZONE
          NAME Z02 #GibodaS
          ALFA -4.26
          BETA 0
          TEST_POINT  17109.70166
       98610.91016    -950
          PLANE P07 #GibodaS_U        #
Distance to testpoint =       -
25.00022809
          PLANE P08 #GibodaS_L        #
Distance to testpoint =
       24.99977191
          PLANE P09 #Giboda1_V        #
Distance to testpoint =
       2184.386585
          PLANE P10 #FE       #
Distance to testpoint =
       2129.092103
END_DEF
# Start defining fracture Z03 #Giboda1--
--------------------------------------
-
BEGIN_DEF PLANE

          NAME P11 #Giboda1_U
          EQUATION    -0.253249198   -
0.967401087    0       100211.5156
```

```
          TYPE UPPER
END_DEF
BEGIN_DEF PLANE
          NAME P12 #Giboda1_L
          EQUATION    -0.253249198   -
0.967401087    0       100311.5156
          TYPE LOWER
END_DEF
BEGIN_DEF PLANE
          NAME P13 #Giboda2_V
          EQUATION    0.95021029     -
0.311609378    0       14509.14099
          TYPE UPPER
END_DEF
BEGIN_DEF ZONE
          NAME Z03 #Giboda1
          ALFA -4.26
          BETA 0
          TEST_POINT  16042.86426
       99440.32031    -950
          PLANE P11 #Giboda1_U        #
Distance to testpoint =       -
50.00087529
          PLANE P12 #Giboda1_L        #
Distance to testpoint =
       49.99912471
          PLANE P04 #ZON12     #
Distance to testpoint =       -
1195.283953
          P_TYPE UPPER
          PLANE P13 #Giboda2_V        #
Distance to testpoint =       -
1233.300617
END_DEF
# Start defining fracture Z04 #Giboda2--
----------------------------------------
BEGIN_DEF PLANE
          NAME P14 #Giboda2_U
          EQUATION    -0.368815809   -
0.929502487    0       98446.88281
          TYPE UPPER
END_DEF
BEGIN_DEF PLANE
          NAME P15 #Giboda2_L
          EQUATION    -0.368815809   -
0.929502487    0       98546.88281
          TYPE LOWER
END_DEF
BEGIN_DEF PLANE
          NAME P16 #Giboda 3_V
          EQUATION    0.940172385    -
0.340699114    0       16646.89234
          TYPE UPPER
END_DEF
BEGIN_DEF ZONE
          NAME Z04 #Giboda2
          ALFA -4.26
          BETA 0
          TEST_POINT  17665.41309
       98957.88281    -950
          PLANE P14 #Giboda2_U        #
Distance to testpoint =       -
49.99901528
          PLANE P15 #Giboda2_L        #
Distance to testpoint =
       50.00098472
          PLANE P13 #Giboda2_V        #
Distance to testpoint =
       458.7940251
          P_TYPE LOWER

          PLANE P16 #Giboda 3_V       #
Distance to testpoint =       -
459.4370845
END_DEF
# Start defining fracture Z05 #Giboda 3-
----------------------------------------
BEGIN_DEF PLANE
          NAME P17 #Giboda 3_U
          EQUATION    -0.312274039   -
0.949992061    0       99448.02344
          TYPE UPPER
END_DEF
BEGIN_DEF PLANE
          NAME P18 #Giboda 3_L
          EQUATION    -0.312274039   -
0.949992061    0       99548.02344
          TYPE LOWER
END_DEF
BEGIN_DEF ZONE
          NAME Z05 #Giboda 3
          ALFA -4.26
          BETA 0
          TEST_POINT  18672.88086
       98597.63281    -950
          PLANE P17 #Giboda 3_U       #
Distance to testpoint =       -
50.00085621
          PLANE P18 #Giboda 3_L       #
Distance to testpoint =
       49.99914379
          PLANE P16 #Giboda 3_V       #
Distance to testpoint =
       610.4931507
          P_TYPE LOWER
          PLANE P10 #FE       #
Distance to testpoint =
       609.1337441
          P_TYPE LOWER
END_DEF
# Start defining fracture Z06 #Imundbo1-
----------------------------------------
BEGIN_DEF PLANE
          NAME P19 #Imundbo1_U
          EQUATION    -0.993672073
       0.112320326    0
       5884.940918
          TYPE UPPER
END_DEF
BEGIN_DEF PLANE
          NAME P20 #Imundbo1_L
          EQUATION    -0.993672073
       0.112320326    0
       5984.940918
          TYPE LOWER
END_DEF
BEGIN_DEF PLANE
          NAME P21 #FN
          EQUATION    -0.241922691   -
0.970295548    0       100553.6797
          TYPE LOWER
END_DEF
BEGIN_DEF PLANE
          NAME P22 #Imundbo2_V
          EQUATION    0.181820482    -
0.983331741    0       93669.15588
          TYPE UPPER
END_DEF
BEGIN_DEF ZONE
          NAME Z06 #Imundbo1
          ALFA -4.26
          BETA 0
          TEST_POINT  17149.77246
       98880.67188    -950
          PLANE P19 #Imundbo1_U       #
Distance to testpoint =       -
49.99970617
          PLANE P20 #Imundbo1_L       #
Distance to testpoint =
       50.00029383
```

```
          PLANE P21 #FN        #
Distance to testpoint =
       461.2848288
          PLANE P22 #Imundbo2_V       #
Distance to testpoint =       -
445.1674352
END_DEF
# Start defining fracture Z07 #Imundbo2-
----------------------------------------
BEGIN_DEF PLANE
          NAME P23 #Imundbo2_U
          EQUATION    -0.887809634   -
0.46021086     0       60422.5
          TYPE UPPER
END_DEF
BEGIN_DEF PLANE
          NAME P24 #Imundbo2_L
          EQUATION    -0.887809634   -
0.46021086     0       60522.5
          TYPE LOWER
END_DEF
BEGIN_DEF PLANE
          NAME P25 #Imundbo3_V
          EQUATION    0.33931808     -
0.940671697    0       86130.85874
          TYPE UPPER
END_DEF
BEGIN_DEF ZONE
          NAME Z07 #Imundbo2
          ALFA -4.26
          BETA 0
          TEST_POINT  17247.68164
       98128.58984    -950
          PLANE P23 #Imundbo2_U       #
Distance to testpoint =       -
50.00062886
          PLANE P24 #Imundbo2_L       #
Distance to testpoint =
       49.99937114
          PLANE P22 #Imundbo2_V       #
Distance to testpoint =       312.180592
          P_TYPE LOWER
          PLANE P25 #Imundbo3_V       #
Distance to testpoint =       -
323.4781467
END_DEF
# Start defining fracture Z08 #Imundbo3-
----------------------------------------
BEGIN_DEF PLANE
          NAME P26 #Imundbo3_U
          EQUATION    -0.977157235   -
0.212517723    0       37742.9375
          TYPE UPPER
END_DEF
BEGIN_DEF PLANE
          NAME P27 #Imundbo3_L
          EQUATION    -0.977157235   -
0.212517723    0       37842.9375
          TYPE LOWER
END_DEF
BEGIN_DEF PLANE
          NAME P28 #Imundbo4_V
          EQUATION    0.17314536     -
0.984896281    0       92141.13429
          TYPE UPPER
END_DEF
BEGIN_DEF ZONE
          NAME Z08 #Imundbo3
          ALFA -4.26
          BETA 0
          TEST_POINT  17526.2832
       97248.37109    -950
          PLANE P26 #Imundbo3_U       #
Distance to testpoint =       -
49.99937035
          PLANE P27 #Imundbo3_L       #
Distance to testpoint =
       50.00062965
          PLANE P25 #Imundbo3_V       #
Distance to testpoint =
       599.0532654
          P_TYPE LOWER

          PLANE P28 #Imundbo4_V       #
Distance to testpoint =       -
603.8301282
END_DEF
# Start defining fracture Z09 #Imundbo4-
----------------------------------------
BEGIN_DEF PLANE
          NAME P29 #Imundbo4_U
          EQUATION    -0.991049409   -
0.13349539     0       30350.07031
          TYPE UPPER
END_DEF
BEGIN_DEF PLANE
          NAME P30 #Imundbo4_L
          EQUATION    -0.991049409   -
0.13349539     0       30450.07031
          TYPE LOWER
END_DEF
BEGIN_DEF PLANE
          NAME P31 #Imundbo5_V
          EQUATION    0.041771564    -
0.999127187    0       94642.42539
          TYPE UPPER
END_DEF
BEGIN_DEF ZONE
          NAME Z09 #Imundbo4
          ALFA -4.26
          BETA 0
          TEST_POINT  17734.7207
       96063.87891    -950
          PLANE P29 #Imundbo4_U       #
Distance to testpoint =       -
49.99917695
          PLANE P30 #Imundbo4_L       #
Distance to testpoint =
       50.00082305
          PLANE P28 #Imundbo4_V       #
Distance to testpoint =
       598.8618081
          P_TYPE LOWER

          PLANE P31 #Imundbo5_V       #
Distance to testpoint =       -
596.8007193
END_DEF
# Start defining fracture Z10 #Imundbo5-
----------------------------------------
BEGIN_DEF PLANE
          NAME P32 #Imundbo5_U
          EQUATION    -0.998733819
       0.050306741    0
       12939.39453
          TYPE UPPER
END_DEF
BEGIN_DEF PLANE
          NAME P33 #Imundbo5_L
          EQUATION    -0.998733819
       0.050306741    0
       13039.39453
          TYPE LOWER

END_DEF
BEGIN_DEF PLANE
          NAME P34 #Imundbo6_V
          EQUATION    0.314365775    -
0.949301933    0       84333.64723
          TYPE UPPER
```

```
END_DEF
BEGIN_DEF ZONE
          NAME Z10 #Imundbo5
          ALFA -4.26
          BETA 0
          TEST_POINT  17795.95801
       95097.21875    -950
          PLANE P32 #Imundbo5_U       #
Distance to testpoint =       -
49.99939674
          PLANE P33 #Imundbo5_L       #
Distance to testpoint =
       50.00060326
          PLANE P31 #Imundbo5_V       #
Distance to testpoint =
       371.5737017
          P_TYPE LOWER

          PLANE P34 #Imundbo6_V       #
Distance to testpoint =       -
347.8861801
END_DEF
# Start defining fracture Z11 #Imundbo6-
----------------------------------------
BEGIN_DEF PLANE
          NAME P35 #Imundbo6_U
          EQUATION    -0.771306515   -
0.636463881    0       73950.40625
          TYPE UPPER
END_DEF
BEGIN_DEF PLANE
          NAME P36 #Imundbo6_L
          EQUATION    -0.771306515   -
0.636463881    0       74050.40625
          TYPE LOWER
END_DEF
BEGIN_DEF ZONE
          NAME Z11 #Imundbo6
          ALFA -4.26
          BETA 0
          TEST_POINT  17991.37305
       94464.97266    -950
          PLANE P35 #Imundbo6_U       #
Distance to testpoint =       -
50.00006197
          PLANE P36 #Imundbo6_L       #
Distance to testpoint =
       49.99993803
          PLANE P34 #Imundbo6_V       #
Distance to testpoint =
       313.7380589
          P_TYPE LOWER

          PLANE P10 #FE       #
Distance to testpoint =
       270.6187872
          P_TYPE LOWER
END_DEF
# Start defining fracture Z12 #Skogsbo--
----------------------------------------
BEGIN_DEF PLANE
          NAME P37 #Skogsbo_U
          EQUATION    -0.893416643   -
0.449229032    0       55382.8125
          TYPE UPPER
END_DEF
BEGIN_DEF PLANE
          NAME P38 #Skogsbo_L
          EQUATION    -0.893416643   -
0.449229032    0       55482.8125
          TYPE LOWER
END_DEF
BEGIN_DEF PLANE
          NAME P39 #F11_V
          EQUATION    0.230849893    -
0.972989377    0       89739.71749
          TYPE LOWER
END_DEF
BEGIN_DEF PLANE
          NAME P40 #Grasbo1_V
          EQUATION    0.60143147     -
0.798924394    0       67537.98224
          TYPE UPPER
END_DEF
BEGIN_DEF ZONE
          NAME Z12 #Skogsbo
          ALFA -4.26
          BETA 0
          TEST_POINT  14087.02881
       95379.46875    -950
          PLANE P37 #Skogsbo_U        #
Distance to testpoint =       -
49.99989031
          PLANE P38 #Skogsbo_L        #
Distance to testpoint =
       50.00010969
          PLANE P39 #F11_V     #
Distance to testpoint =       188.496751
          PLANE P40 #Grasbo1_V        #
Distance to testpoint =       -
190.6195757
END_DEF
# Start defining fracture Z13 #ZON4-----
----------------------------------------
BEGIN_DEF PLANE
          NAME P41 #ZON4_U
          EQUATION    0.504899326
       0.647788985    -0.570478835   -
71115.64964
          TYPE UPPER
END_DEF
BEGIN_DEF PLANE
          NAME P42 #ZON4_L
          EQUATION    0.504899326
       0.647788985    -0.570478835   -
71080.64964
          TYPE LOWER
END_DEF
BEGIN_DEF ZONE
          NAME Z13 #ZON4
          ALFA -4.80406804435028
          BETA 0
          TEST_POINT  15682.58691
       96695.16602    -950
          PLANE P41 #ZON4_U    #
Distance to testpoint =       -
17.50369524
          PLANE P42 #ZON4_L    #
Distance to testpoint =
       17.49630476
          PLANE P06 #ZON1b     #
Distance to testpoint =
       992.6425768
          P_TYPE LOWER
          PLANE P04 #ZON12     #
Distance to testpoint =       -
813.2090093
          P_TYPE UPPER
END_DEF
# Start defining fracture Z14 #ZON1X----
----------------------------------------
BEGIN_DEF PLANE

          NAME P43 #ZON1X_U
          EQUATION    -0.811902642
       0.523052096    -0.259288579   -
37001.07813
          TYPE UPPER
END_DEF
```

```
BEGIN_DEF PLANE
          NAME P44 #ZON1X_L
          EQUATION    -0.811902642
       0.523052096    -0.259288579   -
36966.07813
          TYPE LOWER
END_DEF
BEGIN_DEF PLANE
          NAME P45 #ZON1a_V
          EQUATION    -0.561404754   -
0.827530839    -0.004172976   91859.3691
          TYPE UPPER
END_DEF
BEGIN_DEF ZONE
          NAME Z14 #ZON1X
          ALFA -4.92303804868629
          BETA 0
          TEST_POINT  18408.75488
       98808.74219    -950
          PLANE P43 #ZON1X_U   #
Distance to testpoint =       -
18.75096408
          PLANE P44 #ZON1X_L   #
Distance to testpoint =
       16.24903592
          PLANE P21 #FN        #
Distance to testpoint =
       226.5014684
          P_TYPE LOWER
          PLANE P45 #ZON1a_V   #
Distance to testpoint =       -
238.7103549
END_DEF
# Start defining fracture Z15 #ZON1a----
----------------------------------------
BEGIN_DEF PLANE
          NAME P46 #ZON1a_U
          EQUATION    -0.784903288
       0.562850118    -0.25908789    -
41418.82422
          TYPE UPPER
END_DEF
BEGIN_DEF PLANE
          NAME P47 #ZON1a_L
          EQUATION    -0.784903288
       0.562850118    -0.25908789    -
41383.82422
          TYPE LOWER
END_DEF
BEGIN_DEF PLANE
          NAME P48 #ZON1b_V
          EQUATION    -0.563243702   -
0.826290553    0.000673618
       89428.53451
          TYPE UPPER
END_DEF
BEGIN_DEF ZONE
          NAME Z15 #ZON1a
          ALFA -4.92303804868629
          BETA 0
          TEST_POINT  17596.53076
       97653.4668     -950
          PLANE P46 #ZON1a_U   #
Distance to testpoint =       -
20.00029436
          PLANE P47 #ZON1a_L   #
Distance to testpoint =
       14.99970564
          PLANE P45 #ZON1a_V   #
Distance to testpoint =
       1173.302141
          P_TYPE LOWER
          PLANE P48 #ZON1b_V   #
Distance to testpoint =       -
1173.377671
END_DEF
# Start defining fracture Z16 #ZON1b----
----------------------------------------
BEGIN_DEF PLANE
          NAME P49 #ZON1b_U
          EQUATION    -0.810993612
       0.524575055    -0.259056687   -
37276.35547
          TYPE UPPER
END_DEF
BEGIN_DEF PLANE
          NAME P50 #ZON1b_L
          EQUATION    -0.810993612
       0.524575055    -0.259056687   -
37241.35547
          TYPE LOWER
END_DEF
BEGIN_DEF PLANE
          NAME P51 #ZON1d_V
          EQUATION    -0.592737737   -
0.80539302     -0.00201475
       85571.07787
          TYPE UPPER
END_DEF
BEGIN_DEF ZONE
          NAME Z16 #ZON1b
          ALFA -4.92303804868629
          BETA 0
          TEST_POINT  16277.86938
       95718.42773    -950
          PLANE P49 #ZON1b_U   #
Distance to testpoint =       -
20.00024138
          PLANE P50 #ZON1b_L   #
Distance to testpoint =
       14.99975862
          PLANE P48 #ZON1b_V   #
Distance to testpoint =
       1168.254542
          P_TYPE LOWER
          PLANE P51 #ZON1d_V   #
Distance to testpoint =       -
1166.469129
END_DEF
# Start defining fracture Z17 #ZON1d----
----------------------------------------
BEGIN_DEF PLANE
          NAME P52 #ZON1d_U
          EQUATION    -0.741359591
       0.619191527    -0.258819997   -
47329.12891
          TYPE UPPER
END_DEF
BEGIN_DEF PLANE
          NAME P53 #ZON1d_L
          EQUATION    -0.741359591
       0.619191527    -0.258819997   -
47294.12891
          TYPE LOWER
END_DEF
BEGIN_DEF PLANE
          NAME P54 #Grasbo3
          EQUATION    -0.73063761    -
0.682765424    0       75544.20313
          TYPE UPPER
END_DEF
BEGIN_DEF ZONE
          NAME Z17 #ZON1d
          ALFA -4.92303804868629
          BETA 0
          TEST_POINT  15459.54761
       94517.33594    -950
```

```
          PLANE P52 #ZON1d_U   #
Distance to testpoint =       -
20.00020581
          PLANE P53 #ZON1d_L   #
Distance to testpoint =
       14.99979419
          PLANE P51 #ZON1d_V   #
Distance to testpoint =
       285.9320184
          P_TYPE LOWER
          PLANE P54 #Grasbo3   #
Distance to testpoint =       -
284.2927604
END_DEF
# Start defining fracture Z18 #ZON13a---
----------------------------------------
BEGIN_DEF PLANE
          NAME P55 #ZON13a_U
          EQUATION    0.746134639    -
0.665795088    0       49783.09375
          TYPE UPPER
END_DEF
BEGIN_DEF PLANE
          NAME P56 #ZON13a_L
          EQUATION    0.746134639    -
0.665795088    0       49818.09375
          TYPE LOWER
END_DEF
BEGIN_DEF PLANE
          NAME P57 #ZON14c
          EQUATION    -0.796347499   -
0.604839385    0       69736.42969
          TYPE UPPER
END_DEF
BEGIN_DEF PLANE
          NAME P58 #ZON13b_V
          EQUATION    0.683140325
       0.730287133    0       -
80635.42872
          TYPE UPPER
END_DEF
BEGIN_DEF ZONE
          NAME Z18 #ZON13a
          ALFA -4.92303804868629
          BETA 0
          TEST_POINT  16969.50098
       93815.83984    -950
          PLANE P55 #ZON13a_U  #
Distance to testpoint =       -
17.49909561
          PLANE P56 #ZON13a_L  #
Distance to testpoint =
       17.50090439
          PLANE P57 #ZON14c    #
Distance to testpoint =       -
520.7048053
          PLANE P58 #ZON13b_V  #
Distance to testpoint =       -
530.3776078
END_DEF
# Start defining fracture Z19 #ZON13b---
----------------------------------------
BEGIN_DEF PLANE
          NAME P59 #ZON13b_U
          EQUATION    0.714036226    -
0.700108767    0       53571.875
          TYPE UPPER
END_DEF
BEGIN_DEF PLANE

          NAME P60 #ZON13b_L
          EQUATION    0.714036226    -
0.700108767    0       53606.875
          TYPE LOWER
END_DEF
BEGIN_DEF PLANE
          NAME P61 #ZON13c_V
          EQUATION    0.693951322
       0.720021919    0       -
80587.69745
          TYPE UPPER
END_DEF
BEGIN_DEF ZONE
          NAME Z19 #ZON13b
          ALFA -4.92303804868629
          BETA 0
          TEST_POINT  17579.00391
       94473.0625     -950
          PLANE P59 #ZON13b_U  #
Distance to testpoint =       -
17.49864877
          PLANE P60 #ZON13b_L  #
Distance to testpoint =
       17.50135123
          PLANE P58 #ZON13b_V  #
Distance to testpoint =
       365.9596709
          P_TYPE LOWER
          PLANE P61 #ZON13c_V  #
Distance to testpoint =       -
366.0487409
END_DEF
# Start defining fracture Z20 #ZON13c---
----------------------------------------
BEGIN_DEF PLANE
          NAME P62 #ZON13c_U
          EQUATION    0.725952923    -
0.687744379    0       52188.00391
          TYPE UPPER
END_DEF
BEGIN_DEF PLANE
          NAME P63 #ZON13c_L
          EQUATION    0.725952923    -
0.687744379    0       52223.00391
          TYPE LOWER
END_DEF
BEGIN_DEF PLANE
          NAME P64 #Zon13d_V
          EQUATION    0.668369436
       0.743829481    0       -
83025.6342
          TYPE UPPER
END_DEF
BEGIN_DEF ZONE
          NAME Z20 #ZON13c
          ALFA -4.92303804868629
          BETA 0
          TEST_POINT  18055.0293
       94966.39453    -950
          PLANE P62 #ZON13c_U  #
Distance to testpoint =       -
17.49883236
          PLANE P63 #ZON13c_L  #
Distance to testpoint =
       17.50116764
          PLANE P61 #ZON13c_V  #
Distance to testpoint =
       319.4995836
          P_TYPE LOWER
          PLANE P64 #Zon13d_V  #
Distance to testpoint =       -
319.4005112
END_DEF
# Start defining fracture Z21 #Zon13d---
----------------------------------------
BEGIN_DEF PLANE
          NAME P65 #Zon13d_U
          EQUATION    0.761189878    -
0.648529112    0       47810.82813
          TYPE UPPER
```

```
END_DEF
BEGIN_DEF PLANE
          NAME P66 #Zon13d_L
          EQUATION    0.761189878    -
0.648529112    0       47845.82813
          TYPE LOWER
END_DEF
BEGIN_DEF PLANE
          NAME P67 #FE_V
          EQUATION    -0.457336699   -
0.889293621    0       93395.50056
          TYPE LOWER
END_DEF
BEGIN_DEF ZONE
          NAME Z21 #Zon13d
          ALFA -4.92303804868629
          BETA 0
          TEST_POINT  18400.84277
       95346.31641    -950
          PLANE P65 #Zon13d_U  #
Distance to testpoint =       -
17.49855317
          PLANE P66 #Zon13d_L  #
Distance to testpoint =
       17.50144683
          PLANE P64 #Zon13d_V  #
Distance to testpoint =
       194.3277382
          P_TYPE LOWER
          PLANE P67 #FE_V      #
Distance to testpoint =
       189.2489253
END_DEF
# Start defining fracture Z22 #ZON5-----
--------------------------------------
BEGIN_DEF PLANE
          NAME P68 #ZON5_U
          EQUATION    0.504776895
       0.647777796    -0.570599854   -
70857.25
          TYPE UPPER
END_DEF
BEGIN_DEF PLANE
          NAME P69 #ZON5_L
          EQUATION    0.504776895
       0.647777796    -0.570599854   -
70822.25
          TYPE LOWER
END_DEF
BEGIN_DEF ZONE
          NAME Z22 #ZON5
          ALFA -5.10509804001426
          BETA 0
          TEST_POINT  16551.25488
       95623.82227    -950
          PLANE P68 #ZON5_U    #
Distance to testpoint =       -
17.50027745
          PLANE P69 #ZON5_L    #
Distance to testpoint =
       17.49972255
          PLANE P04 #ZON12     #
Distance to testpoint =       -
1673.338266
          P_TYPE UPPER
          PLANE P10 #FE        #
Distance to testpoint =
       1948.310043
          P_TYPE LOWER
END_DEF
# Start defining fracture Z23 #ZON14a---
--------------------------------------
BEGIN_DEF PLANE
          NAME P70 #ZON14a_U
          EQUATION    -0.788728178   -
0.61474216     0       70544.96875
          TYPE UPPER
END_DEF
BEGIN_DEF PLANE
          NAME P71 #ZON14a_L
          EQUATION    -0.788728178   -
0.61474216     0       70644.96875
          TYPE LOWER
END_DEF
BEGIN_DEF PLANE
          NAME P72 #F11_V
          EQUATION    0.325016763    -
0.945708255    0       87064.67955
          TYPE LOWER
END_DEF
BEGIN_DEF PLANE
          NAME P73 #ZON14_V
          EQUATION    0.599241098    -
0.800568614    0       67644.04635
          TYPE UPPER
END_DEF
BEGIN_DEF ZONE
          NAME Z23 #ZON14a
          ALFA -5.27
          BETA 0
          TEST_POINT  14467.65479
       96274.37891    -950
          PLANE P70 #ZON14a_U  #
Distance to testpoint =       -
49.9978685
          PLANE P71 #ZON14a_L  #
Distance to testpoint =       50.0021315
          PLANE P72 #F11_V     #
Distance to testpoint =       719.434969
          PLANE P73 #ZON14_V   #
Distance to testpoint =       -
760.5864287
END_DEF
# Start defining fracture Z24 #ZON14----
--------------------------------------
BEGIN_DEF PLANE
          NAME P74 #ZON14_U
          EQUATION    -0.812103212   -
0.583513796    0       67906.32813
          TYPE UPPER
END_DEF
BEGIN_DEF PLANE
          NAME P75 #ZON14_L
          EQUATION    -0.812103212   -
0.583513796    0       68006.32813
          TYPE LOWER
END_DEF
BEGIN_DEF PLANE
          NAME P76 #ZON14c_V
          EQUATION    0.594228163    -
0.804296519    0       67136.69396
          TYPE UPPER
END_DEF
BEGIN_DEF ZONE
          NAME Z24 #ZON14
          ALFA -5.27
          BETA 0
          TEST_POINT  15209.26074
       95293.09766    -950
          PLANE P74 #ZON14_U   #
Distance to testpoint =       -
49.99855144
          PLANE P75 #ZON14_L   #
Distance to testpoint =
       50.00144856
          PLANE P73 #ZON14_V   #
Distance to testpoint =       469.39731
          P_TYPE LOWER
```

```
          PLANE P76 #ZON14c_V  #
Distance to testpoint =       -
469.4417076
END_DEF
# Start defining fracture Z25 #ZON14c---
----------------------------------------
BEGIN_DEF PLANE
          NAME P77 #ZON14c_U
          EQUATION    -0.796347499   -
0.604839385    0       69686.42969
          TYPE UPPER
END_DEF
BEGIN_DEF PLANE
          NAME P78 #ZON14c_L
          EQUATION    -0.796347499   -
0.604839385    0       69786.42969
          TYPE LOWER
END_DEF
BEGIN_DEF PLANE
          NAME P79 #F12
          EQUATION    0       1       0
       -93500
          TYPE LOWER
END_DEF
BEGIN_DEF ZONE
          NAME Z25 #ZON14c
          ALFA -5.27
          BETA 0
          TEST_POINT  16019.36572
       94205.91406    -950
          PLANE P77 #ZON14c_U  #
Distance to testpoint =       -
49.99922268
          PLANE P78 #ZON14c_L  #
Distance to testpoint =
       50.00077732
          PLANE P76 #ZON14c_V  #
Distance to testpoint =
       886.3634667
          P_TYPE LOWER
          PLANE P79 #F12       #
Distance to testpoint =
       705.9140625
END_DEF
# Start defining fracture Z26 #NS1------
--------------------------------------
BEGIN_DEF PLANE
          NAME P80 #NS1_U
          EQUATION    1       0       0
       -18058
          TYPE UPPER
END_DEF
BEGIN_DEF PLANE
          NAME P81 #NS1_L
          EQUATION    1       0       0
       -18008
          TYPE LOWER
END_DEF
BEGIN_DEF PLANE
          NAME P82 #FE_V
          EQUATION    -0.121869076   -
0.992546184    0       95013.94116
          TYPE UPPER
END_DEF
BEGIN_DEF ZONE
          NAME Z26 #NS1
          ALFA -5.27
          BETA 0
          TEST_POINT  18033
       96324.58594    -950
          PLANE P80 #NS1_U     #
Distance to testpoint =       -25
          PLANE P81 #NS1_L     #
Distance to testpoint =       25
          PLANE P21 #FN        #
Distance to testpoint =
       2727.770852
          P_TYPE LOWER
          PLANE P82 #FE_V      #
Distance to testpoint =       -
2790.324132
END_DEF
# Start defining fracture Z27 #Grasbo1--
----------------------------------------
BEGIN_DEF PLANE
          NAME P83 #Grasbo1_U
          EQUATION    -0.678791225   -
0.73433131     0       79484.25781
          TYPE UPPER
END_DEF
BEGIN_DEF PLANE
          NAME P84 #Grasbo1_L
          EQUATION    -0.678791225   -
0.73433131     0       79584.25781
          TYPE LOWER
END_DEF
BEGIN_DEF PLANE
          NAME P85 #F11
          EQUATION    -1      0       0
       14000
          TYPE UPPER
END_DEF
BEGIN_DEF PLANE
          NAME P86 #Grasbo2_V
          EQUATION    0.769958973    -
0.638093394    0       49564.44284
          TYPE UPPER
END_DEF
BEGIN_DEF ZONE
          NAME Z27 #Grasbo1
          ALFA -5.27
          BETA 0
          TEST_POINT  14187.29492
       95194.15234    -950
          PLANE P83 #Grasbo1_U        #
Distance to testpoint =       -
50.00006179
          PLANE P84 #Grasbo1_L        #
Distance to testpoint =
       49.99993821
          PLANE P85 #F11       #
Distance to testpoint =       -
187.2949219
          PLANE P86 #Grasbo2_V        #
Distance to testpoint =       -
254.6818738
END_DEF
# Start defining fracture Z28 #Grasbo2--
----------------------------------------
BEGIN_DEF PLANE
          NAME P87 #Grasbo2_U
          EQUATION    -0.59552896    -
0.803333819    0       84844.08594
          TYPE UPPER
END_DEF
BEGIN_DEF PLANE
          NAME P88 #Grasbo2_L
          EQUATION    -0.59552896    -
0.803333819    0       84944.08594
          TYPE LOWER
END_DEF
BEGIN_DEF PLANE

          NAME P89 #Grasbo3_V
          EQUATION    0.746114122    -
0.665818081    0       51633.10875
          TYPE UPPER
END_DEF
BEGIN_DEF ZONE
```

```
            NAME Z28 #Grasbo2
            ALFA -5.27
            BETA 0
            TEST_POINT  14741.01807
         94749.38281    -950
            PLANE P87 #Grasbo2_U        #
Distance to testpoint =       -
50.00075866
            PLANE P88 #Grasbo2_L        #
Distance to testpoint =
        49.99924134
            PLANE P86 #Grasbo2_V        #
Distance to testpoint =
        455.4667298
            P_TYPE LOWER
            PLANE P89 #Grasbo3_V        #
Distance to testpoint =       -
454.2617551
END_DEF
# Start defining fracture Z29 #Grasbo3--
----------------------------------------
BEGIN_DEF PLANE
            NAME P90 #Grasbo3_U
            EQUATION    -0.73063761    -
0.682765424    0       75494.20313
            TYPE UPPER
END_DEF
BEGIN_DEF PLANE
            NAME P91 #Grasbo3_L
            EQUATION    -0.73063761    -
0.682765424    0       75594.20313
            TYPE LOWER
END_DEF
BEGIN_DEF ZONE
            NAME Z29 #Grasbo3
            ALFA -5.27
            BETA 0
            TEST_POINT  15564.28516
         93988.87109    -950
            PLANE P90 #Grasbo3_U        #
Distance to testpoint =       -
50.00042953
            PLANE P91 #Grasbo3_L        #
Distance to testpoint =
        49.99957047
            PLANE P89 #Grasbo3_V        #
Distance to testpoint =
        666.3518999
            P_TYPE LOWER
            PLANE P79 #F12       #
Distance to testpoint =
        488.8710938
            P_TYPE LOWER
END_DEF
# Start defining fracture Z30 #ZON12----
----------------------------------------
BEGIN_DEF PLANE
            NAME P92 #ZON12_U
            EQUATION    -0.999968469   -
0.00794453     0       15619.58105
            TYPE UPPER
END_DEF
BEGIN_DEF PLANE
            NAME P93 #ZON12_L
            EQUATION    -0.999968469   -
0.00794453     0       15654.58105
            TYPE LOWER
END_DEF
BEGIN_DEF PLANE
            NAME P94 #Giboda1
            EQUATION    -0.253249198   -
0.967401087    0       100261.5156
            TYPE LOWER
END_DEF
BEGIN_DEF PLANE
            NAME P95 #ZON12c_V
            EQUATION    -0.013599529   -
0.999907522    0       95838.21984
            TYPE UPPER
END_DEF
BEGIN_DEF ZONE
            NAME Z30 #ZON12
            ALFA -5.41612803567824
            BETA 0
            TEST_POINT  14863.87744
         97698.96875    -950
            PLANE P92 #ZON12_U   #
Distance to testpoint =       -
20.00009202
            PLANE P93 #ZON12_L   #
Distance to testpoint =
        14.99990798
            PLANE P94 #Giboda1   #
Distance to testpoint =
        1983.161986
            PLANE P95 #ZON12c_V  #
Distance to testpoint =       -
2053.855657
END_DEF
# Start defining fracture Z31 #ZON12c---
----------------------------------------
BEGIN_DEF PLANE
            NAME P96 #ZON12c_U
            EQUATION    -0.999382555
         0.035134863    0
         11490.54688
            TYPE UPPER
END_DEF
BEGIN_DEF PLANE
            NAME P97 #ZON12c_L
            EQUATION    -0.999382555
         0.035134863    0
         11525.54688
            TYPE LOWER
END_DEF
BEGIN_DEF PLANE
            NAME P98 #Grasbo2
            EQUATION    -0.59552896    -
0.803333819    0       84894.08594
            TYPE UPPER
END_DEF
BEGIN_DEF ZONE
            NAME Z31 #ZON12c
            ALFA -5.41612803567824
            BETA 0
            TEST_POINT  14863.09229
         95158.13672    -950
            PLANE P96 #ZON12c_U  #
Distance to testpoint =       -
20.00016808
            PLANE P97 #ZON12c_L  #
Distance to testpoint =
        14.99983192
            PLANE P95 #ZON12c_V  #
Distance to testpoint =
        486.7520811
            P_TYPE LOWER
            PLANE P98 #Grasbo2   #
Distance to testpoint =       -
401.0653277
END_DEF
# Start defining fracture Z32 #ZON3X----
----------------------------------------

BEGIN_DEF PLANE
            NAME P99 #ZON3X_U
            EQUATION    0.994184017
        0.10769476     0       -
26713.41992
            TYPE UPPER
```

```
END_DEF
BEGIN_DEF PLANE
          NAME Q00 #ZON3X_L
          EQUATION    0.994184017
       0.10769476     0       -
26663.41992
          TYPE LOWER
END_DEF
BEGIN_DEF PLANE
          NAME Q01 #ZON3a_V
          EQUATION    0.153144411    -
0.98820382     0       95181.19254
          TYPE UPPER
END_DEF
BEGIN_DEF ZONE
          NAME Z32 #ZON3X
          ALFA -5.99
          BETA 0
          TEST_POINT  16096.10938
       99224.1875     -950
          PLANE P99 #ZON3X_U   #
Distance to testpoint =       -
25.00018692
          PLANE Q00 #ZON3X_L   #
Distance to testpoint =
       24.99981308
          PLANE P21 #FN        #
Distance to testpoint =
       382.8781567
          P_TYPE LOWER
          PLANE Q01 #ZON3a_V   #
Distance to testpoint =       -
407.4993538
END_DEF
# Start defining fracture Z33 #ZON3a----
---------------------------------------
BEGIN_DEF PLANE
          NAME Q02 #ZON3a_U
          EQUATION    -0.980147123   -
0.198271438    0       35387.52734
          TYPE UPPER
END_DEF
BEGIN_DEF PLANE
          NAME Q03 #ZON3a_L
          EQUATION    -0.980147123   -
0.198271438    0       35437.52734
          TYPE LOWER
END_DEF
BEGIN_DEF PLANE
          NAME Q04 #ZON3b_V
          EQUATION    0.245539969    -
0.969386468    0       91224.41294
          TYPE UPPER
END_DEF
BEGIN_DEF ZONE
          NAME Z33 #ZON3a
          ALFA -5.99
          BETA 0
          TEST_POINT  16200.18848
       98521.29688    -950
          PLANE Q02 #ZON3a_U   #
Distance to testpoint =       -
25.00004133
          PLANE Q03 #ZON3a_L   #
Distance to testpoint =
       24.99995867
          PLANE Q01 #ZON3a_V   #
Distance to testpoint =
       303.0389794
          P_TYPE LOWER
          PLANE Q04 #ZON3b_V   #
Distance to testpoint =       -
303.0052288
END_DEF
# Start defining fracture Z34 #ZON3b----
---------------------------------------
BEGIN_DEF PLANE
          NAME Q05 #ZON3b_U
          EQUATION    -0.956347585   -
0.2922315      0       44229.66797
          TYPE UPPER
END_DEF
BEGIN_DEF PLANE
          NAME Q06 #ZON3b_L
          EQUATION    -0.956347585   -
0.2922315      0       44279.66797
          TYPE LOWER
END_DEF
BEGIN_DEF PLANE
          NAME Q07 #ZON3c_V
          EQUATION    0.520402038    -
0.853921378    0       73996.73107
          TYPE UPPER
END_DEF
BEGIN_DEF ZONE
          NAME Z34 #ZON3b
          ALFA -5.99
          BETA 0
          TEST_POINT  16474.05078
       97524.5625     -950
          PLANE Q05 #ZON3b_U   #
Distance to testpoint =       -
24.99990725
          PLANE Q06 #ZON3b_L   #
Distance to testpoint =
       25.00009275
          PLANE Q04 #ZON3b_V   #
Distance to testpoint =
       730.4597279
          P_TYPE LOWER
          PLANE Q07 #ZON3c_V   #
Distance to testpoint =       -
708.448092
END_DEF
# Start defining fracture Z35 #ZON3c----
---------------------------------------
BEGIN_DEF PLANE
          NAME Q08 #ZON3c_U
          EQUATION    -0.698079824   -
0.716019928    0       80953.14063
          TYPE UPPER
END_DEF
BEGIN_DEF PLANE
          NAME Q09 #ZON3c_L
          EQUATION    -0.698079824   -
0.716019928    0       81003.14063
          TYPE LOWER
END_DEF
BEGIN_DEF PLANE
          NAME Q10 #ZON3d
          EQUATION    -0.93441987
       0.356173366    0       -
18559.77148
          TYPE LOWER
END_DEF
BEGIN_DEF ZONE
          NAME Z35 #ZON3c
          ALFA -5.99
          BETA 0
          TEST_POINT  16817.82813
       96698.35938    -950
          PLANE Q08 #ZON3c_U   #
Distance to testpoint =       -
24.99824153
          PLANE Q09 #ZON3c_L   #
Distance to testpoint =
       25.00175847
```

```
          PLANE Q07 #ZON3c_V   #
Distance to testpoint =
       175.9668489
          P_TYPE LOWER
          PLANE Q10 #ZON3d     #
Distance to testpoint =
       166.6959141
END_DEF
# Start defining fracture Z36 #ZON3d----
--------------------------------------
BEGIN_DEF PLANE
          NAME Q11 #ZON3d_U
          EQUATION    -0.93441987
       0.356173366    0       -
18584.77148
          TYPE UPPER
END_DEF
BEGIN_DEF PLANE
          NAME Q12 #ZON3d_L
          EQUATION    -0.93441987
       0.356173366    0       -
18534.77148
          TYPE LOWER
END_DEF
BEGIN_DEF PLANE
          NAME Q13 #ZON3c
          EQUATION    -0.698079824   -
0.716019928    0       80978.14063
          TYPE LOWER
END_DEF
BEGIN_DEF PLANE
          NAME Q14 #ZON3e_V
          EQUATION    -0.066556833   -
0.997782636    0       97125.24757
          TYPE UPPER
END_DEF
BEGIN_DEF ZONE
          NAME Z36 #ZON3d
          ALFA -5.99
          BETA 0
          TEST_POINT  16880.7998
       96395.54297    -950
          PLANE Q11 #ZON3d_U   #
Distance to testpoint =       -
25.00121344
          PLANE Q12 #ZON3d_L   #
Distance to testpoint =
       24.99878656
          PLANE Q13 #ZON3c     #
Distance to testpoint =
       172.8650809
          PLANE Q14 #ZON3e_V   #
Distance to testpoint =       -
180.0839364
END_DEF
# Start defining fracture Z37 #ZON3e----
--------------------------------------
BEGIN_DEF PLANE
          NAME Q15 #ZON3e_U
          EQUATION    -0.97344768    -
0.228909627    0       38367.84375
          TYPE UPPER
END_DEF
BEGIN_DEF PLANE
          NAME Q16 #ZON3e_L
          EQUATION    -0.97344768    -
0.228909627    0       38417.84375
          TYPE LOWER
END_DEF
BEGIN_DEF PLANE
          NAME Q17 #ZON3g_V
          EQUATION    0.232093968    -
0.972693369    0       88438.4573
          TYPE UPPER
END_DEF
BEGIN_DEF ZONE
          NAME Z37 #ZON3e
          ALFA -5.99
          BETA 0
          TEST_POINT  16956.92578
       95610.5 -950
          PLANE Q15 #ZON3e_U   #
Distance to testpoint =       -
25.00017405
          PLANE Q16 #ZON3e_L   #
Distance to testpoint =
       24.99982595
          PLANE Q14 #ZON3e_V   #
Distance to testpoint =
       598.1516021
          P_TYPE LOWER
          PLANE Q17 #ZON3g_V   #
Distance to testpoint =       -
625.6418537
END_DEF
# Start defining fracture Z38 #ZON3g----
--------------------------------------
BEGIN_DEF PLANE
          NAME Q18 #ZON3g_U
          EQUATION    -0.971927881   -
0.235279024    0       38946.95703
          TYPE UPPER
END_DEF
BEGIN_DEF PLANE
          NAME Q19 #ZON3g_L
          EQUATION    -0.971927881   -
0.235279024    0       38996.95703
          TYPE LOWER
END_DEF
BEGIN_DEF PLANE
          NAME Q20 #FE_V
          EQUATION    -0.003419999   -
0.999994152    0       92408.1836
          TYPE UPPER
END_DEF
BEGIN_DEF ZONE
          NAME Z38 #ZON3g
          ALFA -5.99
          BETA 0
          TEST_POINT  17421.30566
       93674.75781    -950
          PLANE Q18 #ZON3g_U   #
Distance to testpoint =       -
25.00122979
          PLANE Q19 #ZON3g_L   #
Distance to testpoint =
       24.99877021
          PLANE Q17 #ZON3g_V   #
Distance to testpoint =
       1365.021506
          P_TYPE LOWER
          PLANE Q20 #FE_V      #
Distance to testpoint =       -
1325.607235
END_DEF
# Start defining fracture Z39 #ZON7W----
--------------------------------------
BEGIN_DEF PLANE
          NAME Q21 #ZON7W_U
          EQUATION    -0.517267585   -
0.694337606    0.500329435
       74648.10156
          TYPE UPPER
END_DEF
BEGIN_DEF PLANE

          NAME Q22 #ZON7W_L
          EQUATION    -0.517267585   -
0.694337606    0.500329435
       74683.10156
```

```
          TYPE LOWER
END_DEF
BEGIN_DEF ZONE
          NAME Z39 #ZON7W
          ALFA -6.14509804001426
          BETA 0
          TEST_POINT  15361.47119
       95406.4668     -950
          PLANE Q21 #ZON7W_U   #
Distance to testpoint =       -
17.50029648
          PLANE Q22 #ZON7W_L   #
Distance to testpoint =
       17.49970352
          PLANE P04 #ZON12     #
Distance to testpoint =       -
481.8653022
          P_TYPE UPPER
          PLANE P06 #ZON1b     #
Distance to testpoint =
       577.0459135
          P_TYPE LOWER
END_DEF
# Start defining fracture Z40 #ZON7E----
--------------------------------------
BEGIN_DEF PLANE
          NAME Q23 #ZON7E_U
          EQUATION    0.450557709
       0.739748716    -0.499769568   -
77961.84375
          TYPE UPPER
END_DEF
BEGIN_DEF PLANE
          NAME Q24 #ZON7E_L
          EQUATION    0.450557709
       0.739748716    -0.499769568   -
77926.84375
          TYPE LOWER
END_DEF
BEGIN_DEF ZONE
          NAME Z40 #ZON7E
          ALFA -6.14509804001426
          BETA 0
          TEST_POINT  16969.25171
       94388.71875    -950
          PLANE Q23 #ZON7E_U   #
Distance to testpoint =       -
17.5019573
          PLANE Q24 #ZON7E_L   #
Distance to testpoint =       17.4980427
          PLANE P06 #ZON1b     #
Distance to testpoint =       -
1260.739053
          P_TYPE UPPER
          PLANE P10 #FE        #
Distance to testpoint =       1243.93142
          P_TYPE LOWER
END_DEF
# Start defining fracture Z41 #ZON8-----
--------------------------------------
BEGIN_DEF PLANE
          NAME Q25 #ZON8_U
          EQUATION    0.660662293
       0.750683248    0       -81694.375
          TYPE UPPER
END_DEF
BEGIN_DEF PLANE
          NAME Q26 #ZON8_L
          EQUATION    0.660662293
       0.750683248    0       -81659.375
          TYPE LOWER
END_DEF
BEGIN_DEF PLANE
          NAME Q27 #FS_V
          EQUATION    -0.885594755
       0.46445875     0       -
28597.28429
          TYPE LOWER
END_DEF
BEGIN_DEF ZONE
          NAME Z41 #ZON8
          ALFA -6.14509804001426
          BETA 0
          TEST_POINT  15914.09863
       94797.67969    -950
          PLANE Q25 #ZON8_U    #
Distance to testpoint =       -
17.50000455
          PLANE Q26 #ZON8_L    #
Distance to testpoint =
       17.49999545
          PLANE P04 #ZON12     #
Distance to testpoint =       -
1029.638791
          P_TYPE UPPER
          PLANE Q27 #FS_V      #
Distance to testpoint =
       1338.885238
END_DEF
#Below planes and zonesdefined by hand
BEGIN_DEF PLANE
          NAME Q42 #ZON13a
          EQUATION    0.746134639    -
0.665795088    0       49800.59375
          TYPE UPPER
END_DEF
BEGIN_DEF PLANE
          NAME Q43 #ZON3e
          EQUATION    -0.97344768    -
0.228909627    0       38392.84375
          TYPE LOWER
END_DEF
BEGIN_DEF PLANE
          NAME Q44 #ZON9U
          EQUATION    0.284240693
       0.03143223     -0.958237588   -
7432.802246
          TYPE LOWER
END_DEF
BEGIN_DEF PLANE
          NAME Q45 #ZON7W
          EQUATION    -0.517267585   -
0.694337606    0.500329435
       74665.60156
          TYPE UPPER
END_DEF
BEGIN_DEF PLANE
          NAME Q46 #ZON9L
          EQUATION    0.243971271
       0.05488769     -0.968227949   -
9123.708783
          TYPE UPPER
END_DEF
BEGIN_DEF PLANE
          NAME Q47 #ZON11U
          EQUATION    0.572371185
       0.039318778    -0.819051445   -
13445.73242
          TYPE LOWER
END_DEF
BEGIN_DEF PLANE
          NAME Q48 #ZON1a
          EQUATION    -0.784903288
       0.562850118    -0.25908789    -
41398.82422
          TYPE UPPER
END_DEF
BEGIN_DEF PLANE
          NAME Q49 #ZON11L
```

```
          EQUATION    0.57
       0.039323669    -0.819237292   -
13545.16797
          TYPE UPPER
END_DEF
BEGIN_DEF PLANE
          NAME Q50 #ZON14c
          EQUATION    -0.796347499   -
0.604839385    0      69686.42969
          TYPE UPPER
END_DEF
BEGIN_DEF PLANE
          NAME Q51 #ZON1d
          EQUATION    -0.741359591
       0.619191527    -0.258819997   -
47294.12891
          TYPE UPPER
END_DEF
BEGIN_DEF PLANE
          NAME Q52 #F100
          EQUATION    0       0       -1
       -100
          TYPE UPPER
END_DEF
BEGIN_DEF PLANE
          NAME Q53 #F850
          EQUATION    0       0       -1
       -850
          TYPE UPPER
END_DEF
BEGIN_DEF PLANE
          NAME Q54 #FS
          EQUATION    0.241921857
       0.970295727    0       -
95198.67969
          TYPE LOWER
END_DEF
BEGIN_DEF PLANE
          NAME Q55 #ZON5
          EQUATION    0.504776895
       0.647777796    -0.570599854   -
70839.75
          TYPE UPPER
END_DEF
BEGIN_DEF PLANE
          NAME Q56 #F1600
          EQUATION    0       0       -1
       -1600
          TYPE UPPER
END_DEF
# Start defining fracture Z51 #ZON11-
Defined by hand-------------------------
BEGIN_DEF ZONE
          NAME Z51 #ZON11
          ALFA -6.38
          BETA 0
          TEST_POINT  16250   94500-600
          PLANE Q47 #ZON11U
          PLANE Q49 #ZON11L
          PLANE Q48 #ZON1a
          P_TYPE UPPER
          PLANE P06 #ZON1b
          P_TYPE UPPER
          PLANE Q50 #ZON14c
          P_TYPE UPPER
          PLANE P10 #FE
          P_TYPE LOWER
          PLANE Q54 #FS
          P_TYPE LOWER
END_DEF
# Start defining fracture Z60 #NorthA---
----------------------------------------
BEGIN_DEF ZONE
          NAME Z60 #NorthA
          ALFA -6.42
          BETA 0
          TEST_POINT  15500   96500   -50
          PLANE P04 #ZON12     #
Distance to testpoint =       -
626.5773501
          P_TYPE UPPER
          PLANE Q55 #ZON5      #
Distance to testpoint =
          P_TYPE UPPER
          PLANE P06 #ZON1b     #
Distance to testpoint =
        807.6891558
          P_TYPE LOWER
          PLANE P05 #ZON14     #
Distance to testpoint =       -
940.3530049
          P_TYPE UPPER
          PLANE Q50 #ZON14c    #
Distance to testpoint =       -
1023.957155
          P_TYPE UPPER
          PLANE Q51 #ZON1d     #
Distance to testpoint =
        979.7208165
          P_TYPE LOWER
          PLANE Q52 #F100      #
Distance to testpoint =       -50
          P_TYPE UPPER
END_DEF
# Start defining fracture Z61 #NorthB---
----------------------------------------
BEGIN_DEF ZONE
          NAME Z61 #NorthB
          ALFA -7.51
          BETA 0
          TEST_POINT  15500   96500-600
          PLANE P04 #ZON12
          P_TYPE UPPER
          PLANE Q55 #ZON5
          P_TYPE UPPER
          PLANE P06 #ZON1b
          P_TYPE LOWER
          PLANE P05 #ZON14
          P_TYPE UPPER
          PLANE Q50 #ZON14c
          P_TYPE UPPER
          PLANE Q51 #ZON1d
          P_TYPE LOWER
          PLANE Q52 #F100      #
Distance to testpoint =       500
          P_TYPE LOWER
          PLANE Q53 #F850      #
Distance to testpoint =       -250
          P_TYPE UPPER
END_DEF
# Start defining fracture Z62 #NorthC---
----------------------------------------
BEGIN_DEF ZONE
          NAME Z62 #NorthC
          ALFA -7.51
          BETA 0
          TEST_POINT  15500   96000-1000
          PLANE P04 #ZON12
          P_TYPE UPPER
          PLANE Q55 #ZON5      #
Distance to testpoint =       -
258.4398768
          P_TYPE UPPER
          PLANE P06 #ZON1b
          P_TYPE LOWER
          PLANE P05 #ZON14
          P_TYPE UPPER
          PLANE Q50 #ZON14c
          P_TYPE UPPER
          PLANE Q51 #ZON1d
```

```
          P_TYPE LOWER
          PLANE Q53 #F850      #
Distance to testpoint =       150
          P_TYPE LOWER
END_DEF
# Start defining fracture Z63 #South1A--
----------------------------------------
BEGIN_DEF ZONE
          NAME Z63 #South1A
          ALFA -6.78
          BETA 0
          TEST_POINT  16000   95000   -50
          PLANE P06 #ZON1b     #
Distance to testpoint =-384.6702321
          P_TYPE UPPER
          PLANE Q55 #ZON5      #
Distance to testpoint =       -
1195.899086
          P_TYPE UPPER
          PLANE Q10 #ZON3d     #
Distance to testpoint =
       325.9803889
          P_TYPE LOWER
          PLANE Q50 #ZON14c    #
Distance to testpoint =-514.8718276
          P_TYPE UPPER
          PLANE Q52 #F100      #
Distance to testpoint =       -50
          P_TYPE UPPER
END_DEF
# Start defining fracture Z64 #South2A--
----------------------------------------
BEGIN_DEF ZONE
          NAME Z64 #South2A
          ALFA -6.78
          BETA 0
          TEST_POINT  16800   94500   -50
          PLANE Q10 #ZON3d     #
Distance to testpoint =       -
599.6421906
          P_TYPE UPPER
          PLANE Q43 #ZON3e     #
Distance to testpoint =
       406.9630041
          P_TYPE LOWER
          PLANE Q55 #ZON5
          P_TYPE UPPER
          PLANE Q42 #ZON13a
          P_TYPE UPPER
          PLANE Q50 #ZON14c    #
Distance to testpoint =       -
849.5301344
          P_TYPE UPPER
          PLANE Q52 #F100      #
Distance to testpoint =       -50
          P_TYPE UPPER
END_DEF
# Start defining fracture Z65 #SouthB---
----------------------------------------
BEGIN_DEF ZONE
          NAME Z65 #SouthB
          ALFA -7.87
          BETA 0
          TEST_POINT  16000   95000-600
          PLANE P06 #ZON1b     #
Distance to testpoint =-242.189054
          P_TYPE UPPER
          PLANE Q55 #ZON5
          P_TYPE UPPER
          PLANE Q43 #ZON3e
          P_TYPE LOWER
          PLANE Q42 #ZON13a
          P_TYPE UPPER
          PLANE Q50 #ZON14c    #
Distance to testpoint =       -
514.8718276
          P_TYPE UPPER
          PLANE Q52 #F100      #
Distance to testpoint =       500
          P_TYPE LOWER
          PLANE Q53 #F850      #
Distance to testpoint =       -250
          P_TYPE UPPER
END_DEF
# Start defining fracture Z66 #SouthC---
----------------------------------------
BEGIN_DEF ZONE
          NAME Z66 #SouthC
          ALFA -7.87
          BETA 0
          TEST_POINT  16000   95000-1000
          PLANE P06 #ZON1b     #
Distance to testpoint =-138.5663791
          P_TYPE UPPER
          PLANE Q55 #ZON5
          P_TYPE UPPER
          PLANE Q43 #ZON3e
          P_TYPE LOWER
          PLANE Q42 #ZON13a
          P_TYPE UPPER
          PLANE Q50 #ZON14c    #
Distance to testpoint =-514.8718276
          P_TYPE UPPER
          PLANE Q53 #F850      #
Distance to testpoint =       150
          P_TYPE LOWER
END_DEF
# Start defining fracture Z67 #SRD other
above 100 m----------------------------
BEGIN_DEF ZONE
   NAME Z67 #SRD other A
          ALFA -7.16
          BETA 0
          TEST_POINT  16000   97500   -50
          PLANE Q52 #F100      #
Distance to testpoint =       -50
          P_TYPE UPPER
          PLANE P10 #FE
          P_TYPE LOWER
          PLANE Q54 #FS
          P_TYPE LOWER
          PLANE P21 #FN
          P_TYPE LOWER
END_DEF
# Start defining fracture Z68 #SRD other
below 100 m----------------------------
BEGIN_DEF ZONE
          NAME Z68 #SRD other B
          ALFA -8.26
          BETA 0
          TEST_POINT  16000   97500-600
          PLANE Q52 #F100
          P_TYPE LOWER
          PLANE Q56 #F1600
          P_TYPE UPPER
       END_DEF
#
END_BLOCK
```

APPENDIX H. Information on Coordinate Transform

The simulations for Beberg are performed using coordinates in a local system based on the RAK system, but with an off-set subtracted. This means that the all input data in form of e.g. stream tube starting positions and fracture zones are defined for that system. The model is set up in the local system with the origin for the model cube at (14050, 94610, -1505). The HYDRASTAR modelling terms "user system" and "world system" are defined using that point in the local system. The HYDRASTAR "cube system" is rotated 14 degrees clock-wise in relation to the local system. The used definitions of coordinate systems give output data for e.g. exit locations, which could be extracted from the lines_<real>.hyp files, in the local system. (The rotation of the cube system is made internally in HYDRASTAR).

The Beberg local coordinate system used in the groundwater simulations here is set up with an off-set of 1 600 000 and 6 600 000 in east and north, in relation to RAK. The coordinate systems for Beberg are right-handed with X towards east and Y towards north. The Z-direction is given in meter above sea level (m.a.s.l). To translate the modelling coordinates to RAK the following equations have been used:

$$X_{RAK} = X_{Off\text{-}set} + X_B$$

$$Y_{RAK} = Y_{Off\text{-}set} + X_B$$

where X_{RAK} and Y_{RAK} stand for east and north, respectively, X_B and Y_B are Beberg modelling coordinates, $X_{Off\text{-}set}$ = 1 600 000 and, $Y_{Off\text{-}set}$ = 6 600 000.

ISSN 1404-0344
CM Gruppen AB, Bromma, 1999